Semi-Trailer Structural Failure Analysis

Using Finite Element Method

A thesis submitted in partial fulfilment of the requirements for the

Degree of Master of Engineering in Mechanical Engineering in the

University of Canterbury

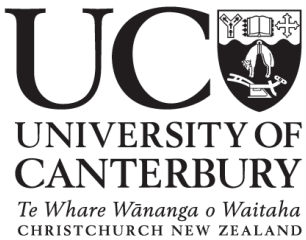

Author: Chetan Chandrakant Baadkar

Department of Mechanical Engineering

University of Canterbury

2010

TABLE OF CONTENTS

ACKNOWLEDGMENTS

I wish to acknowledge Steelbro New Zealand ltd for this research project and infrastructure.

I would like to thank Engineering Manager, Greg Muirsmith for giving me the opportunity to work on this project as a part of my Master of Engineering degree and special thanks to Product development Engineer, Greg Lowe for his support and guidance throughout my service with Steelbro. I have gained a lot of practical knowledge and expertise through working alongside him.

I would like to extend my gratitude to my supervisory team Dr. Elijah Van Houten and Dr. David Aitchison for accepting my project and guiding me throughout the project.

I would like to thank Adam Latham and Paul Southward for their technical support, particularly when there were computer problems.

I am very grateful for the technical help I received during the strain gauge installation from Julian Philip.

Thank you to all my friends and fellow students on the third floor mechanical\civil engineering building, who have made my time here interesting and enjoyable.

I would like to thank my parents, Chandrakant Baadkar and Shalini Baadkar for believing in my dreams and supporting the best possible way they could.

Most importantly, I would like to thank my dear wife, Reshma Baadkar for her continued support, encouragement, and understanding. Although life got hard at times, we made it through; you deserve as much credit for this work as I do.

Finally, I would like to thank my baby daughter, Medha Baadkar whose beautiful face always motivated me to carry on during the stressful times.

LIST OF FIGURES

LIST OF TABLE

LIST OF SYMBOLS

Roman

k_t	Stress concentration factor
M	Bending moment at the maximum stress
F	Applied force at the free end of the plate
L	Length of the plate form the free end to the point of maximum stress
B	Breadth of the cross section of the plate
I	Area moment of inertia for the plate cross section
H	Height of the cross section at free end of the plate
C	Vertical height from the natural axis to the outer fibre at the free end
[M]	Mass matrix
[C]	Damping matrix
[K]	Global stiffness matrix
$\{\ddot{x}\}$	Acceleration vector
$\{\dot{x}\}$	Velocity vector
$\{x\}$	Displacement vector
t	Time
$\{F\}$	Force vector
FOS	Factor of safety
ΔL	Change in length
L	Initial length
E	Elastic modulus or Yong's modulus
D	diameter
ΔD	Change in diameter

K_c	Fracture toughness of the material for the thickness of interest
b	fatigue strength exponent
K_a	Surface condition modification factor
K_b	Size modification factor
K_c	Load modification factor
K_d	Temperature modification factor
K_e	Reliability factor
K_f	Miscellaneous modification factor
s_e	Endurance limit of the actual component
S'_e	Endurance limit of the test specimen
c	Fatigue ductility exponent
$2N_f$	Fatigue life in reversals to failure
H'	Cyclic strain coefficient of the material
n'	Cyclic hardening exponent
S	Nominal elastic stress
e	Nominal elastic strain

Greek

σ_{max}	Maximum stress
σ_{min}	Minimum stress
σ_m	Mean stress
R	Stress ratio
$\Delta\sigma$	Stress range
ΔK	Stress intensity range
ν	Poisson's ratio

σ_f'	Fatigue strength coefficient of the material
ε_f'	Fatigue ductility coefficient of the material
σ_{nom}	Nominal stress
σ_y	Yield stress
$\rho_{\max}$	Moment arm for tyre and the ground contact surface area (constant)
N	Normal force on the wheels
σ	Stress at the contact surface area
μ	Coefficient of friction
ε	Strain
ε_L	Longitudinal strain
ε_T	Transverse strain
ε_1	Strain in axis 1
ε_2	Strain in axis 2
ε_3	Strain in axis 3
σ_{uts}	Ultimate tensile strength
σ_{ys}	Yield strength
σ_a	Fatigue strength when $\sigma_m \neq 0$
σ_{ar}	Fatigue strength in fully reversed loading condition, when $\sigma_m = 0$
$\in_{ea}$	Elastic strain amplitude
$\in_{pa}$	Plastic strain amplitude
$\in$	Total local strain
$\in_a$	Strain amplitude
σ_a	Stress amplitude

ABSTRACT

This project is centred on an ongoing trailer component failure problem at the STEELBRO New Zealand Ltd due to cracks. In this research the problem has been systematically approached using ANSYS finite element analysis software. The approach involves investigation of the problem and structural analysis of the trailer subjected to two types of service conditions. The service conditions are simulated in ANSYS which involved CAD and finite element modelling of the trailer, and then the finite element model is validated experimentally by strain gauges and geometrically by ANSYS element shape checking capability. The finite element model subjected to static structural analysis confirmed the crack locations and indicated the cause of the failure. Further fatigue analysis on one of the loading condition revealed it's potential to cause failure at the crack locations. Finally, this research concludes with a proposal of revised component design to overcome the failure at the crack locations and recommendations for further analysis on the trailer.

1 INTRODUCTION

1.1 Background of the study

1.1.1 Company profile

STEELBRO New Zealand Ltd is a world leader in self-loading container trailer manufacture. The product base has evolved over a number of years since Steelbro first began producing innovative and imaginative solutions for the transport industry in 1878. Since then, Steelbro has manufactured a broad range of road-going equipment, including conventional and specialised trailers, now sold in more than 100 countries.

Since 1979, the primary product for modern day STEELBRO is the self-loading semi-trailer or truck, known as a Sidelifter. The Sidelifter consists of two sets of cranes that deploy to the side of the trailer and typically load/unload an ISO container (generally conforming to ISO 668) from the ground, a dock, a companion trailer or a rail wagon. The Steelbro Sidelifter is manufactured for a wide range of container types. Standard machines handle 40', 20' and double 20’ ISO containers. Other container sizes can be accommodated including 10', 24', 30’, 45' or 48' units. Other than standard trailer chassis, the company has been involved in manufacturing trombone and drop-deck trailers. The trombone trailer has feature of extending and contracting between 20' and 40' container loading positions and the drop-deck trailers are manufactured to very low deck heights. These two types of trailers are built to suit very specific applications.

Steelbro is currently manufacturing Sidelifters in Europe, China, Malaysia and New Zealand (Christchurch) and widely acknowledged within the industry as a world leader in the design and manufacture of road-going container handling equipment.

1.1.2 SB330 Side-Lifter Trailer

The unit of particular interest in the study described below is the SB330 Sidelifter trailer, which is shown in the Figure 1-1. This unit has a maximum lift capacity of 33 tonnes (72,800 lbs), a container carrying capacity from 10' to 45' and can handle full and empty containers. In this model, the cranes move along the length of the chassis and each crane is independently activated by hydraulic cylinders. The hydraulic and electrical systems are operated by a Kubota 42HP diesel engine. This machine can pick up and transport one 40' container or two 20' containers simultaneously. It can also be used to double stack 9'6" hi-cube containers on the ground and trailer-to-trailer transfers.

Figure 1-1: SB330 side-lifter semi-trailer

1.1.3 Problem definition

A Trailer chassis is a large welded structure, mainly constructed of two I-section beams running along its entire length of 13600 mm. These I beams are called the mainframes of the chassis. Roughly the chassis is formed by welding the cross-member at several locations along the length of the mainframes. Structural integrity of these cross-member joints is very important for a trailer chassis, as it can drastically influence the induced strains and stresses in the trailer and therefore affects the life of the trailer. The rub-plate cross-member group is at the front of the trailer chassis and is an important structural part of the chassis. As shown in Figure 1-2, the cross-member pressings are welded to the rub-plate along with a couple of Rolled Hollow Sections (RHS). The King-pin is a mechanical junction between truck and trailer, which acts as support point at the front end and carries significant amount of payload. As can be seen the figure below, the King-pin is bolted to the Rub-plate assembly.

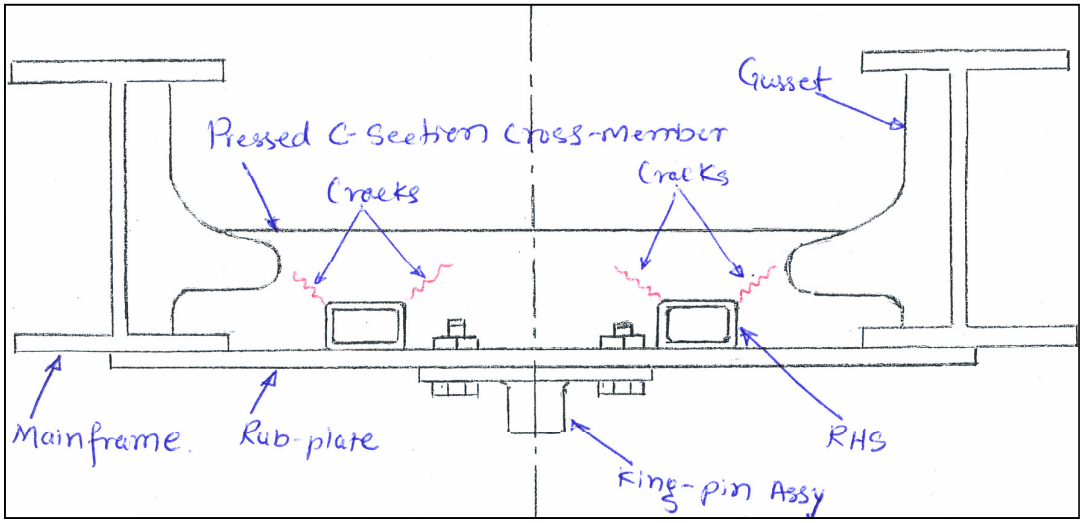

Figure 1-2: Pictorial view of the Rub-plate assembly; showing the typical weld crack appearance on cross-member pressing

In this particular SB330 trailer chassis, cracks have appeared in various cross-member joints in early stages of its lifetime. Pictorial view of the cracks on the rub-plate cross-member pressing is shown in Figure 1-2. Also, cracks ground for welding is shown in Figure 1-3. So far a quick fix at service stations has eliminated all the cracks in the cross-member joints. An additional strengthening plate added to the cross-member pressing can be seen in Figure 1-4, which has eliminated further cracking of the cross-member pressing. However an alternative design level solution is sought for the rub-plate cross-member group based on its structural importance in the trailer chassis.

Figure 1-3: Cracks at the corner of the cross-member and RHS ground for welding is shown on the actual trailer.

Figure 1-4: Showing the additional strengthening plates welded to the Rub-plate cross member

1.1.4 Speculations of cause

There are two main factors considered to be seriously contributing to the above explained problem. The factors are explained below:

Firstly, when the trailer is transporting loaded container, it tends to deflect (bow and hog) up and down at the unsupported span of the chassis. This is perhaps due to change in inertia forces, which causes the swinging action to act like a cyclic loading on the chassis. Also a frequent loading/unloading operation can produce the same effect on the chassis. Altogether this may exceed the fatigue limit of the material causing failure due to fatigue.

Secondly, Yard manoeuvres are as important as on road movements of a trailer, it can be crucial if certain aspects are considered such as lateral deflection of the chassis. When the trailer moves in a congested yard environment, manoeuvres such as turning around a sharp corner or reversing in a confined space could produce a bowing effect on the chassis. If the intensity of the lateral deflection due to yard manoeuvres is very high it could cause the

working stress to exceed yield stress of the material or repeated yard manoeuvres could cause cyclic effects on the chassis leading to fatigue failure.

1.2 Research objectives

- Investigate and confirm the reasons behind the rub-plate cross-member cracks.
- Conduct the static and fatigue analysis on the current design using FEA techniques.
- Restructuring the cross-member joint design to overcome the particular cracking problem.
- Develop suitable finite element procedure, which can be incorporated into the STEELBRO's conventional product development process.

1.3 Outline of the thesis

This section provides an outline of the organization and brief description of the remaining sections of the thesis.

The body of this thesis consists of mainly seven chapters as shown in Figure 1-5. Initially the problem is defined and sufficient literature survey is done to identify and gain knowledge form the previous research in the related field. Then a suitable problem approach is adopted to solve the problem. An experimental method, which employs the strain gauge technology, is also used to validate the FEA predicted results. A chapter wise briefing is as follows:

Chapter 2 discusses some of the relevant literature such as journal papers, publications, articles, theses on finite element method, stress analysis, trailer design, Sub-modelling technique in FEA, fatigue analysis and so on.

Chapter 3 details the physical structure of the trailer. It shows complete solid modelling of the trailer and presents associated technical details up to the discretization stage of the finite element analysis.

Chapter 4 covers the static structural analysis of the trailer. The analysis is performed on the trailer for two cases namely, static loading/unloading and perceived “worst case” condition. This chapter also includes discussion on the causes of the failure based on the results obtained from the finite element analysis of the trailer.

Chapter 5 validates the finite element model used for the static analysis using ANSYS shape checking feature and strain values recorded for the rosette strain gauges. It also reports the differences between the analytically calculated stress values and the linear strain gauge results.

Chapter 6 use finite element analysis technique for the fatigue analysis of the current design to determine the fatigue life. It also includes the redesign of the problem area to overcome

the failure of the component based on the outcome of the static and fatigue analysis of the current design.

Finally, Chapter 7 summarises the conclusions based on the findings of the analysis and provides recommendations for the future work.

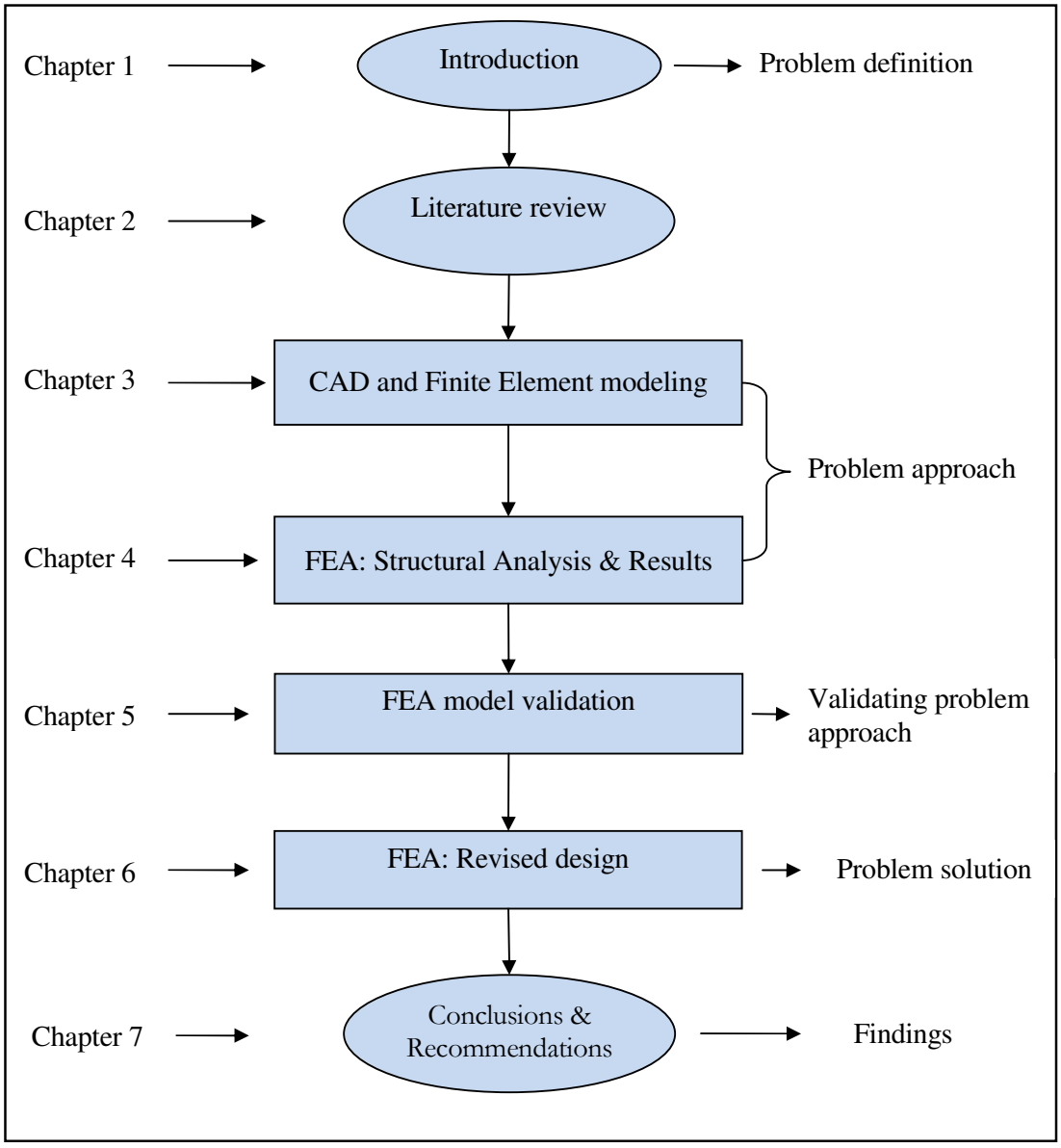

Figure 1-5: Organization of the thesis; Showing the logical approach to the problem

1.4 Scope and limitations of the research

In this research the trailer design is verified for two important known loading conditions. The outcome of the analysis could become the basis for further complex design analysis. In any type of design analysis, engineering practice is to keep the working stress well below the yield stress of the material. Therefore the approach followed in this study could be widely used in trailer manufacturing industries.

In this study only linear elastic material model is used for the static analysis and non-linear material behaviour is not considered, which could be important for further design analysis of the structure. Also, the true characteristics of the shock absorbers in the suspension have not been built into the model, which could be significant for further dynamic analysis of the trailer. Finally, fatigue analysis performed on the current design is only based on FEA method, which will have to be validated experimentally.

2 LITERATURE SURVEY

2.1 Introduction

The finite element method is now used in wide range of industries in research and product development process. This is a result of continuous development of the technology over five decades, ever since it was introduced in 1950s. In the past two decades, the technological advancement in the field of the digital computers has turned finite element method into a very sophisticated tool, which can analyze complex field problems. Hence rapid growth in application of the FEA technology can be seen in this era. The advantages of using FEA were soon realized in competitive industrial world and triggered research and development within the industry for the effective use of the finite element tool. The investigation done in this thesis is an ideal example of such a type. Scholarly and commercial research literatures surveyed in the field of structural analysis using FEA indicates the commercial value of this tool. Some of the researches, which are relevant to this research include static analysis, sub-modeling, fatigue analysis, strain gauging, etc are briefed below.

Forest Engineering Research Institute of Canada (FERIC) has developed software for designing light weight trailers for logging operations. This is interactive software based on finite element analysis technique. To validate the trailer design software experiments were conducted on the actual trailer for stress and deflection and also modal testing of the chassis was carried out. For instance strain gauges and accelerometers were mounted on the chassis to measure strain and acceleration at critical locations respectively. They found that the experimental results obtained showed good correlation with the results of the trailer design software and ANSYS, commercially available analysis software as well. Then prototype was

designed using trailer design software and manufactured. The experimental test showed the results were well within the safe working limit [3].

According to Rahman, Tamin, and Kurdi (2008), highest stress point can be identified for components by performing the stress analysis, which is essential for the fatigue life prediction of components. In this research finite element analysis of the truck model is performed using ABACUS analysis software. In the static structural analysis performed on the truck, the static forces created by the truck body and the cargo are applied on the chassis. Then the boundary condition resembling the physical situation is applied to constraint the truck model. The model is discretized using 3D tetrahedral elements. The results showed the highest stress point and maximum deflection in the chassis. The deflection is validated using the analytical formula. As the highest stress point can be the initiation point for the fatigue failure, this paper concludes with recommendation to reduce the magnitude of the stress at the critical point [4].

According to Kassahun (2008), responses of the vehicle structural components to the static and dynamic loads are very important to produce good quality vehicles with longer fatigue life, greater strength, low weight and low cost. In this research this is achieved by studying the structural response in terms of stress, strains, deflections and vibration and noise in the components. In this study an ISUZU NPR commercial vehicle with van body is subjected to the static and dynamic loading in finite element analysis software, ANSYS, and a van model was also developed using the same software. Particularly static, modal and random vibration analysis was done in ANSYS. As a result of these analyses the various structural components of the van chassis, which are influenced by higher values of stress and deflection due to different static and dynamic loading conditions, were identified [5].

Wang, and Rauch (2008) worked on fatigue analysis and design optimization of a trailer hitch system. It involved testing the trailer hitch according to the customer specifications. Locations of the failure were identified by the experimental testing. Design Modeler module in ANSYS was used to model the global model of the trailer hitch. Then it was meshed using uniform finite elements and a coarse finite element model was prepared. Later this model was analyzed to identify the "hot spots". It was found that the "hot spots" identified in the analysis matched with the failure points identified in the experimental testing. The sub-model was created form the global model of the trailer hitch at the area of interest and again it was done in Design Modeler. The sub-model is then analyzed to obtain the local stress at the area of interest. The data from the structural analysis then fed to the fatigue module of the ANSYS to predict the fatigue life of the trailer hitch. Finally, parameter driven hitch geometry was created and DesignXplorer ANSYS module was used to optimize the trailer hitch design based on the simulation results [6].

Bekah, (2004), carried out fatigue analysis of a car door hinge using finite element analysis and validated the results by experimental testing. This process involved modeling finite element model of the door hinge. A couple of models were tried in the geometry check and one of them was found more accurate. This led to the further verification in the static analysis and one of the FE model was confirmed to be more accurate. The static analysis was carried out on the FE model for uni-axial and multi-axial loading. The analysis was carried out in MSC.NASRAN and the model was solved for stress and strains. The results obtained from the static analysis were used in the fatigue analysis to predict the fatigue life of the door hinge. Finally, on the basis of FE based fatigue analysis, the door hinge design was optimized and fatigue life of the door hinge was improved [7].

Petracconi, Ferreira, and Palma (2009) presented a paper that investigated current life of a rear tow hook assembly of a passenger car by experimental testing. It was found that the life of the product was less than the expected life of the tow hook during service. Care was taken to conduct the experimental testing according to the actual service condition. As result of the testing failure region were identified. FE-based simulation of the tow hook confirmed the failure region as it was identified in the experimental fatigue testing. Rosette strain gauges were used to record the micro-strain at the failure region of the tow hook. The data was recorded on a computer from the strain gauges through data acquisition system. Then the fatigue life identified from the experimental fatigue testing is compared with the life estimated from the FE-based simulation and it was found that the results are within the acceptable limit. Based on this methodology new configurations of the tow hook were simulation tested and best of design was proposed for manufacturing. Finally, the prototype was experimentally tested for fatigue life and it was found that no cracks were found during the expected service life of the tow hook [8].

Topac, Gunal, & Kuralay (2008) presented a paper that studied fatigue failure of a rear axle housing and proposed a solution to increase its fatigue life. In this study prototype axle housing was experimentally tested for fatigue life using hydraulic test rig. The results of the test showed that the cracks appeared before the expected design life of the axle housing. The next step in the research was to create the detailed model of the axle housing in the CATIA V5R15 software. Then the solid model was imported into ANSYS Workbench 11 for the static and fatigue analysis. The material properties and the S-N curve for the material were obtained from the tensile test of the housing material test specimen. The FE-based fatigue analysis performed in the ANSYS confirmed the critical region identified in the experimental fatigue testing and the results showed that this is due to the stress concentration, which

reduced the expected life of the axle housing. Finally the study was concluded that the stress concentration should be reduced to increase the fatigue life and proposed the design change at the critical region and increase in the thickness of the reinforcement ring of the axle housing [9].

Fermer & Svensson, (2001) presented a paper that discuses about FE-based fatigue analysis methodology used in automotive industries. Generally spot welds and seam welds are commonly used joining method in car and truck body building. The failures of these welds have prompted continuous research and development in FE-based fatigue simulation to minimize the cost of the production. This paper details few experiences of using FE-based fatigue analysis in predicting fatigue life of the spot and seem welded joints. These analyses showed that the method used for the fatigue analysis is good enough to be incorporated in the design process. It also mentions about the growing trend of the finite element analysis in the automotive industry. Finally, this paper conclude with the finding that the FE-based fatigue life prediction of the weld in conjunction with the results obtained from the analytical methods were in good correlation with the results obtained from the experimental fatigue testing.[10]

Yongming, Startman, & Mahadevan, (2006) proposed a new multi-axial fatigue damage model and “elasto-plastic” finite element model. In this paper a multi-axial fatigue damage model was developed for railroad wheel, where complex rolling contact stresses are involved, which is capable of predicting “both the initiation crack plane orientation and fatigue initiation life”. In the next step of the research finite element model of the wheel/rail contact was developed. This involved modeling a full scale model of the wheel/rail contact and analyzing in ANSYS 7 software. In order to increase the efficiency and accuracy of the finite element analysis, the sub-modeling technique is also included in the proposed finite

element model. Then the numerical example was used to qualitatively validate the proposed models. Finally the proposed models were used to study the different parameters of the wheel and its effects on the fatigue damage were investigated and recommendations were suggested for the future work [11].

Ye & Moan, (2007) investigated aluminium box-stiffener /web frame connection for fatigue life. Three types of designs used in this study these connections were designed in such a way that the cost of fabrication could be reduced without compromising the fatigue strength. Finite element analysis (FEA) and experimental fatigue tests were carried out to study the static and fatigue behaviour of the connection. FEA analyzed the effect of weld parameters and local geometry at the cracking area for stress gradient and stress concentration. Twelve specimens of the three designs were experimentally tested for fatigue life. Experimental data indicated that two of the three designs should be avoided due to possible defects introduced by the welding procedure, which can reduce the fatigue life. Finally the study showed that the size of the fillet weldment has a greater influence on the fatigue life of the joint [12].

Zhao, Li, & Shen, (2008) presented a paper on improving the fatigue life of the rubber mount on the crack-shaft of an automobile wheel. In this research they investigated the fatigue crack using the finite element model of the mount and the model was analyzed for fatigue in MSC.MARC analysis software. Stress concentration was found at the interface of the rubber and metal of the mount. Then the stress concentration was minimized by modifying the structural parameters of the mount and the rubber material. As a result, fatigue life of the rubber mount was increased. This new FEA process and methodology was also backed up by experimental testing. Finally on this basis, a new FEA process and methodology was proposed, which can improve product quality. The proposed technique was also cost effective due to shortened product development cycle [13].

Karaoglu & Kuralay, (2002) conducted a study on stress analysis of a truck chassis with riveted joints. The purpose of this study was to reduce the magnitude of the stress near the riveted joints. Three geometric parameters of the components of the joints were varied and analyzed in ANSYS version 5.3 analysis software. Three variables of the joints were thickness of the sidebar and connection plate and length of the connection plate. During the analysis it was found that increasing the sidebar thickness can reduce the stress but at the consequence of high overall weight. This problem was overcome by just increasing the local thickness of the sidebar using the local plate. Increasing the thickness of the connection plate also reduced the stress in the connection plate with slightly increased stress in the sidebar. As a final option, increase in the length of the connection plate also decreased the stress distribution near the riveted joints. Finally, comparison of all three results of the analysis concluded that stress near the riveted joints can be reduced by using local plate at the joints. If not, increasing the length of the connection plate can be a better option to minimize the stresses [14].

Colquhoun & Draper, (2000) presented a paper, which discusses the local strain-based fatigue analysis using finite element model. In this analysis local strain based fatigue analysis was integrated into software using finite element technique. This paper also discusses few industrial experiences to validate the analysis. It was found that the experimental results were in good agreement with the analysis results. The analysis process involved creating a CAD model, exporting it to FEA software, initial stress analysis and then fatigue analysis. It was found during the analysis that the fatigue results were mesh dependent and simple mesh can estimate non-conservative fatigue life. This problem was overcome by using refined mesh. Finally this paper concluded that the crack locations can be accurately determined and very reliable fatigue life estimates can be done using finite element model [15].

Cowell, (2006) developed a methodology to predict the fatigue life of the rotary-wing aircraft components using commercially available analysis software, namely, ANSYS and Fe-safe. The primary objective of the research was to predict the fatigue life of the components and confirm the suitability of the repaired ones for further use in the same service conditions. Fatigue analysis of a flat plate with a centrally located hole is carried out using this methodology and predicted fatigue life the plate is compared with the simulated life obtained from stress and strain fatigue life algorithms based on previously published experimental data. The predicted fatigue life found to be in good agreement with the simulated results. When this methodology is applied to the helicopter main gear drag beam, it was found to be effective in identifying the influence of beam thickness on fatigue life of the component. Finally, it was concluded that developed methodology was effective enough to predict the fatigue life of the aircraft components and also can be used to confirm the continuous use of the repaired parts [16].

He, Wang, & Gao, (2010) investigated a failure of an automobile damper spring tower. In this investigation, firstly, the service conditions of the suspension assembly were identified in order to establish the failure analysis procedure. Then the finite element analysis was done to determine the static stress distribution on the damper spring tower. Later the strain gauges were mounted on the critical location to record the strain gauge signals during the service conditions. The data available from the strain gauges and the strain-life approach was used to predict the fatigue life of the component and compared with the failure records. The estimated life calculated from the damper spring tower with broken damper spring test was found to be in good agreement with the failure records. Thus the research showed that the failure of the damper spring tower was due to the early failure of the spring damper and finally, the study recommended further test to improve the spring damper [17].

Palma & Santos, (2002) conducted a fatigue damage analysis of an automobile stabilizer bar. In this research fatigue damage was calculated using a “linear damage rule” with the data obtained from experimental test performed in the laboratory and the actual service environment. The results were also verified by analytical method. Finite element analysis was used to identify the critical stress locations on the stabilizer bar to mount the strain gauges. The comparison of the results of the stress analysis from all the methods used in this study showed that the magnitude of the stress distribution was similar. Finally the fatigue damage and life of the stabilizer bar was calculated for extreme field conditions and a fatigue failure criterion was set for laboratory testing conditions [18].

3 FEA: CAD AND FINITE ELEMENT MODELING

3.1 Introduction

The Finite Element Analysis (FEA) or Finite Element Method (FEM) is a numerical technique, which could give near accurate solutions to complex field problems. Basically this method involves dividing the complex structures into known number of smaller structures or elements. This ability of the method is called discretization or meshing, which makes the technique more effective in analyzing irregular shaped structures in a variety verity of engineering problems [19]. Mathematically it is nothing but representing most of physical problems in terms of mathematical models formed by differential and integral equations. Complexities such as irregular shape of the object or boundary conditions involved in the physical problems can make these equations almost impossible to solve directly. In this situation finite element analysis technique is adopted to obtain near accurate solution for the physical problem by approximately solving the governing equations, which could not be solved otherwise [20].

The traditional product development process is based on fundamental engineering equations and effective in analyzing regular shaped simple problems. However for complex physical problems the design process is more dependent on extensive testing, which normally makes the process expensive. The modern product development process with FEA technology does not eliminate the product testing process, but its ability to analyze complex physical problem easily and effectively can reduce the initial prototype testing in the design stages of the product development process [1]. This makes FEA technology valuable in today's competitive industrial environment. Therefore in this research the solution is sought for a structural problem, originally designed by the traditional method. The following section

discusses how the FEA technology is adopted in the product development process of the trailer, which is originally designed by the traditional product development process.

3.2 Overview of the FEA Process

The outline of the finite element analysis procedure used in this research is shown in Figure 3-1. The complete process could be categorized into two main objectives; Firstly, the design analysis stage and secondly, the design revision stage. The design analysis stage can be seen as two loops, first, an inner loop and second, an outer loop. The inner loop is responsible for achieving desirable accuracy of the finite element model and outer loop is responsible for achieving good quality model for the analysis. Therefore these two loops collectively contribute to the accuracy of the final solution. [20] The verification step in the design analysis decides which loop the analysis will get into. This decision is mainly based on factors such as maximum stress, visual inspection of the discretized model and quality of the element used for finite element modeling. In the first stage of the FEA process, it is necessary to analyze the existing or initial design in order to determine the causes of the problem, which could indicate the right direction to achieve better design against failure and provide solution to the problem. This is because the revised design strategy solely depends on the results of the initial assessment of the current design. The initial analysis of the trailer involves understanding the physical problem, constructing the CAD model of the trailer, finite element modeling of the CAD model, and, stress analysis of the trailer model using ANSYS software. These topics are explained in their own sections and outcome of the stress analysis dictated the design improvement, which is discussed later in chapter 6, in context with the stress analysis results obtained for the trailer. But for now the first stages of the FEA analysis is explained in detail in the following sections.

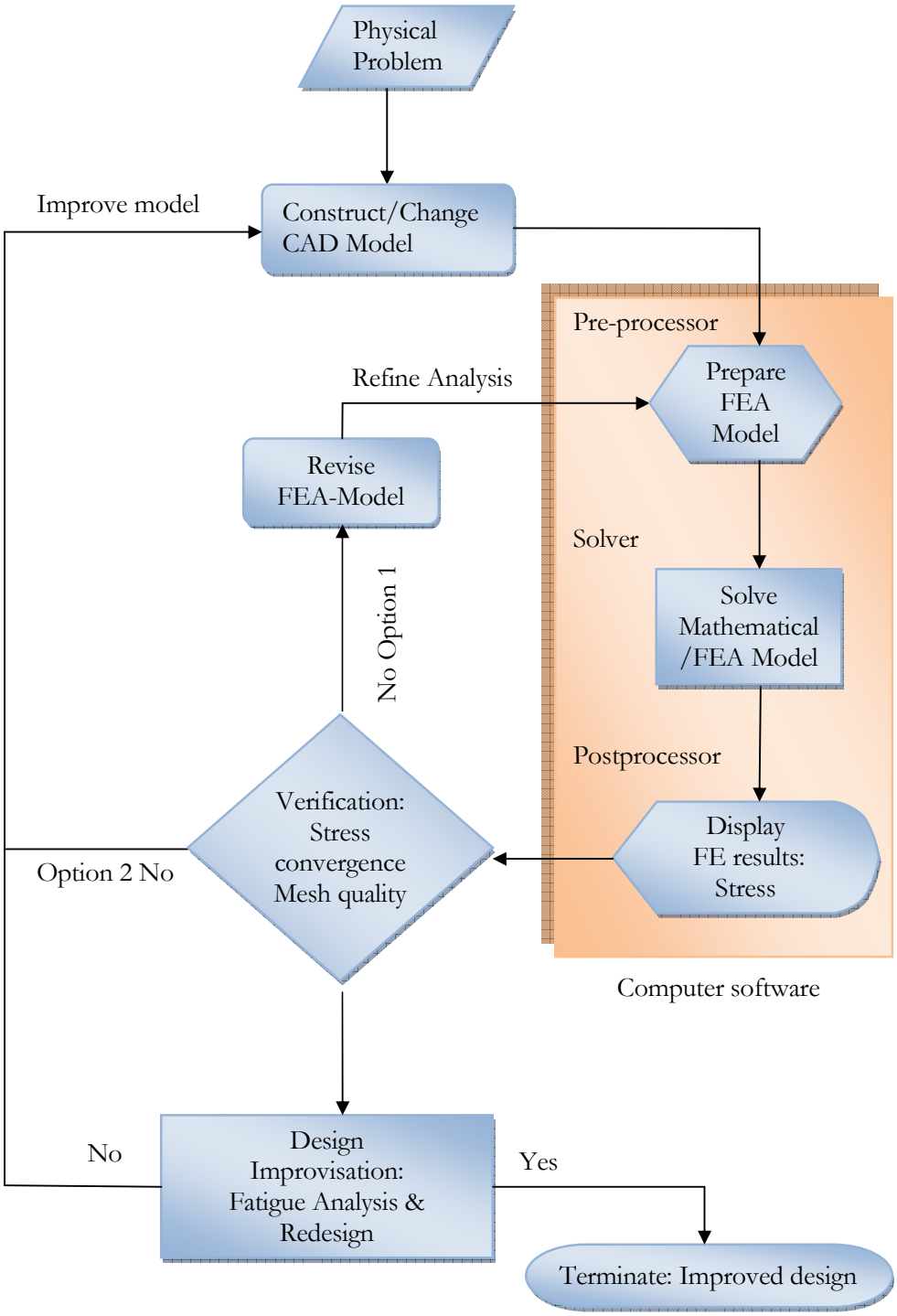

Figure 3-1: Overview of the FEA process [20] [21]

3.3 Building the Model in the CAD system for FEA

The seamless integration of FEA into the current product development process of the company can only be achieved if CAD and FEA activities are co-linear. In a company like STEELBRO, where design engineer and design analyst are a single role, there is a good opportunity to build CAD geometry best suited for FEA modelling, which could be used in the production line after the successful completion of the analysis. The ideal conditions for using the CAD model for FEA and all downstream applications with minimum effort is achieved if CAD modeling is done with either 3D solids or surfaces to form to complete volumes. The volumes created in this way can be meshed with tetrahedral 3D elements or brick elements discussed later in this chapter or should be capable of providing mid-surface extraction to create finite element model using shell elements [1]. This concept of utilising same model for CAD and FEA is further explored to determine its suitability for the company's general purpose finite element analysis requirement and for trailer analysis as well.

3.3.1 Physical Model of the trailer

The SB330 trailer chassis is a completely welded large structure as shown in Figure 3-2. It is made up of A709M Grade 345w structural steel. The mechanical properties of the steel are given in the Table 3-1. I-section beams called mainframes are the main structural members of the trailer. These mainframes are connected together at various locations using structural members such as plates, rectangular hollow sections and C-sections. The suspension is welded at the rear of the chassis.

Modulus of Elasticity (E) MPa	Poisson Ratio (ν)- typical value for steel	Yield Stress (σ_y) MPa
186200	0.29	353

Table 3-1: showing the mechanical properties of A709M Grade 345 W [29]

3.3.2 Modeling the Geometry

The aim of this section is to create an understanding of the necessity of building the solid model for FEA use. However, the same model should also be able to create production drawings with no or little effort. This could be achieved if the solid model is built with the consideration of the downstream applications, for example using proper parent-child relationship in feature building, which could be used to suppress features not necessary in FEA modelling. To satisfy finite element modelling needs of the solid model, a clean geometry is essential. Clean geometries can be built by building the solid models with features, which enhances the chances of quality FEA meshing without compromising the accuracy of the solid model. This can be achieved by modelling the features in such a way that the solid model does not challenge the meshing process, but allows the creation of quality elements and manipulating the solid model in such a way that it does not affect the structural integrity of the part, for instance by simplification of the part away from the area of interest [1].

The objective of building CAD model for FEA is to ensure a good quality mesh is produced in the finite element modelling of the solid model. The first step in this process is to identify the features that could potentially lead to a poor mesh. One of the very common solid modeling issues from the point of view of FEA use of the solid model is short edges and sliver surfaces, which were frequently encountered in this project's solid modelling. An example of such a problem is shown in Figure 3-3.

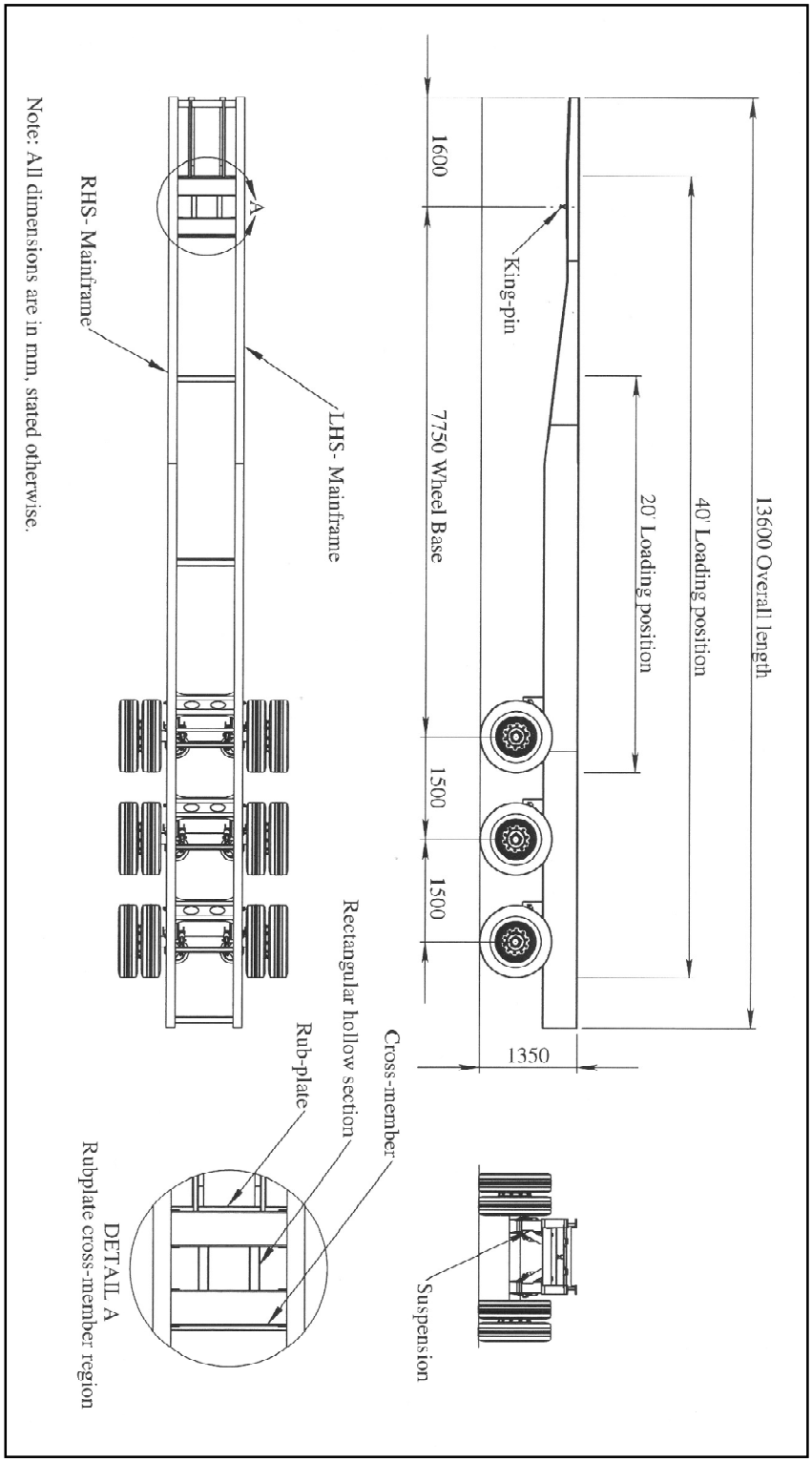

Figure 3-2: 2D drawing of the SB330 trailer showing the 20' and 40' container loading positions.

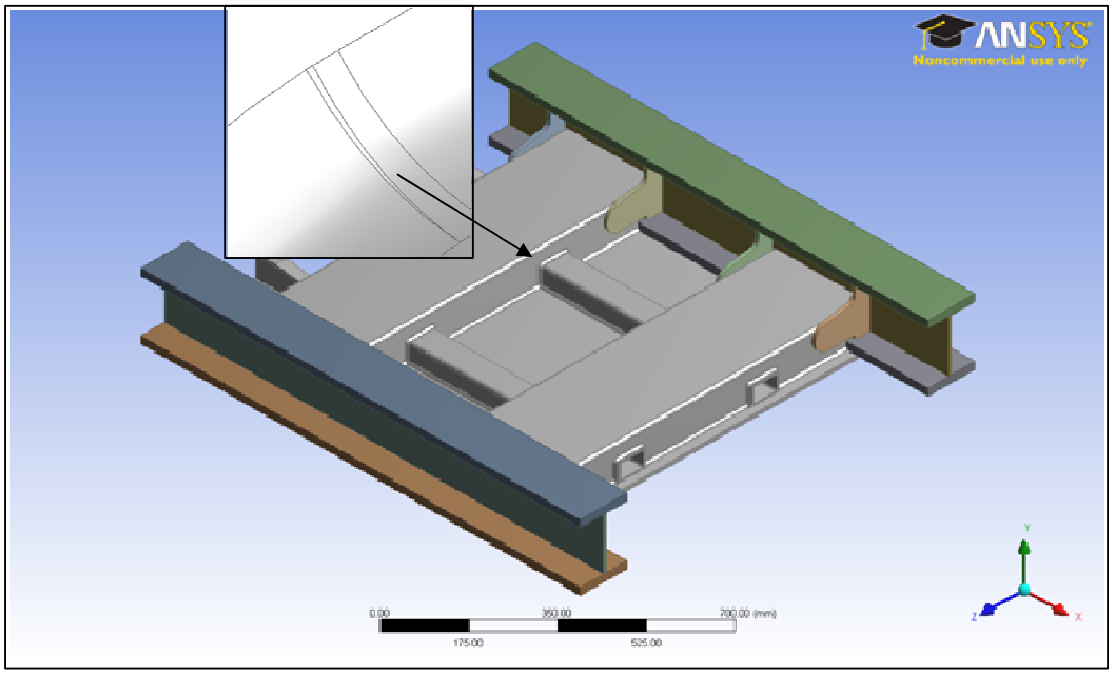

Figure 3-3: showing the potential sliver geometry in the filet feature of the weld-beed in the solid model.

Normally in CAD model filet edges close to the other edges of the geometry or misalignment of the features can create short edges. If such edges are smaller than the smallest edge of the model or nominal element size in a mesh, it could create element distortion, where one edge of the element is much shorter than the others. Similarly Sliver surfaces are narrow faces with very high aspect ratio. More often, automeshers create sliver surfaces by placing very flat element on short edges encountered in the geometry during meshing. Therefore, as a good modeling practice, the length of the edges in the solid model should be kept more than one-third of the desired element edge length of the finite element mesh [1].

3.3.3 Finalising the trailer geometry for FEA

Physical model of the whole trailer including suspension was modelled using SolidWorks modelling software. The assembly modelling was done such a way that the co-ordinate system of the physical model coincides with the co-ordinate system of the FEA model later in the simulation environment for the simplicity of the analysis. The suspension model was obtained from Hendrickson Asia Pacific Pty Ltd. The imported suspension model was converted from surface body to solid body with the intension of using it as a rigid body in the analysis. The primary objective of this research is to study and analyze the chassis of the trailer. The suspension being the third party component for STEELBRO, it is not of great importance to the company. However, in reality, suspension does play an important role in the load distribution along the length of the chassis. Therefore considering the geometric importance of the suspension in relation with the chassis, the suspension is modeled as a single component. Parent-child relations are suitably managed to create parts for the chassis considering the future needs of the FEA modeling, where parts or features of the component that could be insignificant for the finite element analysis can be easily suppressed. The chassis is modeled as an assembly of various structural members. The entire SolidWorks assembly is saved as a parasolid file, which can be imported into the Ansys Design Modeler software. This is done due to an ANSYS license restriction to import SolidWorks files directly into Design Modeler environment. Design Modeler was used to prepare the solid model for the analysis due to its greater ability to simplify and prepare CAD model for further analysis in the ANSYS simulation, e.g. “Inprint” faces, which allows applying point load on a surface. “Inprint” faces are created on the chassis at the 20’ and 40’ container mounting positions. Finalized geometry of the trailer which is used for the analysis is shown in Figure 3-4.

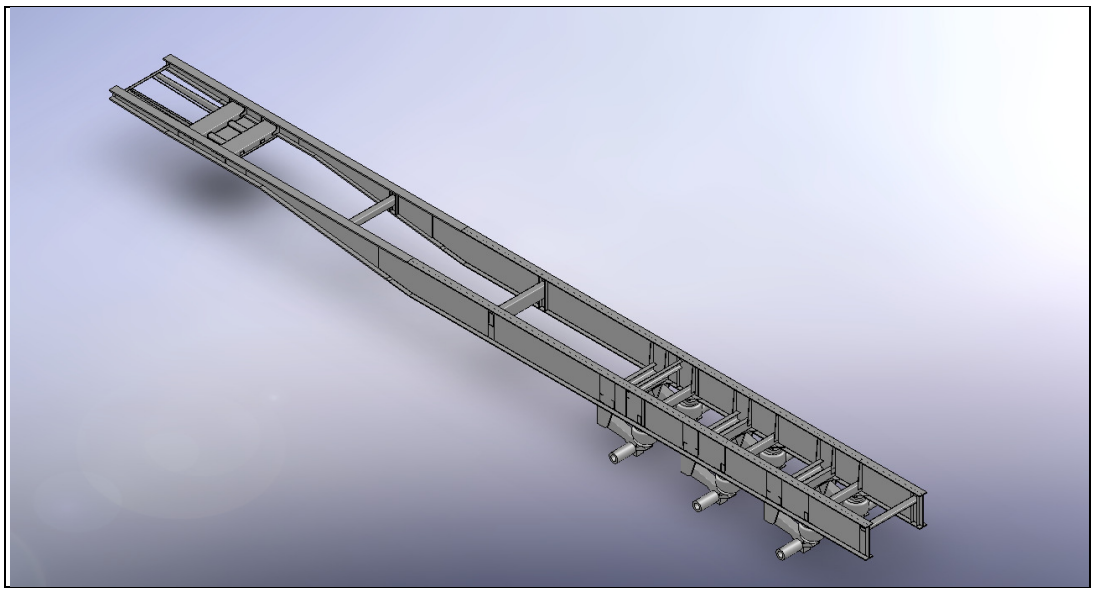

Figure 3-4: Showing the Final geometry for the FEA

3.4 Modelling with Finite Elements

The accuracy of the solution of the physical problem depends on the finite element modelling of the problem and accuracy of the finite element model depends on how well it represents the physical behaviour of the problem, which is largely dependent on the quality and quantity of the elements used to build the finite element model. If care is not taken, the model can be too inaccurate or can waste valuable computer resources and time during the analysis. As the whole modeling process is numerical approximation using polynomial interpolation at elemental nodes [21][22], it is necessary to understand the capabilities and limitation of the finite element method in order to ensure the proper finite element modelling techniques are employed to achieve the desired results.

The following illustrative example obtained from the text book of 'ANSYS Workbench Software Tutorial' [23] is used to demonstrate the effect of proper finite element modelling technique in combination with proper element type on the accuracy of the results, which is

compared with the analytical solution calculated for the problem. It also serves as a basis for the more complex analysis performed on the trailer chassis in the following chapter.

3.4.1 Analytical approach

The physical object shown in the Figure 3-5 is a bar with shoulder fillet, loaded as a cantilevered beam. Three faces at left side of the flat bar are fixed; Left, top and bottom face. The free end of the part on the right face carries a bending load acting vertically downward can be seen in Figure 3-5. The shape of the geometry shown in the figure can be assumed as a cut off part from the rectangular plate. In this case, the total load carried by the original rectangular plate cross section will now be loaded on to the remaining cross section of the plate. Therefore the uniformly distributed stress over the original area of the plate now will be concentrated at the change of cross section of the part. [24] Hence it can be predicted that the stress concentration will occur at the fillet region of the part, where the fillet meets the rectangular section of the unsupported part of the flat bar. The maximum stress at this location can be calculated from elasticity theory using stress concentration factor (k_t) and the equation (3.1). Stress concentration factor (k_t) can be obtained from the graph shown in Figure 3-6 [23]. The graph is plotted based on theoretical elastic, homogeneous and isotropic material considering only the shape of the part.

$$\sigma_{max} = k_t \times \sigma_{nom} \quad (3\text{-}1)$$

Where,

$$\sigma_{nom} = \frac{M \times c}{I} \quad (3\text{-}2)$$

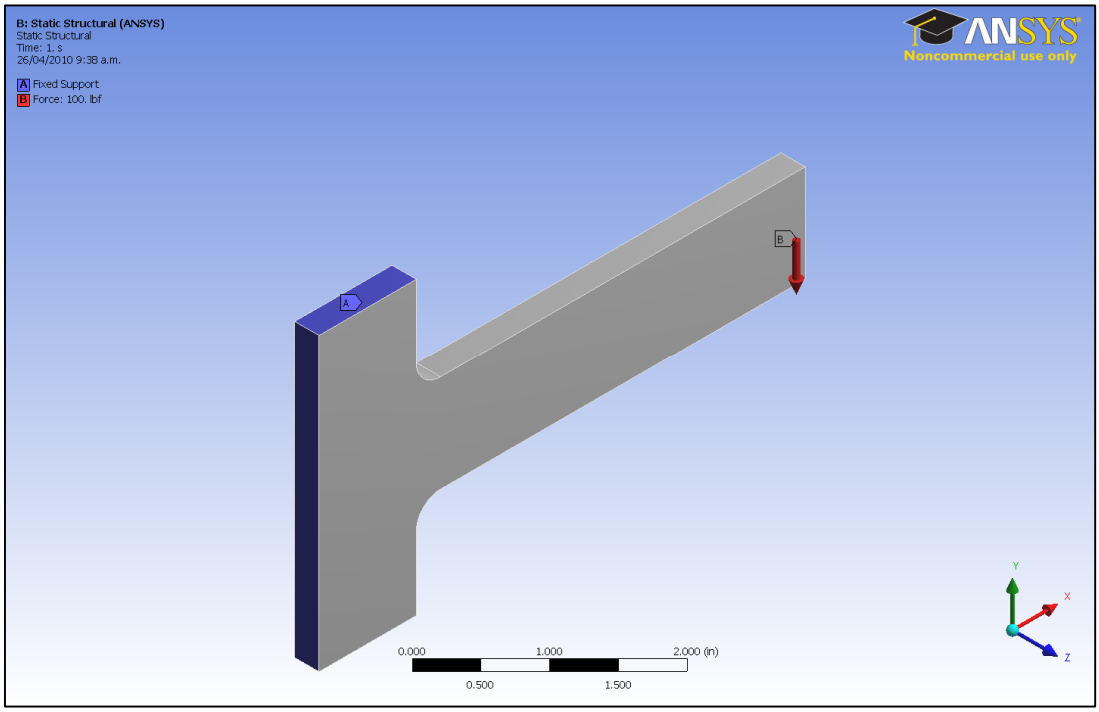

Figure 3-5: Flat bar with shoulder fillet loaded as cantilevered beam [23].

M is the moment at the point where maximum stress will occur.

$$M = F \times L \tag{3-3}$$

C is the perpendicular distance from the neutral axis to the layer of maximum stress and *I,* is the area moment of inertia.

$$I = \frac{B \times H^3}{12} \tag{3-4}$$

The curve is selected based on the geometric parameters (H/h) of the part as shown in figure below and the stress concentration factor (k_t) is determined for r/h of the geometry. Then the stress concentration factor is multiplied with the nominal stress to obtain the maximum

stress at the stress concentration. The maximum stress value obtained form the analytical calculation is tabulated later in the Table 3-2.

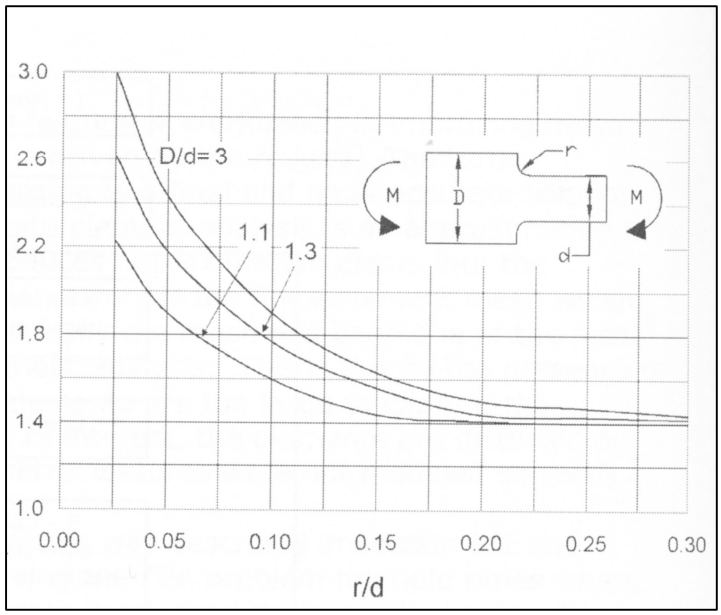

Figure 3-6: Graph showing stress concentration factor with respect to shape of the geometry [23]

3.4.2 Finite element approach

Analytical method itself may be sufficient for this type of simple problem. However, more complex finite element method for solving this problem has been developed for the following reasons:

- Developing generalised finite analysis method for the company utilising ANSYS Workbench capabilities.
- Verifying the accuracy of the approach using the analytical results.
- Finally, to develop guideline for more complex analysis performed on the trailer chassis.

3.4.2.1 Automeshing solid model using ANSYS workbench

Meshing is the process of dividing the solids or surfaces into discrete elements. It can be either done manually or automatically. In case of manual discretization, the model will be built by specifying the coordinates of each nodes and connecting the nodes to form the elements, which will eventually acquire the shape of the object being discretized. This process can be tedious and laborious and may not be feasible for very complex parts. On the other hand, ANSYS workbench automeshing algorithm extracts the geometric information from the CAD model submitted for the analysis and uses the default setting based on the analysis type to produces the mesh. [23] This mesh can be altered after the initial assessment of the discretized model. The quality of the finite element model produced by automeshing is governed by three factors. Namely, quality of the CAD model, mesh refinement at the transition between the features, and the meshing algorithm's ability to reform badly shaped elements. Although the last one is not user controlled, the first two factors greatly influence the third factor and in turn the accuracy of the result [1]. Building the proper geometry for FEA use is already discussed in the previous section and the following sections deals with the second factor. This includes element type and modelling procedure using ANSYS meshing algorithm to obtain accurate solution.

Generally, idealisation of a geometric shape and physical behaviour of a problem influences the finite element modelling of the problem with proper element type such as line, area, or volume elements. Therefore, the elements could be broadly classified as line, area, and volume elements as shown in Figure 3-7. These are elements in one-dimension (1D), two-dimension (2D), and three-dimension (3D) space respectively. [19] Typically, 1D elements are used to simulate beam or bar like geometries.

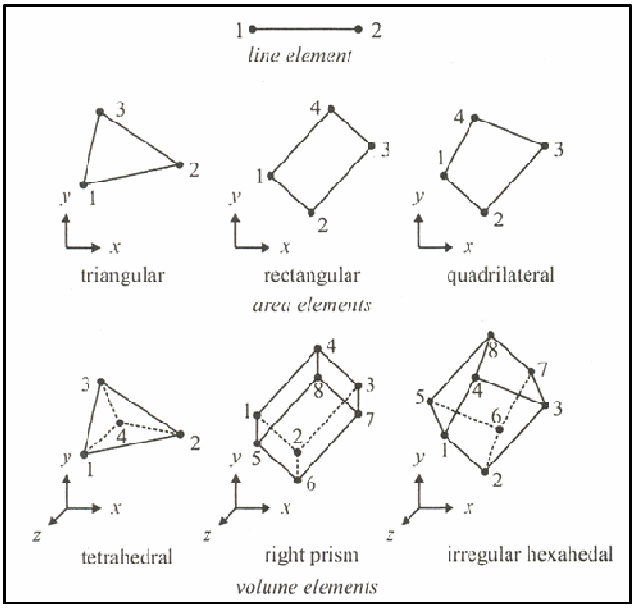

Figure 3-7: showing the common type of elements used in FEA. [19]

The shell can be categorised as area element with a small thickness with respect to its area and normally ideal for plate like geometries. For objects with symmetrical geometries, the shell elements can be effectively utilised at a cost of mid-surface creation for the parts. This process can be laborious and tedious for complex parts even with symmetry. This was realised when an effort was made to create the surface geometry for the semi-trailer chassis. The next obvious choice is 3D elements, which appear suitable for the company's general purposes and short product development cycle. Solid elements suit the company's interest of using the CAD model with little or no preparation for the analysis. Even though solid elements are more resource intensive, it is possible to make the process less resource intensive and achieve good quality results with special modelling technique like the sub-modeling technique used in this project.

ANSYS Workbench pre-processor algorithm can default select solid elements depending on the model to be analysed and provides options to select suitable elements. In order to analyse

the plate problem both default as well as user selection settings were used in the analysis. Tetrahedron and hexahedron solid elements are considered for the analysis and the result of the analysis is compared with the analytical solution obtained in the previous section. An overview of different solid elements and its suitability for the analysis is discussed in the following sections.

Constant strain Tetrahedron: The 4-node tetrahedron element is shown in Figure 3-8. Each corner of the element has a node with three displacement degrees of freedom in X, Y, and Z direction. In total, it has 12 displacement degrees of freedom for an element. The element is a first order element and computes only a constant strain over span of the element. Therefore, the element may be suitable where the strain is nearly constant for the length of the element. The element is also inaccurate in modelling physical problem involving bending and torsion, if the axis of such forces passing through or close to the element [21]. Therefore, it may not be a good choice to use this element in the plate analysis as bending is involved.

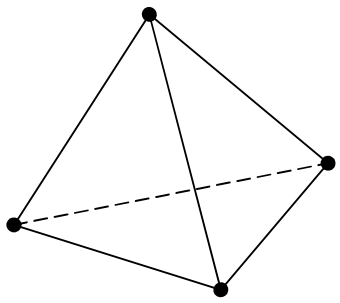

Figure 3-8: 3D 4-node tetrahedron element

Linear strain tetrahedron: Linear strain 10-node tetrahedron is shown in Figure 3-9 below. ANSYS identifies the element as SOLID187 and describes as 3D 10-node tetrahedral structural solid element. The element has three displacement degrees of freedom at each

node in x, y, and z direction. In total, it has 30 degrees of freedom for 10 nodes of an element. It's a higher order element with quadratic displacement behaviour, capable of meshing irregular shapes modelled from CAD systems. The element is also capable of being used in a situation of plasticity, creep, stress stiffening, large deflection, and large strain capabilities [26]. In addition, the ability to compute linear strain along the length of the element enables it to model the bending situation more accurately [21]. Therefore this element may be used for the analysis of the plate problem, where bending is involved.

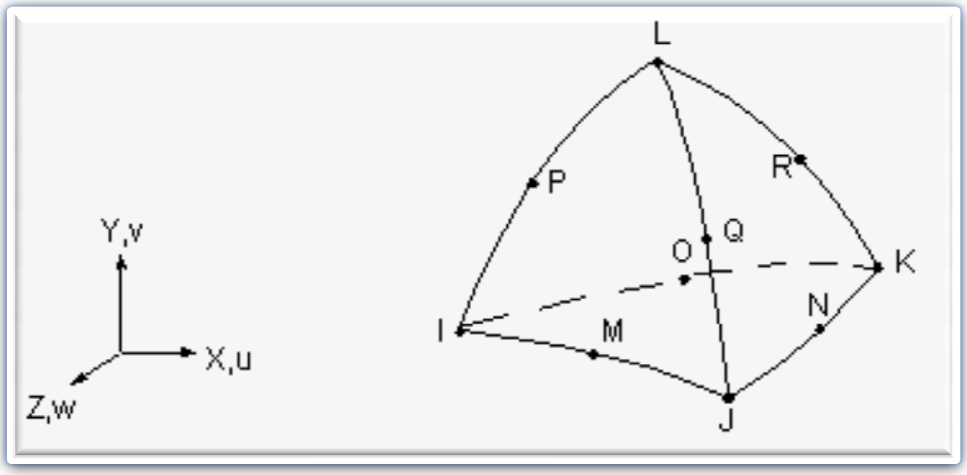

Figure 3-9: 3D 10-node tetrahedron element [26]

Trilinear Hexahedron: This element is popularly known as 8-node brick element as shown in Figure 3-10. In ANSYS, the element is identified as SOLID185 and described as 3-D 8-node structural solid. The element has three translation degrees of freedom at each node in X, Y, and Z direction. In total the element has 24 translation degrees of freedom [26]. The translation formulation of the element is missing few quadratic modes due to which, the edges of the element remains straight during deformation and undergoes shear locking in bending. Therefore, the element is unable to represent beam behaviour very well [21]. The remedy for shear locking may be possible but seems unnecessary when higher order

hexahedron element is available. In ANSYS, it is possible to use the element as tri-linear tetrahedron with 6-node wedge element, by collapsing two of its edges.

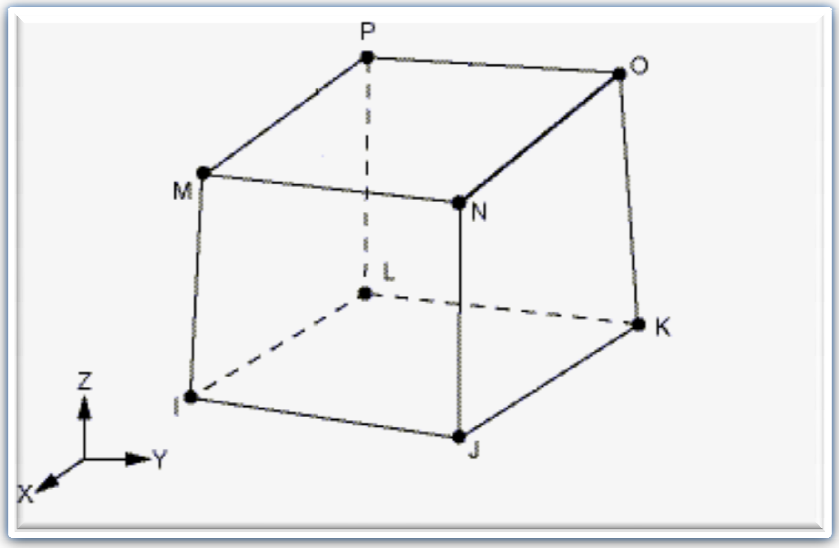

Figure 3-10: 3D 8-node hexahedron element [26]

Quadratic Hexahedron: this element is shown in Figure 3-11. It is identified as SOLID186 and described as 3D 20-node structural solid in ANSYS workbench product. It is a higher order element with quadratic displacement behaviour. As shown in the above figure, it has a node at every corner of the element and a mid-side node on the every edge of the element. It has three translation degrees of freedom at every node making up total 48 degrees of freedom for the element. The mid-side node of the element could be used to form straight or curved edges. When the element is rectangular, it is able to compute linear strain field more correctly for the length of the element. Similar to linear strain tetrahedron, it is capable of supporting plasticity, large deflection, large strain, etc and it is well suitable for modeling solid models produced form CAD packages. [26] The element can be modified to 15-node wedge element and 13-node pyramid element, when hex-dominant mesh is selected for the analysis in ANSYS workbench.

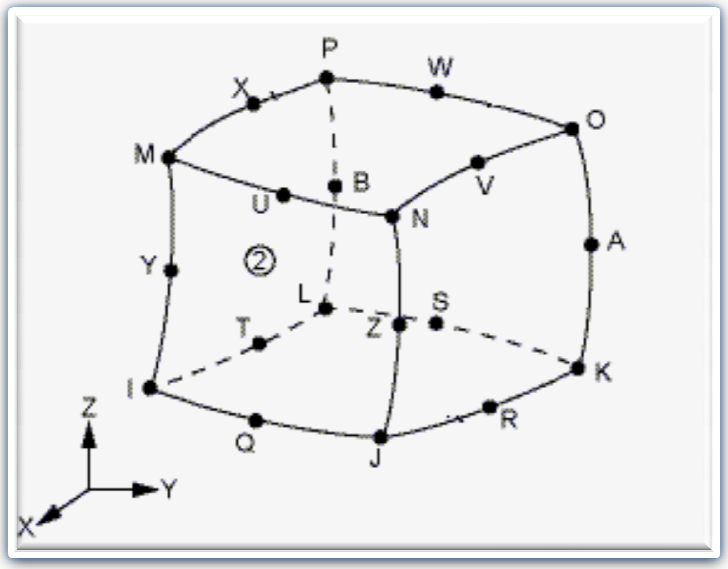

Figure 3-11: 3D 20-node hexahedron solid element [26]

From the above discussion of the solid elements available in ANSYS workbench, it is seen that the use of higher order elements such as linear strain tetrahedron and quadratic hexahedron may improve result quality and therefore, these elements selected for further analysis. Figure 3-12 shows the 20-node hexahedron mesh produced by ANSYS Workbench default setting and Figure 3-13 shows the 10-node tetrahedron mesh produced by changing the user element setting to tetrahedron respectively.

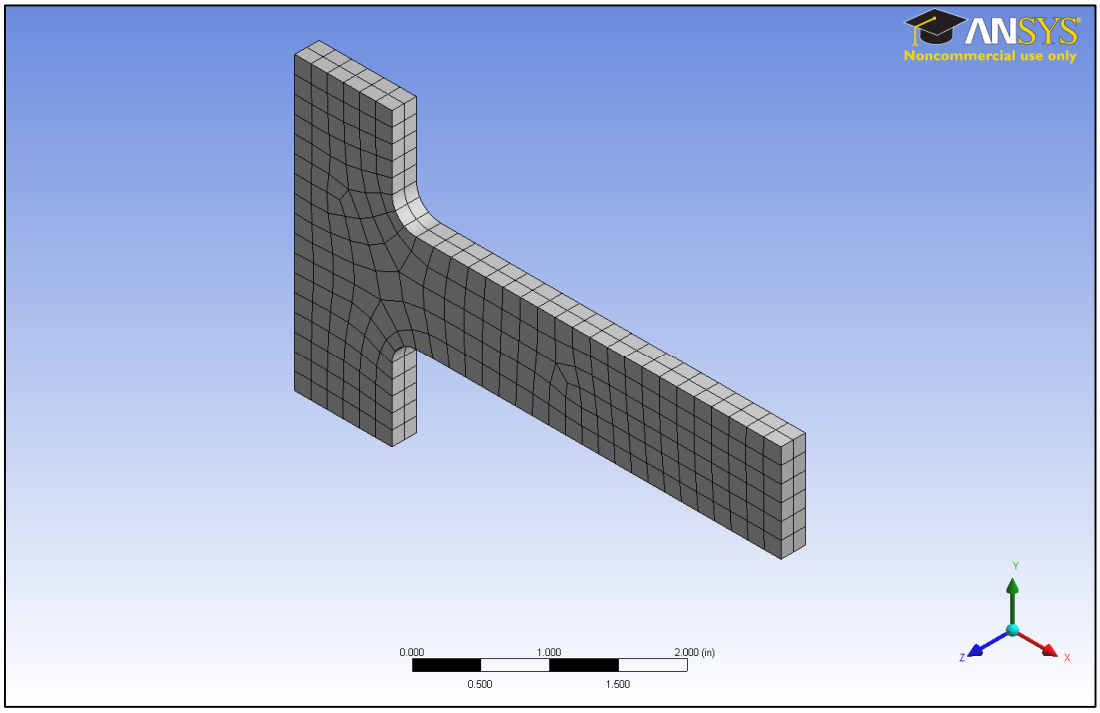

Figure 3-12: showing the plate meshed with 20-node hexahedron elements

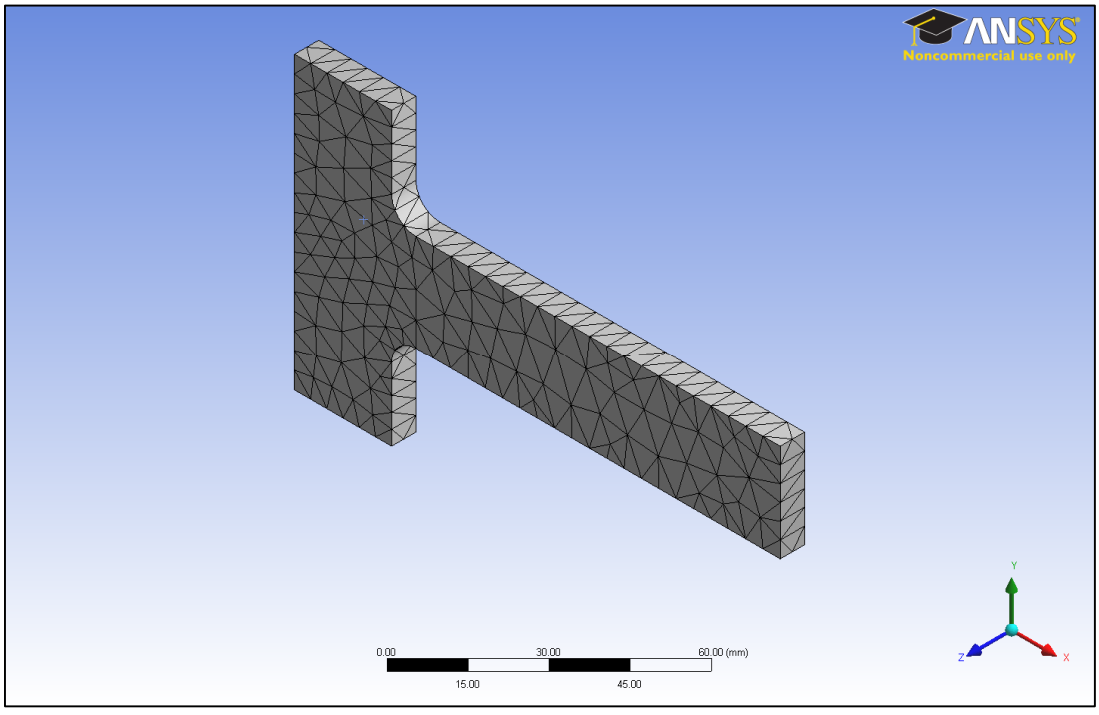

Figure 3-13: showing the part meshed with 10-node tetrahedron elements

	FEA Results (MPa)	*Analytical Result (MPa)*	*% deference*	*No of elements*	*Computation time (s)*
σ_{max} Initial mesh	82.06	92.46	0.12	448	4
σ_{max} Convergence	93.85		0.0149	37041	13
σ_{max} Sub-modeling	93.69		0.013	32942	25
Direct refinement	93.81		0.0144	32844	24

Table 3-2: Analysis results for 20-node hexahedron elements

	FEA Results (MPa)	*Analytical Result (MPa)*	*% deference*	*No of elements*	*Computation time (s)*
σ_{max} Initial mesh	78.12	92.46	0.168	1084	3
σ_{max} Convergence	93.24		0.0084	31682	10
σ_{max} Sub-modeling	93.18		0.0077	7334	5
Direct refinement	93.48		0.0109	36957	10

Table 3-3: Analysis results for 10-node tetrahedron elements

Results obtained for the initial mesh for both the, hexahedral and tetrahedral elements is tabulated in Table 3-2 & 3-3 respectively. The results for the initial mesh show a large difference from the analytical result. This is because the initial mesh is very coarse and does not accurately represent the geometry and mechanics of the plate. This indicates that mesh refinement is required to accurately represent the physical model. This can be achieved by reducing the size of the element, which will increase the number of elements in the mathematical model as the size and number of elements are inversely related in a model. Generally this course of action leads to the increase in mathematical accuracy of the model [22]. The mesh refinement is achieved by three following methods; namely, manual mesh refinement, adaptive mesh refinement technique and sub-modeling in combination with adaptive mesh refinement.

Manual Mesh refinement: The convergence of the result is the basic goal in all three methods of mesh refinement. ANSYS Workbench can produce reasonable sized mesh to start with, which in this instance calculated a result that seems to be far away from the analytical result. The mesh may then be further refined using element size control in ANSYS until the result of the two final analyses is nearly the same. Figure 3-14 and Figure 3-15 shows the final mesh produced by this method using 20-node hexahedron and 10-node tetrahedron respectively. By observing these figures, it is clear that the mesh is a result of reduction in nominal size of the element across the entire geometry, resulting in a very large number of elements. This can be avoided by the use of local mesh refinement, which targets mesh refinement areas of rapid change in stresses. However, it seems to be unnecessary for the example problem of this size. Automatic stress convergence of local regions can be easily achieved in ANSYS through the use of Adaptive Mesh refinement.

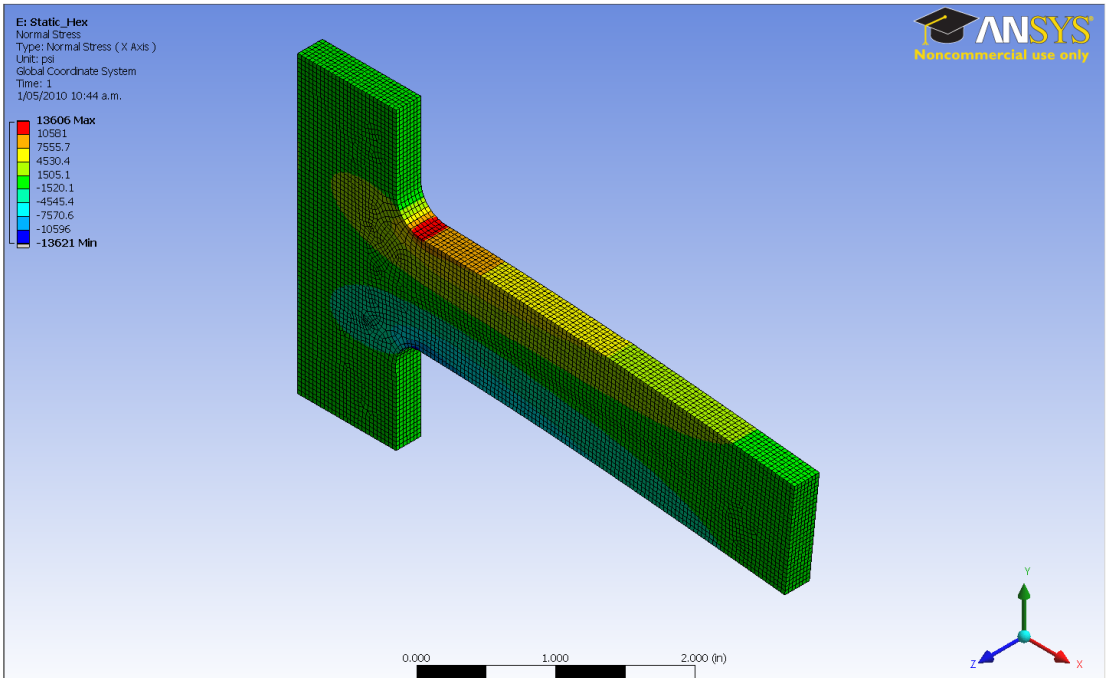

Figure 3-14: Final mesh with 20-node hexahedron element by manual refinement

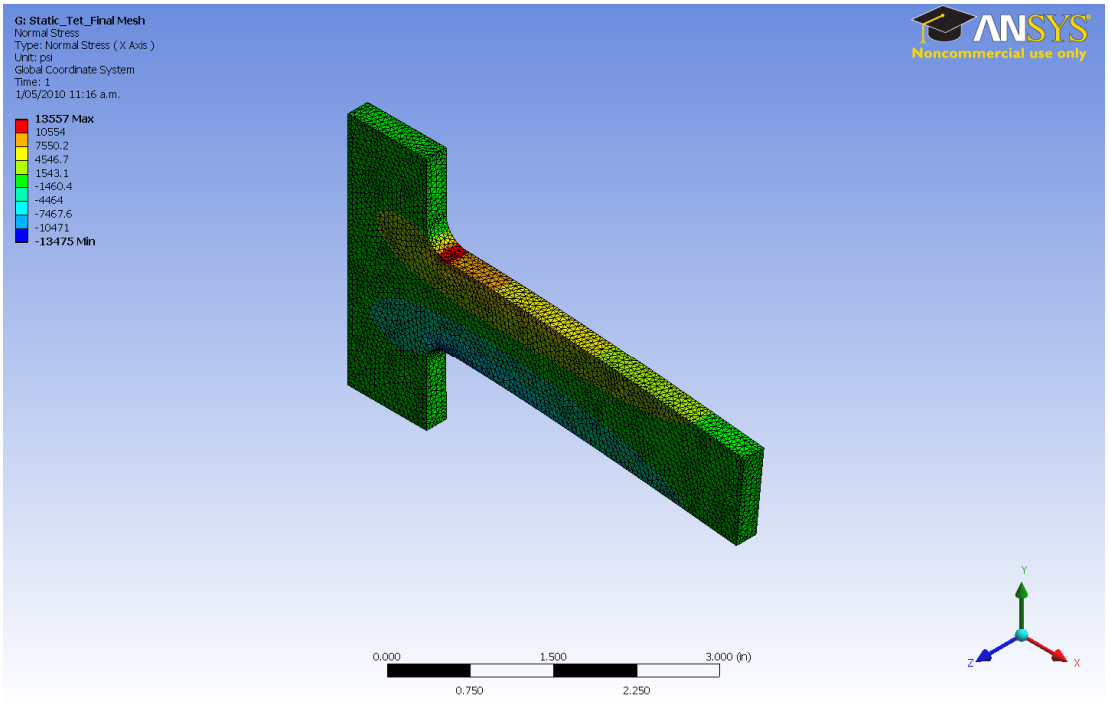

Figure 3-15: Final mesh of the plate for 10-node hexahedron element by manual

Adaptive mesh refinement: The Workbench meshing algorithm can perform mesh refinement in such a way that the refinement takes place in regions where rapid change in stress is occurring. This means that additional elements are added only where the FE model needs to be improved. The refinement in the region of high stress gradient can be observed in Figure 3-16. As this process is entirely automatic in ANSYS Workbench, it was observed that even though the initial mesh refinement was started with hexahedron 20-node elements the final mesh is turned out to be of 10-node tetrahedron elements. This indicates that, according the ANSYS Workbench meshing algorithm, tetrahedron elements can also be used effectively for shaping small intricate details.

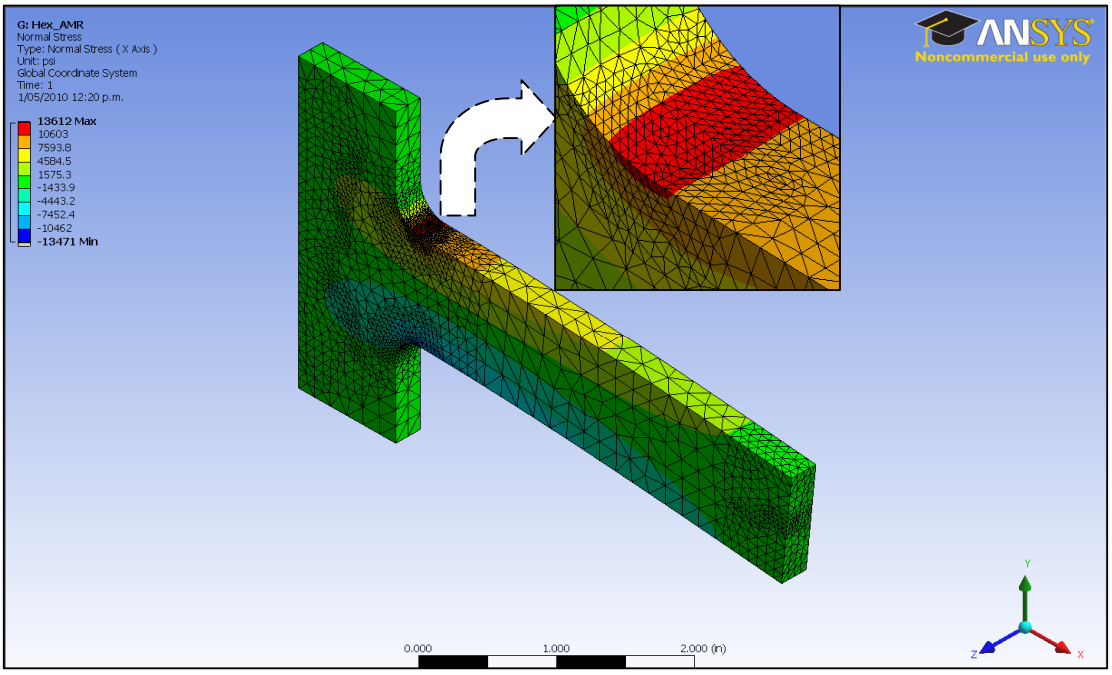

Figure 3-16: showing the fine mesh refinement only at the high stress gradient

Sub-modeling: Sub-modeling is based on St. Venant's principal, which states that:

> "If an actual distribution of forces is replaced by a statically equivalent system, the distribution of stress and strain is altered only near the region of load application". [27]

According to this statement, stress concentration is a localised effect, which indicates that accurate solution could be calculated for the area of interest, if the cut boundaries of the area of interest covering the local stress are far away from the stress concentration. [27]

At this stage of the plate analysis, it is clear that the mesh density is extremely important; Very coarse mesh can contain serious errors and finer mesh can require intensive computer resources which make solution time relatively long. If the initial mesh reveals patches of high stress gradient or any particular region of interest in a large structure, the sub-modelling technique may be used to analyse the area of interest with very fine mesh. This technique

significantly reduces the degrees of freedom by facilitating smaller, localised model to be used in the analysis [22].

The sub-modelling technique is demonstrated using the example problem as shown in the Figure 3-17. Sub-modelling is carried out in two stages. First, the whole structure is modelled with reasonably fine mesh and analysed as usual. Second, the result of this mesh analysis is applied to the sub-model, which is the area of interest cut-off from the larger structure as shown in the figure below. The first stage of the analysis determines the displacements for the complete model, which are then applied as boundary conditions to the sub-model which is finely meshed to accurately determine the stresses. The result of the analysis using sub-modelling technique for the plate problem is tabulated in Tables 3-2 and 3-3.

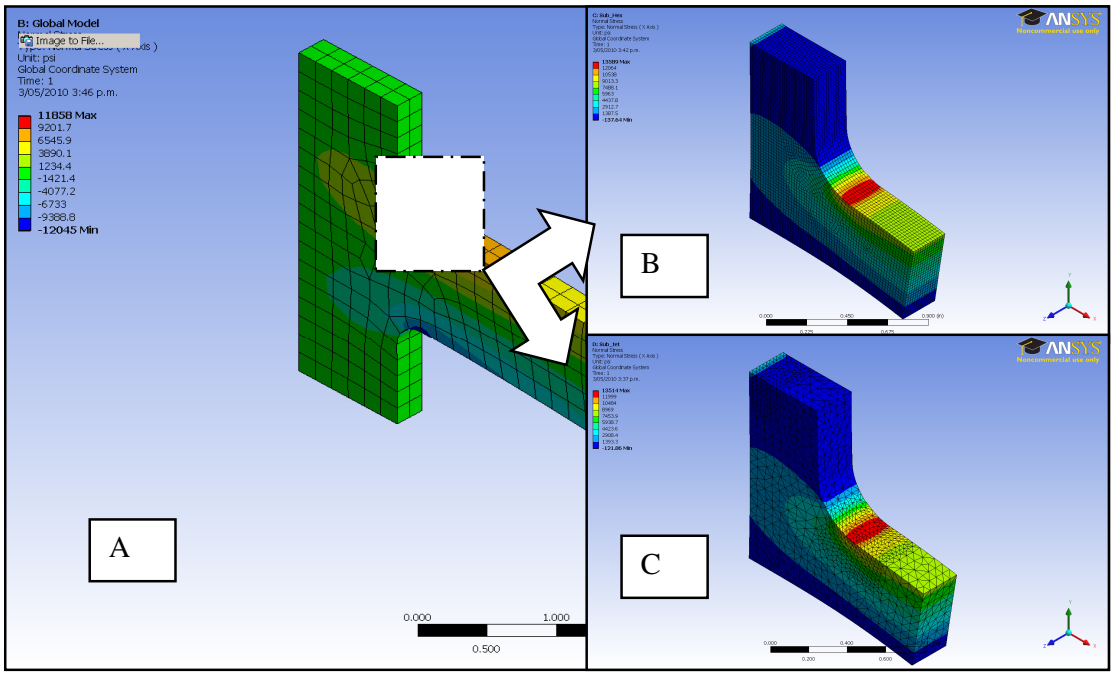

Figure 3-17: (A) Showing the global model with cut boundary region (B) Sub-model with 20-node Hexahedron, and (C) Sub-model with 10-tetrahedron.

The sub-model is analysed using both hexahedron and tetrahedron elements and Figure 3-17 (B) and (C) show mesh refinement by manual and adaptive methods, respectively. From the

result of the analysis, it is observed that accurate results were obtained with minimum number of elements using adaptive mesh refinement and sub-modeling methods.

In the example problem, it is possible to compare the result of the FEA analysis to the analytical result. However, for complex geometries like the STEELBRO trailer, it is not feasible to calculate the analytical result to compare with the FEA result. In this case, element shape checking could be used as a tool to ensure the accuracy of the geometry of the physical part to be within the acceptable limit. Otherwise it could be primary source of error in discretization and could lead to inaccurate result. As the result of the plate analysis is within an acceptable accuracy limit, this example problem is used to create a guideline for the shape checking of the elements for similar structural analysis. The various shape checking criteria in relation to the example problem are as follows:

- Aspect ratio
- Jacobian ratio
- Warping factor
- Maximum corner angle
- Skewness

Aspect ratio: In 3D solid elements, the aspect ratio is calculated using the corner nodes of the element, For triangular faced elements, a basic rectangle is constructed as shown in Figure 3-18 (i), connecting the apex of the triangle and the mid-points of the opposite edges. The process is repeated for the remaining apexes of the triangle. Then the aspect ratio of the face is calculated as the ratio of the longer side to the shorter side of the most distorted rectangle, divided by square root of 3. Similarly, in quadrilateral faced elements, the basic rectangles are constructed by joining the mid-points of quadrilateral edges and centring about the element. One of the rectangles constructed of the quadrilateral face is shown in Figure

3-18 (ii). Then the aspect ratio for the face is calculated by dividing the longest edge to the shortest edge of the most distorted rectangle. Likewise, the process is repeated for all the faces of the quadrilateral element and the most distorted value of the aspect ratio among all the faces of the element is considered the aspect ratio of the element. [26]

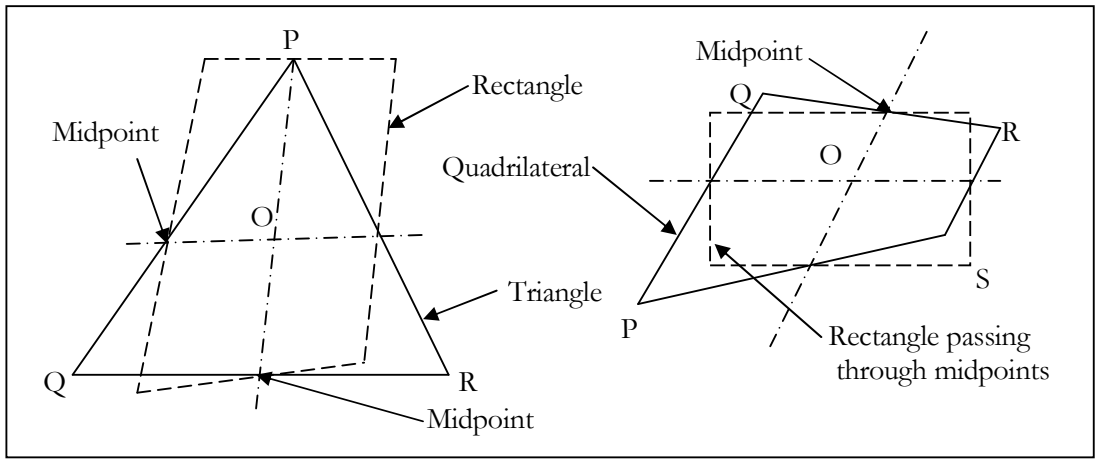

Figure 3-18: Aspect ratio calculation for (i) Triangle and (ii) Quadrilateral [26]

The ideal aspect ratio is 1 for a quadrilateral element and 1.15 for an equilateral triangle [22]. Large deviations from this will introduce some error into the calculations. The graph of aspect ratios obtained for the example problem is shown in Figure 3-19 and Figure 3-20 for hexahedral and tetrahedral elements respectively. In the graph of the hexahedral element, it is observed that the aspect ratio for the hexahedral mesh ranged from 1 to 3. However, 90% of the mesh has an aspect ratio close to 1. Similarly, the graph plotted for the tetrahedral mesh of the same plate, shown in Figure 3-20, revealed that the aspect ratio ranged from 1 to 8.24, with nearly 96% of the tetrahedral mesh is having an aspect ratio less than 3.

The percentage difference between the FEA result and the analytical result of the plate problem and above observations confirms that aspect ratio from 1 to 3 can produce good results and aspect ratios greater than 3 may be acceptable as long as it occurs away from the area of interest [22].

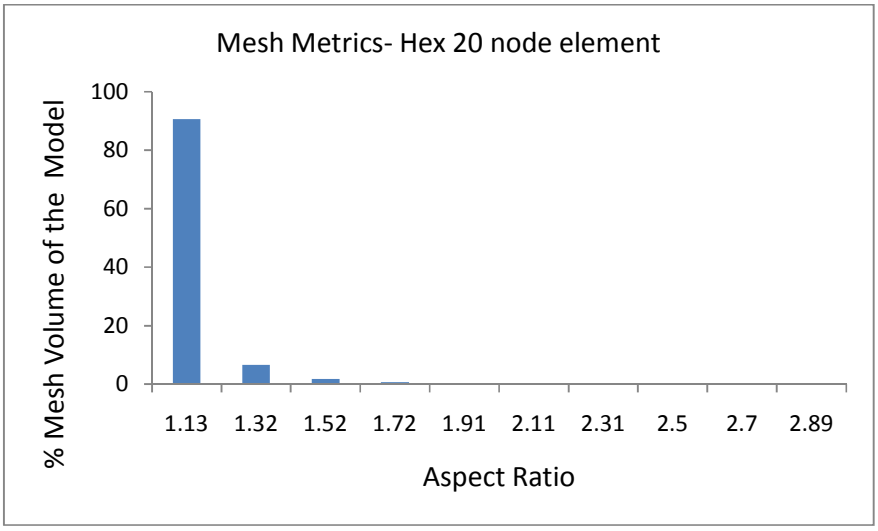

Figure 3-19: Graph showing the aspect ratio distribution for Hexahedra 20-node element

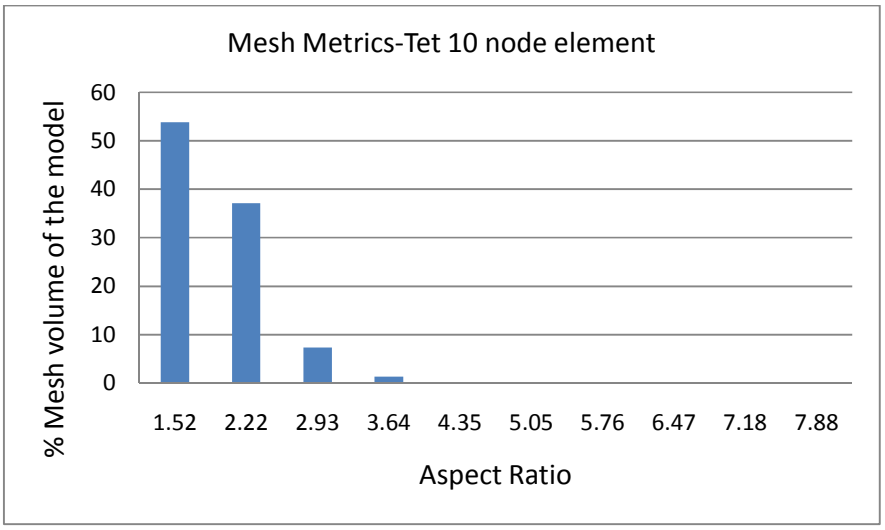

Figure 3-20: Graph showing the aspect ratio distribution for tetrahedra 10-node element

Maximum corner angle: The maximum corner angle check for 3D elements is also calculated in reference to its faces or cross-section in 3D space as the angel between the adjacent edges of the triangular or quadrilateral face or cross-section through the element. The ideal maximum corner angle (α) for triangular and quadrilateral faces is 60^{o} and 90^{o}, respectively. The Figure 3-21 shows triangular and quadrilateral faces with ideal maximum corner angle [26].

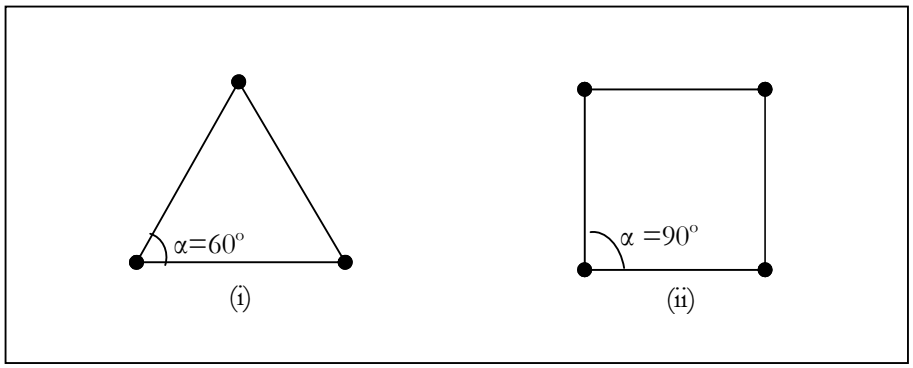

Figure 3-21 : Ideal maximum corner angle (i) triangle face (ii) Quadrilateral face

Mesh metrics obtained for maximum corner angle showed that for 20-node hexahedron elements the maximum corner angle ranged from 70^o to 132^o. Even though the range appears to be wider, 92% of the elements of the entire mesh is close to the ideal angle of 90^o. The remaining small volume of mesh, which has high deviation from the ideal angle, may have contributed some approximation error. However, the FEA analysis of the plate has produced acceptable quality of result, which is confirmed when compared to the analytical result. This indicates that the range of maximum corner angle for hexahedron may be acceptable as long as high percentage of the mesh is close to the ideal angle of 90^o. In case of 10-node tetrahedral elements the maximum corner angle ranged from 75^o to 150^o. However, nearly 88% of the total volume was within 110^o. Again even though this angle appears is greater than the ideal angle for triangular face of 60^o, it had little effect on the accuracy of the result in the plate analysis, which indicates that this range of maximum corner angle for tetrahedral elements may be acceptable. The graphs of maximum corner angle for 20-node hexahedral and 10-node tetrahedral element mesh are shown in Figure 3-22 and Figure 3-23, respectively.

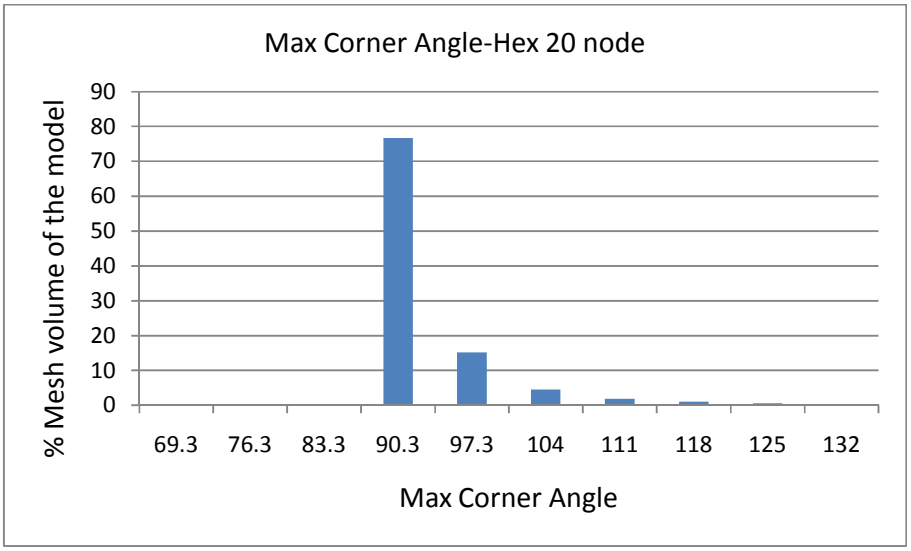

Figure 3-22: Graph showing the maximum corner angle distribution for Hex 20-node element

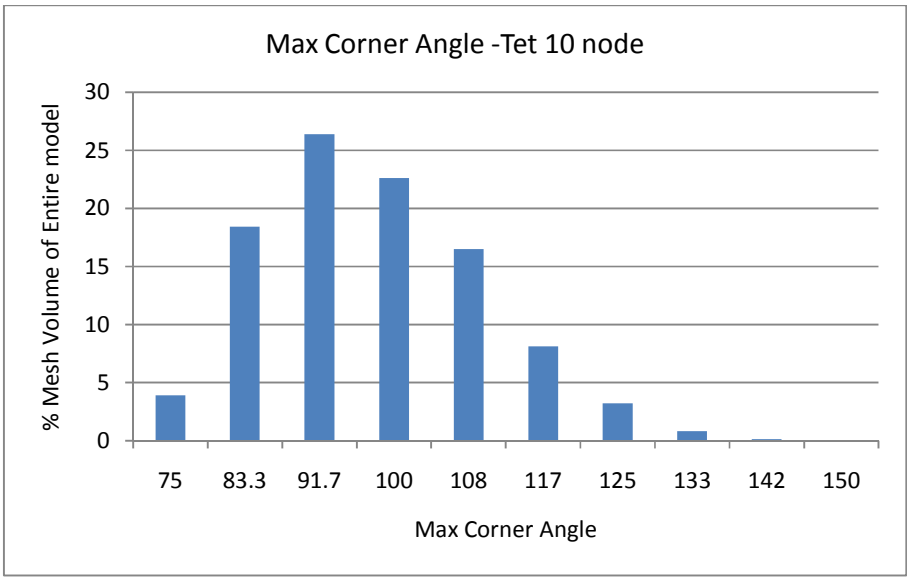

Figure 3-23: Graph showing the maximum corner angle distribution for Tetrahedra 10-node element

Skewness: Skewness is defined as the deviation of the triangular or quadrilateral face from the perfect equilateral and equiangular face respectively as shown in Figure 3-24 [28].

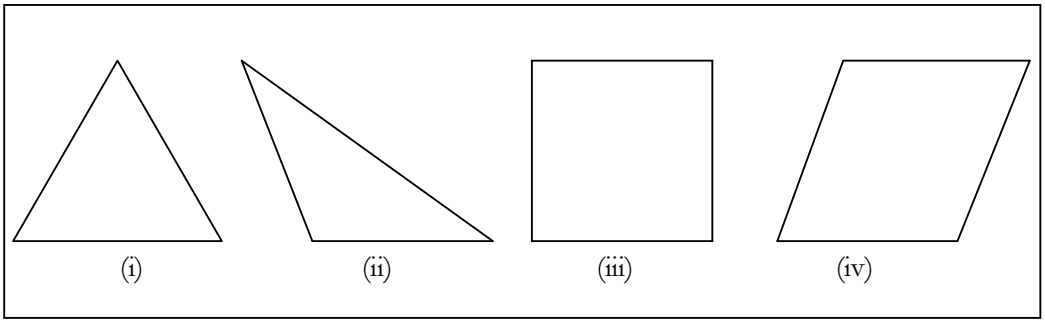

Figure 3-24: showing (i) Equilateral Triangle (ii) Skewed triangle (iii) Equiangular Quad, and (iv) Skewed quad [28]

ANSYS measures the skewness using following two methods [28]:

Equilateral volume based method:

$$Skewness = \frac{Optimal\ Cell - Cell\ Size}{Optimal\ Cell\ Size}$$

Where, the optimal cell size = size of an equilateral cell.

Normalised volume deviation method:

$$Skewness = max\left[\frac{\theta max - \theta e}{180 - \theta e}, \frac{\theta e - \theta min}{\theta e}\right]$$

Where, max , θmin , are the largest, smallest angle within the cell and θe is the angle for an equiangular face or cell.

According to the definition of skewness, the ANSYS calculates the value of 0 to be an equilateral cell and a value of 1 to be the worst possible cell. Therefore, the value of skewness ranged from 0 to 0.5 is considered to be good, a value from 0.5 to 0.75 is fair, and values beyond 0.75 should be avoided [28]. Skewness values obtained for the example problem using 20-node hexahedron and 10-node tetrahedron is shown in Figure 3-25 and Figure 3-26 respectively. The skewness observed in both meshes is within the guidelines explained above and the FEA results obtained for the example problem confirms that the skewness can be a good measure of mesh quality.

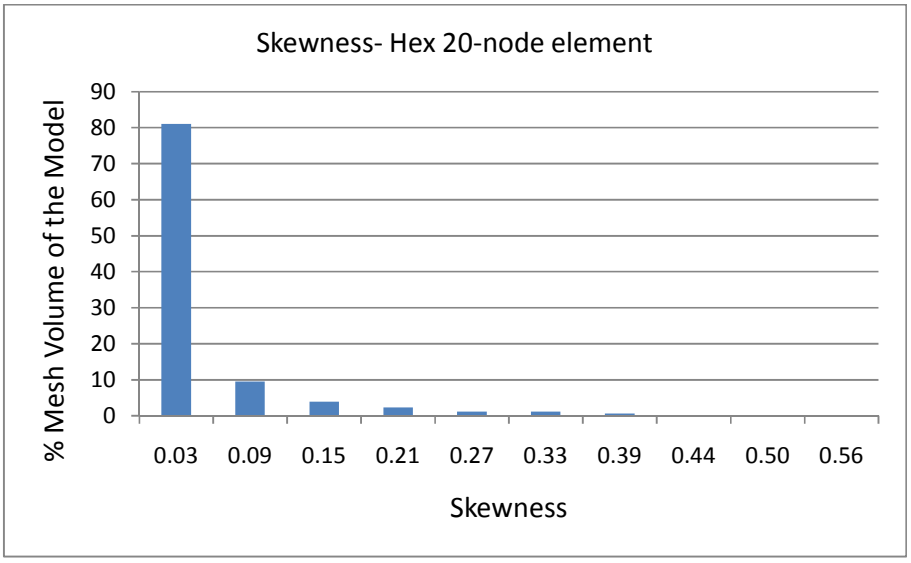

Figure 3-25: Graph showing the skewness distribution for Hexahedra 20-node element

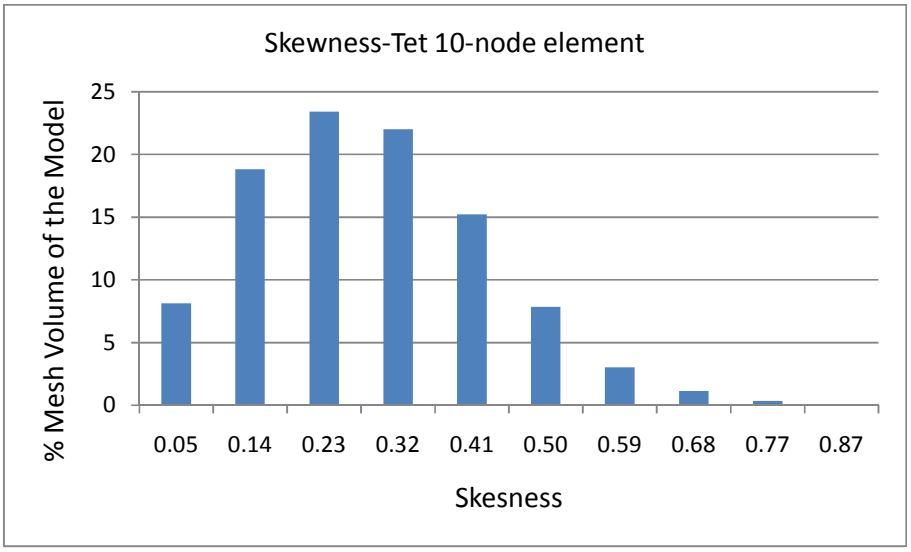

Figure 3-26: Graph showing the skewness distribution for Tetrahedra 10-node element

Warping factor: warping factor is only calculated for quadrilateral faces of the element. For 3D solid elements, as 4 nodes make up a face, the warping factor is calculated by dividing the edge height difference of the twisted or lifted face by its square root of area. The warping factor of 0 is a perfect shape of the element and a value beyond 1 is a poor shape. Figure

3-27 (i) & (ii) show a brick element with warping factor of 0 and approximately 0.2, respectively [28].

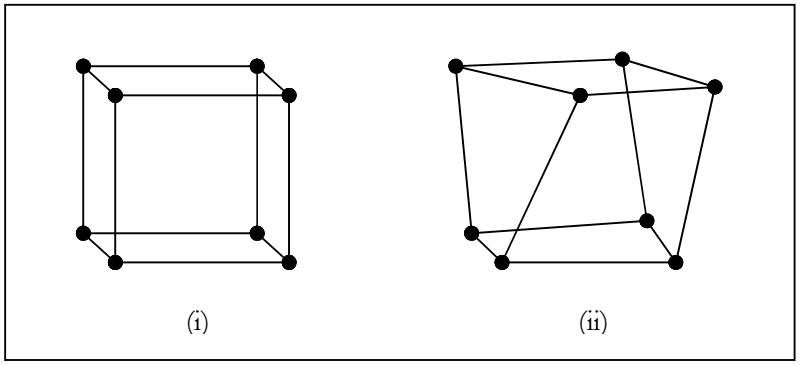

Figure 3-27: Showing brick element with warping factor (i) Zero (ii) approximately 0.2 [28]

The warping factor obtained for the example problem using 20-node hexahedron element indicates that nearly all of the elements are perfectly shaped in the mesh, as shown in Figure 3-28 below.

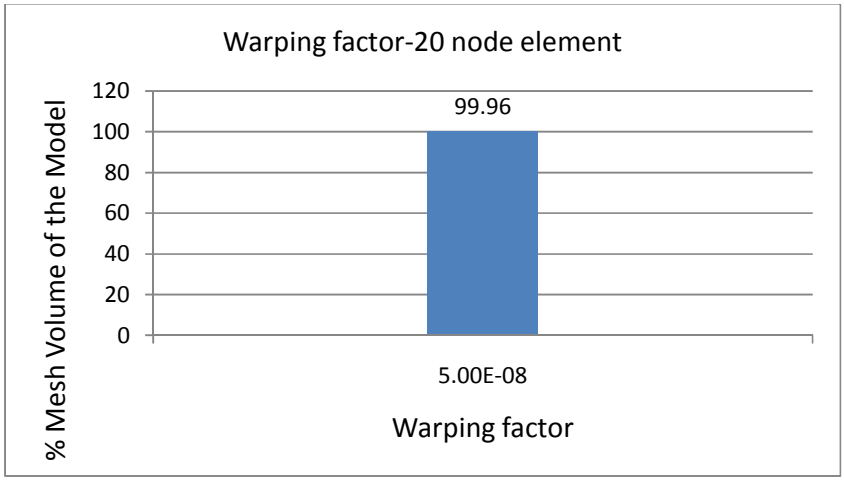

Figure 3-28: Graph showing warping factor for 20-node element mesh

Jacobian ratio: ANSYS calculates the determinant of the Jacobian matrix at integration points for 10-node tetrahedron and at all nodes and centroids for 20-node hexahedral elements. The Jacobian ratio is computed for the element by dividing the maximum and the minimum values of the Jacobian determinant for the element. Figure 3-29 shows the graph of

the Jacobian ratio obtained for the 10-node tetrahedron and 20-node hexahedron. Form the observation of the graphs; it is clear that the Jacobian ratio for both element types is close to unity, which is an indication of well-shaped elements [28].

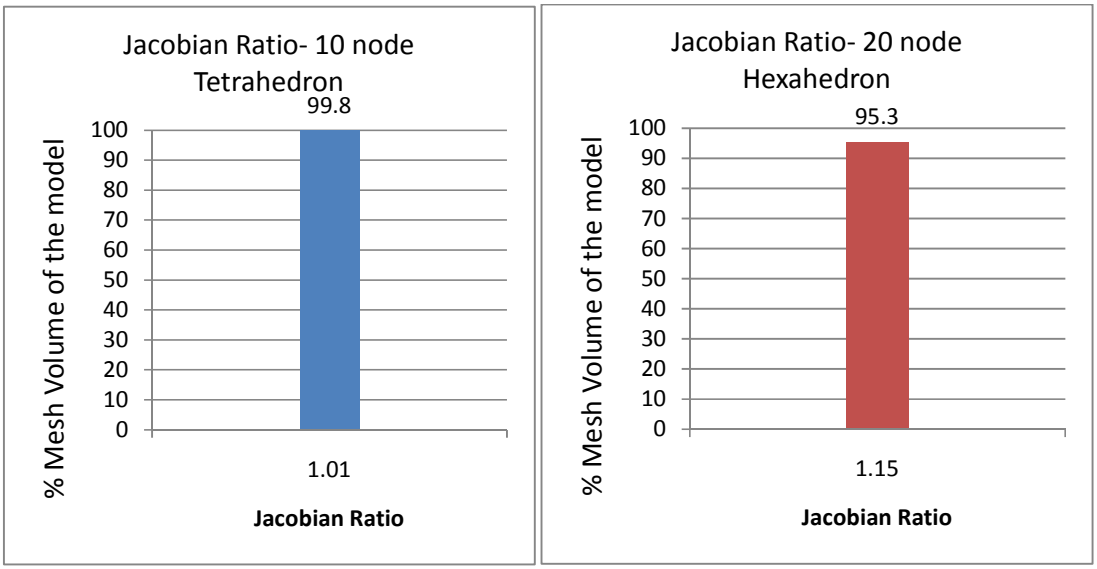

Figure 3-29: Graph showing the Jacobian ratio for the example problem for the element mesh

3.4.3 Discretization of the trailer solid model

The trailer solid model prepared according to the guidelines discussed in the CAD modeling section is discretized using the knowledge gained by the analysis of the example problem in the previous section. An initial mesh as shown in Figure 3-30 revealed that the model is very large and requires too many elements if direct automeshing is applied. To avoid this over discrimination, local meshing needed to be applied depending on the area of interest. The area of interest in this study is the crack region at the rub-plate cross member as explained in the Chapter 1. This area of interest is further discritised during the static analysis of the trailer and will be discussed in the following chapter. The meshed finite element model of the whole trailer chassis, which will be the "global model" in the finite element analysis, is shown in Figure 3-30.

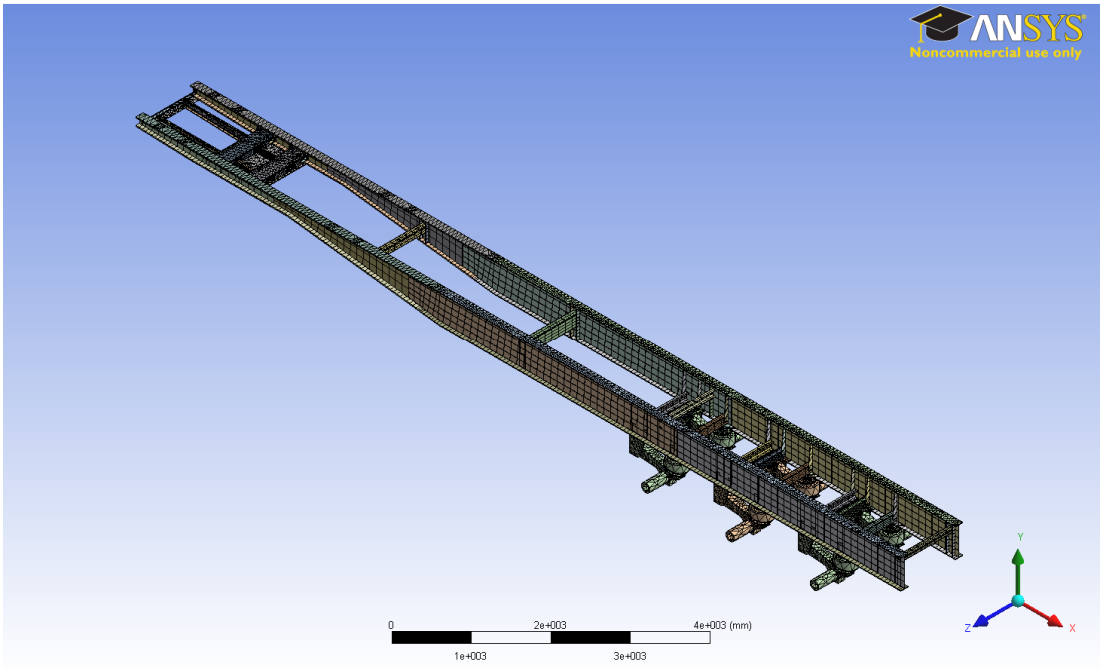

Figure 3-30: Initial mesh of the trailer solid model

4 FEA: STATIC STRUCTURAL ANALYSIS & RESULTS

4.1 Introduction

Generally, when designing mechanical structures, various analyses must be performed to determine the strength of the structure against possible loads acting on the system. Among these analyses, static analysis is the most common analysis performed on structures to determine it's strength against static loads acting on structure. This analysis is performed to ensure the response of the structure to the static loads are within acceptable limit, otherwise the structures would have little chance against other complex loads such as dynamic and/or cyclic loads. Therefore, static analysis could be considered as the first step in structural design analysis.

In this chapter, structural analysis is conducted on the trailer for two sets of static loading situations. This is carried out to determine the effect of the static loading at the location of the crack, as explained in the problem definition in the first chapter. The static structural analysis is carried out with FEA numerical techniques using ANSYS finite element analysis software. The systematic methodology for conducting the structural analysis of the trailer using ANSYS software is proposed in this chapter. The procedure adopted in the analysis is explained in the following sections.

4.2 Modes of operation of the trailer

The trailer model SB330 is designed for on-road container transport in New Zealand. It is understood that the main use of the trailer is for transporting containers between shipyards and warehouses in cities. The trailer typically carries 20' or 40' containers loaded within the permissible payload. The trailer is equipped with two set of cranes, which facilitates loading and unloading of containers. A typical trailer service would include loading the container at the shipyard, carrying it to point of delivery and unloading with the help of cranes mounted on the chassis or the reverse. Based on it's normal service conditions, the following loading conditions are considered for the analysis.

4.2.1 Normal loading/unloading condition

In this operating condition, the trailer is loaded with a 20'or 40' container. The containers are positioned at "optimum" loading positions on the chassis as shown in Figure 3-2. The container is placed on four docking points on the chassis and locked in its position by devices called twist-locks. It is assumed that the load from the container is transferred to the chassis at these four loading points. For this analysis, the maximum design load is applied on the chassis and equally divided among the four docking points of the container. As mentioned above, the cranes are also mounted on the chassis and the weight of the crane is also equally divided between four contact points where it rests on the mainframe of the chassis. The total load acting on the chassis is the weight of the container itself (in this case maximum design load) and the weight of the two cranes. These loads acting on the chassis form the force boundary condition on the chassis, as shown in Figures 4-1 & 4-2. The king-pin connection to the trailer allows free rotation around Y-axis and Z-axis as shown in Figure 4-1 & Figure 4-2. The displacement and the rotation along the rest of the axes are fixed. This

boundary condition is visualised based on the interaction between the kingpin and the truck rub-plate. The third set of boundary condition is considered to be the interaction between the suspension system and the ground. As the chassis only rests on the ground at these locations, this is considered to be a compression only support. This boundary condition restricts the movement of the system in the direction of the force, keeping rest of the movements free in the remaining directions. This boundary condition is suited to capture the interaction at the support points in the static loading condition. The boundary conditions for the 20' and 40' container loading condition are shown in the Figure 4-1 &Figure 4-2, respectively.

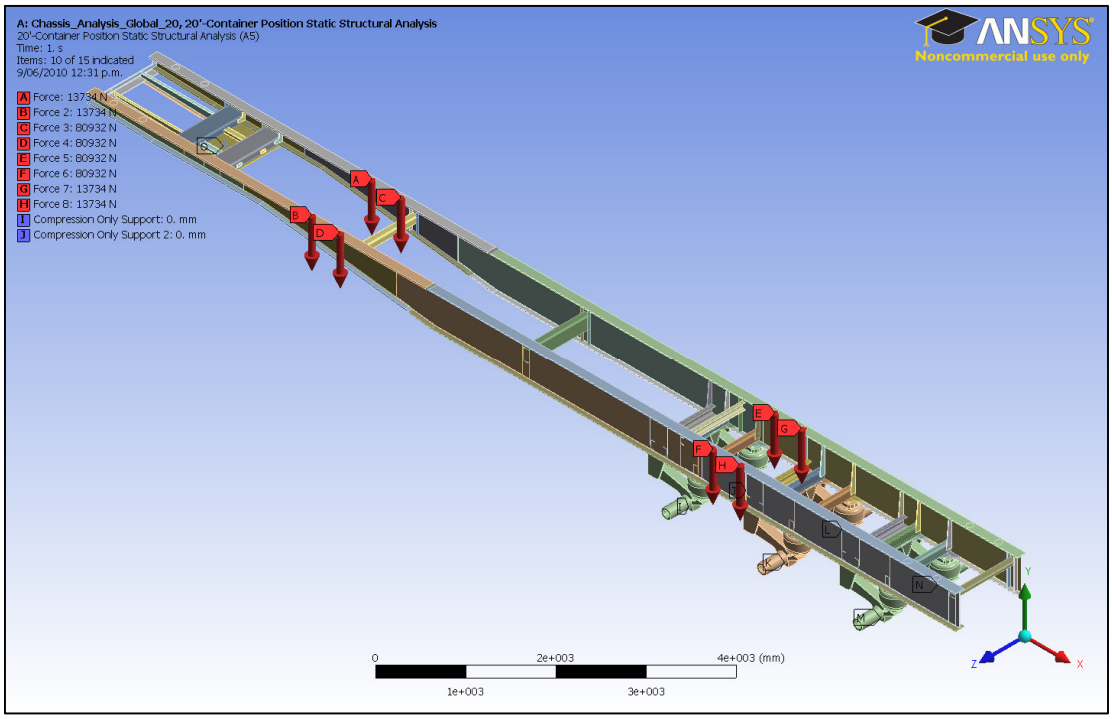

Figure 4-1: Showing the boundary conditions in 20' container normal loading condition.

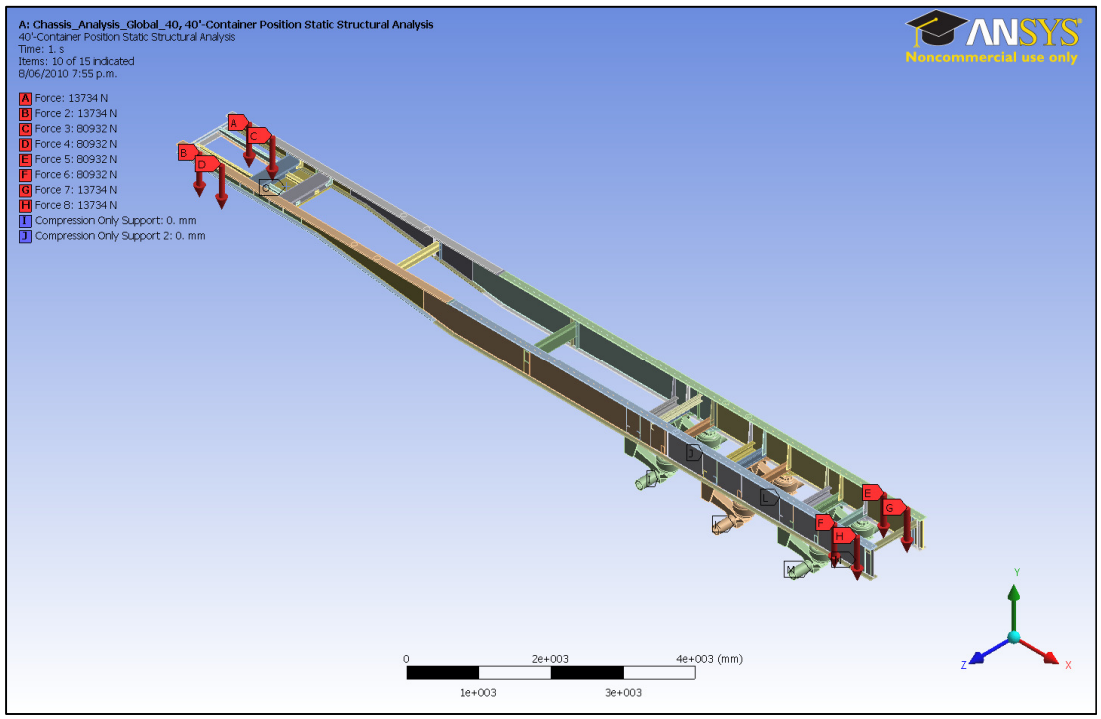

Figure 4-2 Showing the boundary conditions in 40' container normal loading condition.

4.2.2 "Worst case" service condition

One possible reason for the appearance of the cracks at the rub-plate cross-member region is the critical yard manoeuvres performed during service. In order to simulate the critical yard manoeuvres, a hypothetical "worst case" scenario was developed where the trailer is reversed into a shipyard gateway through the tightest possible corner. This condition is simulated for both 20' and 40' container positions. This process is idealised as a quasi-static case, where the trailer is being reversed at a very low speed. Meaning there is little or no effect from dynamic forces. The pictorial representation of this situation is shown in Figure 4-3. As shown the trailer pivots at the king-pin. The pushing or pulling force at the king-pin would produce turning moments at the wheels of the trailer, which could cause high stresses at the rub-plate region. This boundary condition is simulated by applying the calculated turning moment at the wheels and fixing the kingpin, as this would create a same effect of

applying the driving force at the kingpin. The boundary conditions representing the turning moment is shown in the Figure 4-4 and Figure 4-5 for 20' and 40' container positions, respectively. The turning moment is applied on the first set off suspension in the 20' loaded condition and on the third set off suspension in the 40' loaded condition. The assumption behind this action and theoretical calculations performed to obtain the turning moment is explained in the next section.

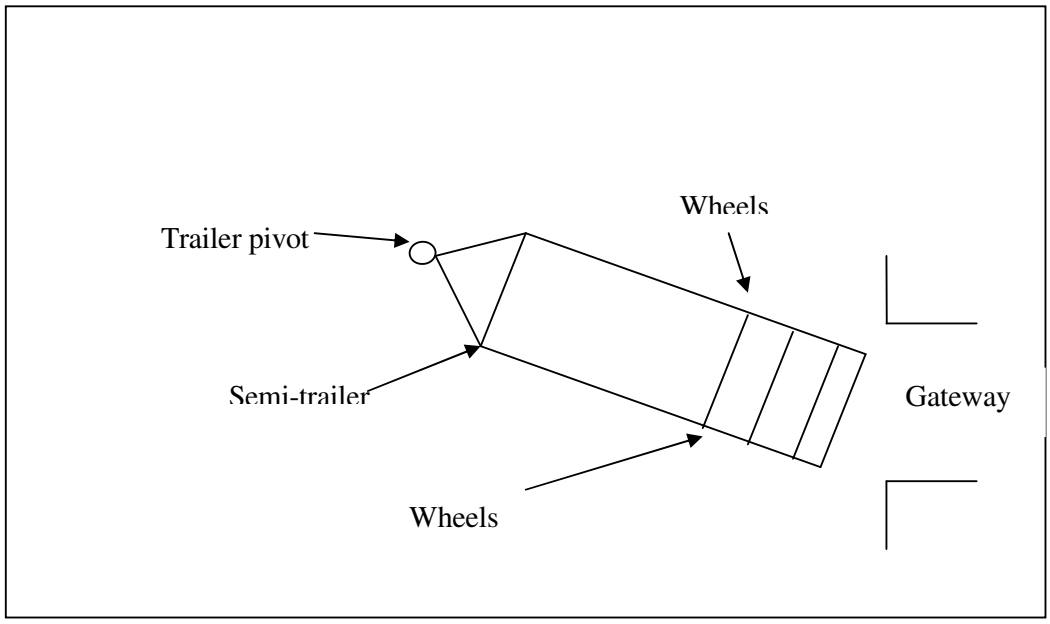

Figure 4-3: Top view of the trailer being reversed into a gateway showing the turning action at rear of the trailer

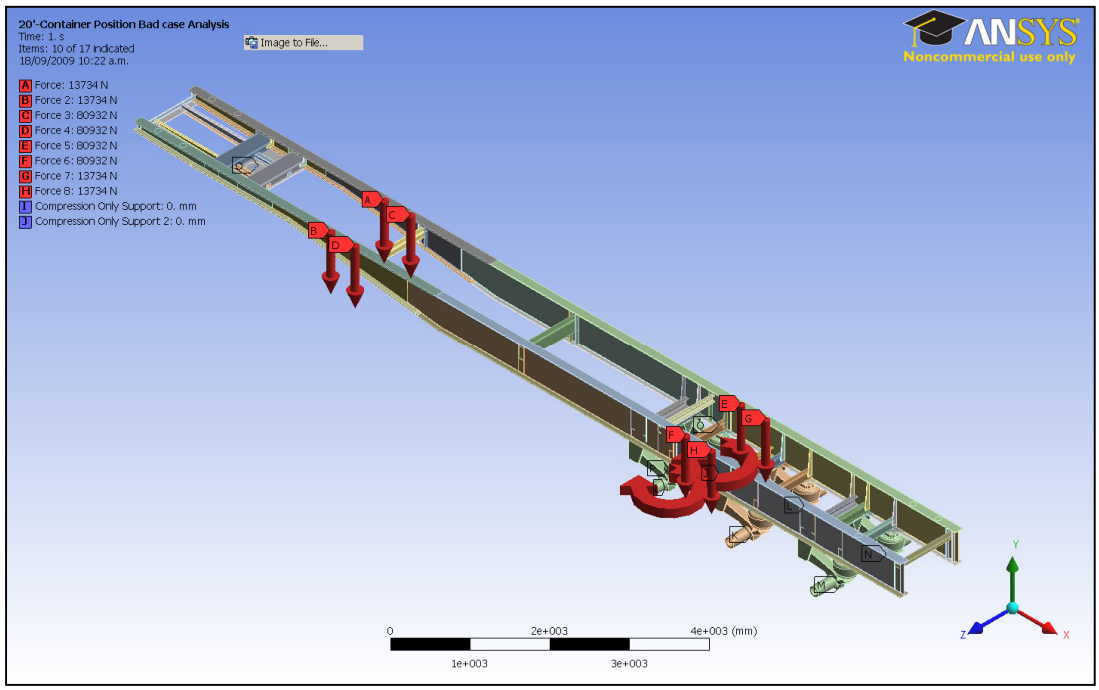

Figure 4-4: representing the boundary conditions for "worst case" analysis in 20' container position

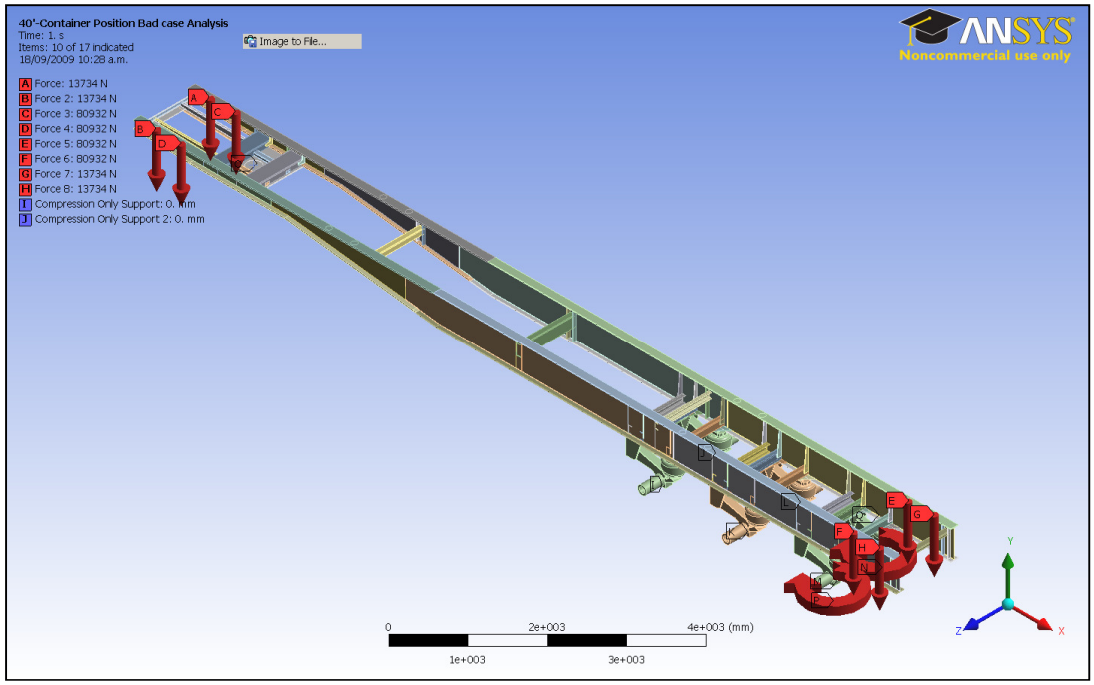

Figure 4-5: representing the boundary conditions for "worst case" analysis in 40' container position

4.3 FE static analysis of the trailer

4.3.1 Introduction

The FE static analysis is performed to determine the response of a structure to applied loads independent of time. This response includes displacements, reaction forces, stresses and strains and so on, depending on the purpose of the study. The purpose of the study in this static analysis is to confirm the location of the high stresses (as indicated by the crack appearance) and to determine the maximum stress at that location induced by the applied loads. In order to calculate these stresses, the finite element method utilises displacements calculated at each nodal point, which are then converted to strains and then stresses by continuity and constitutive relations, respectively. The displacements are calculated by solving a system of equilibrium equations for each nodal point. The general equilibrium equation of motion is given below [30]:

$$[\mathrm{M}]\{\ddot{x}\} + [\mathrm{C}]\{\dot{x}\} + [\mathrm{K}]\{x\} = \{\mathrm{F}(t)\} \qquad (4\text{-}1)$$

where,

[M] is the mass matrix

[C] is the damping matrix

[K] is the global stiffness matrix

$\{\ddot{x}\}$ is the acceleration vector

$\{\dot{x}\}$ is the velocity vector , and

$\{x\}$ is the displacement vector

This equation of equilibrium could be modified to suite the static case by removing all time dependent terms, as shown below:

$$[K]\{x\} = \{F\} \quad (4\text{-}2)$$

Where, the global stiffness matrix [K] is composed of elemental stiffness matrices[k]'. With the application of known boundary conditions, the system of equation 4.2 is solved for displacements at the nodes. These displacements are used to calculate strains and then corresponding stresses are obtained. This numerical technique is performed on the trailer using ANSYS workbench simulation environment to determine the stress distribution in the structure.

4.3.2 Analysis strategy for the trailer

Success of the finite element method in today's commercial world is largely because of the computing power of the modern day computers. As the number of finite elements is directly proportional to the accuracy of the mathematical model of the simulation environment, computer memory and processing speed plays an important role in the analysis. It is important to develop a finite element model that respects computing resources available for the analysis. Without it, the analysis may not be feasible or it may be inaccurate. For instance, the trailer is a large welded structure and analysing the full structure to obtain accurate stresses across the entire structure may not be possible without exceeding the elements or memory size limits. In this situation, the sub-modeling technique [31] offered in ANSYS workbench appears to be a practical way reducing the size of the analysis while retaining accuracy.

4.3.2.1 Global Model Simulation

The sub-modeling technique requires solving the global model or structure as usual by applying the global boundary conditions, and then transforming the global loads to the area of interest in the local region. The global model still needs to be solved with reasonable

degree of mesh, refinement as the local deformation is interpolated from the global deformation. Each part of the trailer model is connected using face-to-face bonded contact, as it would be in welded assembly and the parts in the assembly are modelled using local meshing methods suitable for the geometry of the parts.

In the global static analysis of the chassis, basically there are two supports; one at the front of the front of the chassis, king-pin, and the other at rear of the chassis. The rear support is a group of three suspensions. These two boundary conditions for the chassis is idealised as a simply supported beam. This assumption is consistent with the reaction force obtained at the suspension, which indicates that the total load at the rear is taken up by the suspension closest to the applied load. This is due to the rigid suspension model relative to the chassis. However, in reality, pneumatic suspension is designed to loads in all three suspensions. Although, the load is distributed equally in all there suspension sets, the whole suspension assembly is considered as single support due to their close proximity to each other for a structure over 13m long. In addition point should be noted that the other boundary condition at the area of interest, King-pin, represents the actual physical behaviour and more than 7m away form the suspension support.

The reaction forces obtained at the three suspension supports as shown in Table 4-1 and Table 4-2.

	Suspension 1		Suspension 2		Suspension 3	
	LW	RW	LW	RW	LW	RW
Reaction Force (KN)	123.10	125.37	0	0	0	0

Table 4-1: Reaction force at the suspensions in 20' container loading position

	Suspension 1		Suspension 2		Suspension 3	
	LW	RW	LW	RW	LW	RW
Reaction Force (KN)	0	0	0	0	94.47	94.45

Table 4-2: Reaction force at the suspensions in 40' container loading position

Based on the reaction forces obtained in the global static analysis, the turning moment is applied at the first axle in the case of 20' "worst case" container position, while it is applied to the third axle in the case of 40' "worst case" container position. The turning moment is calculated from the normal force acting at suspension support (reaction force) and the contact surface area of the tyres in laden condition, as shown in the Figure 4-6 below. The contact area of 245mm x 510mm for the tyres is taken from company records, which is 245mm x 510mm for the tyres normally used for the trailer. The turning moment at the support is calculated as follows and tabulated in Table 4-3.

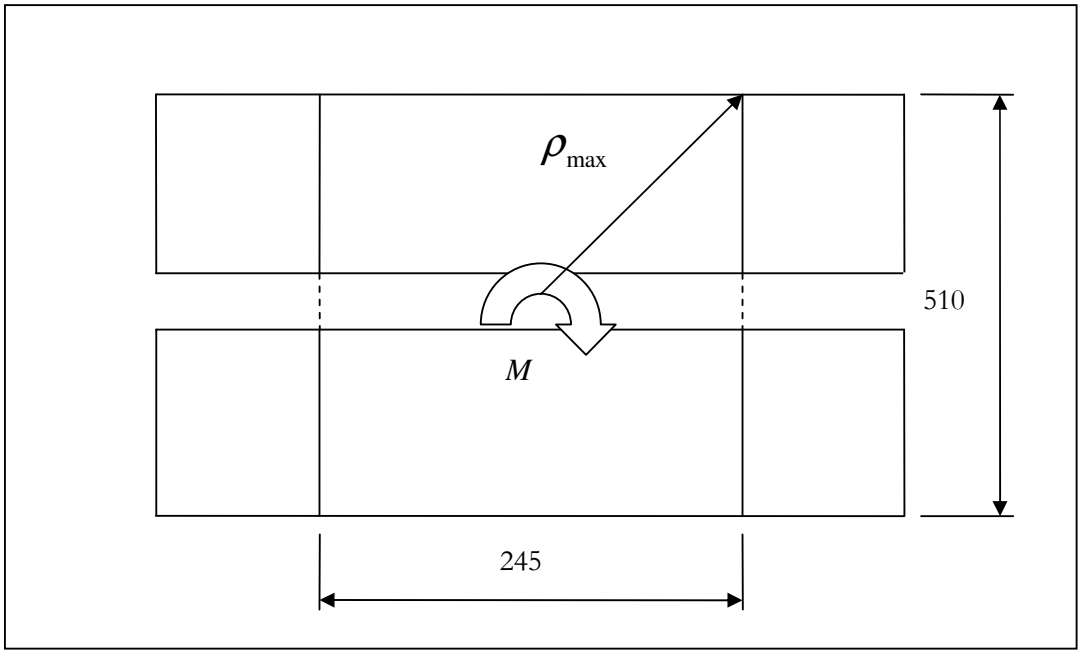

Figure 4-6: showing the contact surface area for twin tyre for calculating the turning moment.

$$\delta M = \rho * \delta F \qquad (4\text{-}3)$$

$$\Rightarrow \delta M = \rho * \sigma * \delta A \qquad (4\text{-}4)$$

Assuming the moment arm and stress is constant at the contact surface and integrating the equation (4-4) on both sides gives:

$$\int \delta M = \int \rho * \sigma * \delta A \approx \rho_{\max} * \sigma \int \delta A \quad (4\text{-}5)$$

$$M \approx \rho_{\max} * \sigma * A = \rho_{\max} * \mu * N \quad (4\text{-}6)$$

Substituting $\sigma = \mu * \left[\frac{N}{A}\right]$ in the above equation (4-7)

$$M \approx \rho_{\max} * \mu * N \quad (4\text{-}8)$$

Where, M = turning moment at the wheel

$\rho \approx \rho_{msx}$ = moment arm for tyre ground contact surface area (constant)

N = Normal force on the wheels

$\sigma =$ Stress at the contact surface area (constant)

μ = coefficient of friction for rubber on asphalt (dry) = 1.2 [40]

	20' loading condition-suspension 1		40' loading condition-suspension 3	
	LW	RW	LW	RW
Moment in KN-mm	41789.98	42560.61	32070.68	32063.89

Table 4-3: calculated turning moment at the supports in 20' and 40' container position.

The purpose of the global analysis is to identify the region of highest stresses as shown in Figure 4-7 to Figure 4-10 for the loading conditions investigated in this project. As a result of global analysis very high stress are identified at the King-pin region, which is the area of interest. The high stresses in this region are due to the stress raiser, as the global CAD model does not represent a very accurate geometry at the kingpin region. Therefore, it is required to model the geometry with accurate details including weldment. The analysis of the detailed

model of the kingpin region using sub-modeling analysis is explained in the following section. The results obtained in the global analysis is saved and further used in the sub-modeling analysis of the king-pin region.

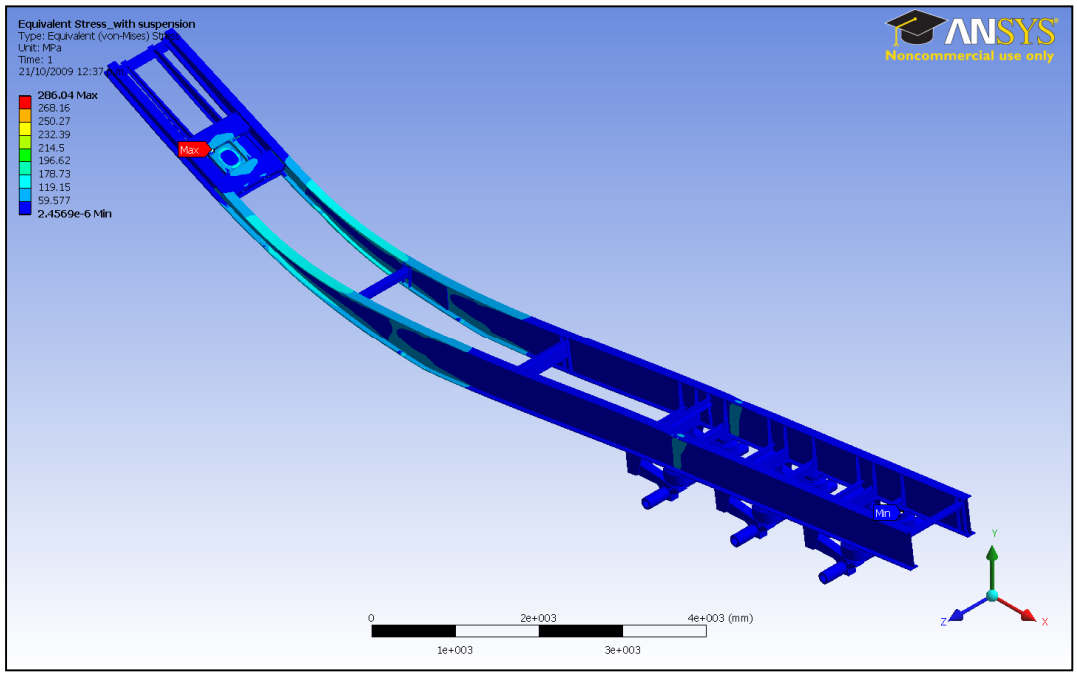

Figure 4-7: showing the stress distribution in the global model in 20'container loading position

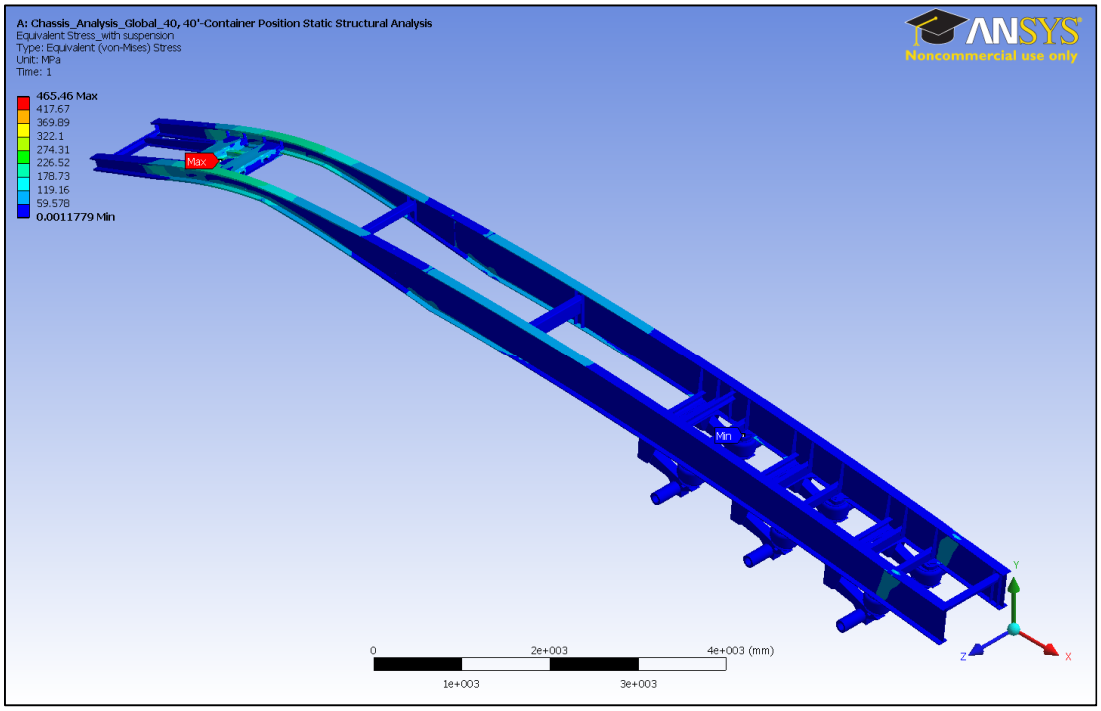

Figure 4-8: showing the stress distribution in the global model in 40'container loading position

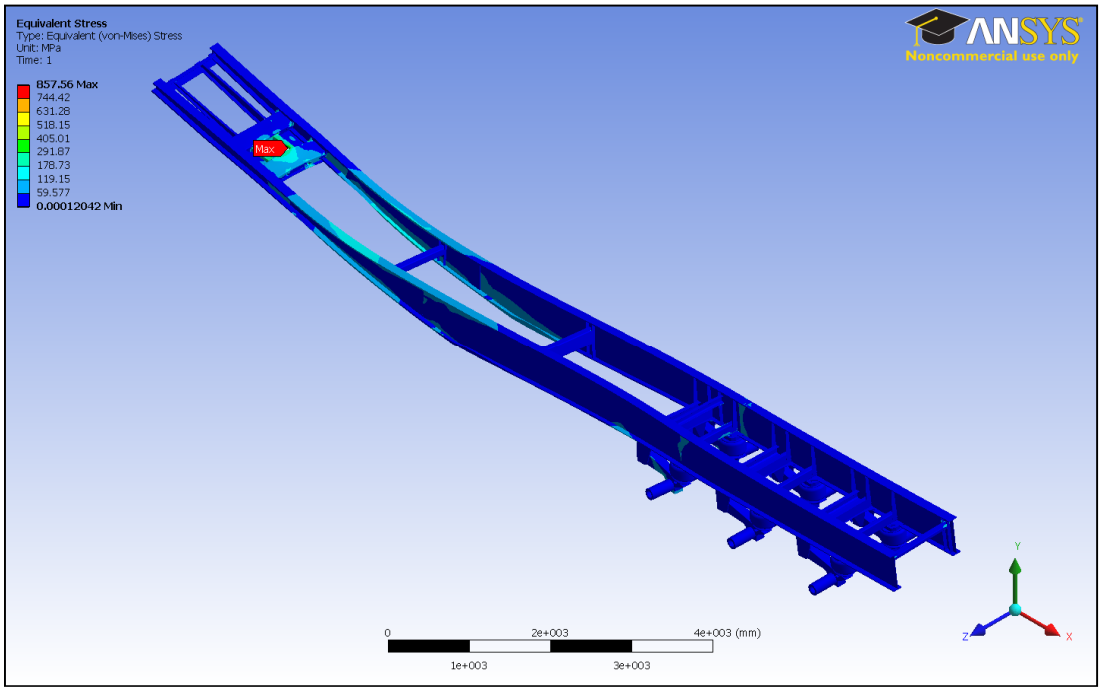

Figure 4-9: showing the stress distribution in the global model for "worst case" in 20'container loading position

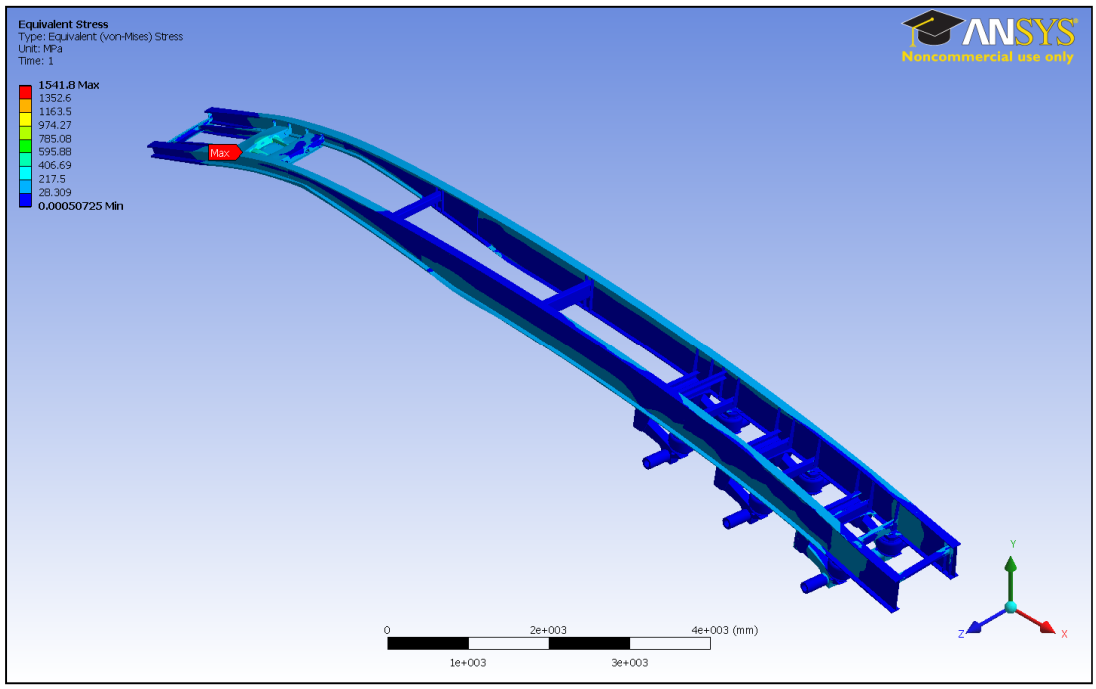

Figure 4-10: showing the stress distribution in the global model for "worst case" in 40'container loading position

4.3.2.2 Sub-model Simulation

The sub-model is created by removing the region of interest from the global model. In this process, it is important to keep the cut boundaries as far away as possible from the location of the high stress, so the displacement interpolation from the global model does not affect the final results. Removing the sub-model from the global model achieves the geometric consistency, as it does not change the location with respect to the global coordinate system. This allows the displacement boundary condition to be interpolated correctly. In the sub-model analysis, the interpolation of the global displacement is done using APDL (ANSYS Parametric Database Language) commands provided by ANSYS. These commands are inserted as a macro in the sub-modeling simulation to retrieve the database and result files from the global model in order to perform the displacement interpolation. Then the sub-model is solved using the interpolated boundary conditions and the local boundary condition present in the sub-model [6].

As mentioned in the section 1.1.3, cracks are observed at the cross-member weld beeds. This necessitates a detailed geometry of the sub-model including the weld beed. However, it is difficult to build the exact solid model of the weld beed, as such geometries can cause stress singularities and CAD models may not be suitable for FE modelling. Therefore, the weld beed requires some geometric idealisation to suit the finite element modelling. The R1MS (Radius 1 Maximum Stress) concept proposed by ANSYS appears rewarding to ensure non-singular stress state in the sub-model [6]. According to this concept, the fillet weld beed is represented as a chamfer and the transition from the weld seem with the surrounding material is smoothened with a 1mm radius. The sub-model developed on these guidelines is shown in Figure 4-11.

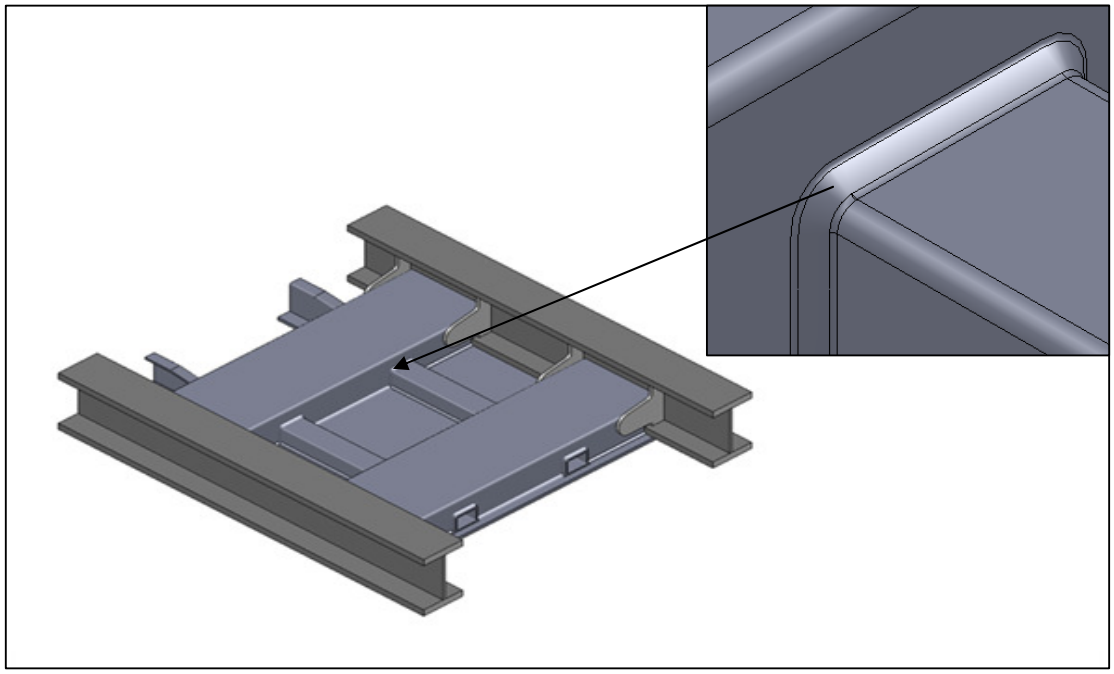

Figure 4-11: showing the sub-model highlighting the weld beads at the cross-member and cut boundary faces

Along with these guidelines for building the sub-model the following assumptions are also incorporated in the simulation of the sub-model;

- Material properties of the weld bead will remain linear, isotropic, and homogeneous.

- Weld and HAZ (Heat Affected Zone) have the same properties as the base metal.
- Full penetration of the weld is attained.
- No residual stress due to forming will be included.

The sub-model is then meshed with fine elements to accurately represent the geometry. In this sub-model, very fine mesh discretization was obtained using the "sphere of influence" method available in ANSYS workbench platform, which allows local mesh control at the area of interest in the sub-model [31]. The sub-model meshed using the "sphere of influence" mesh control is shown in Figure 4-12 below.

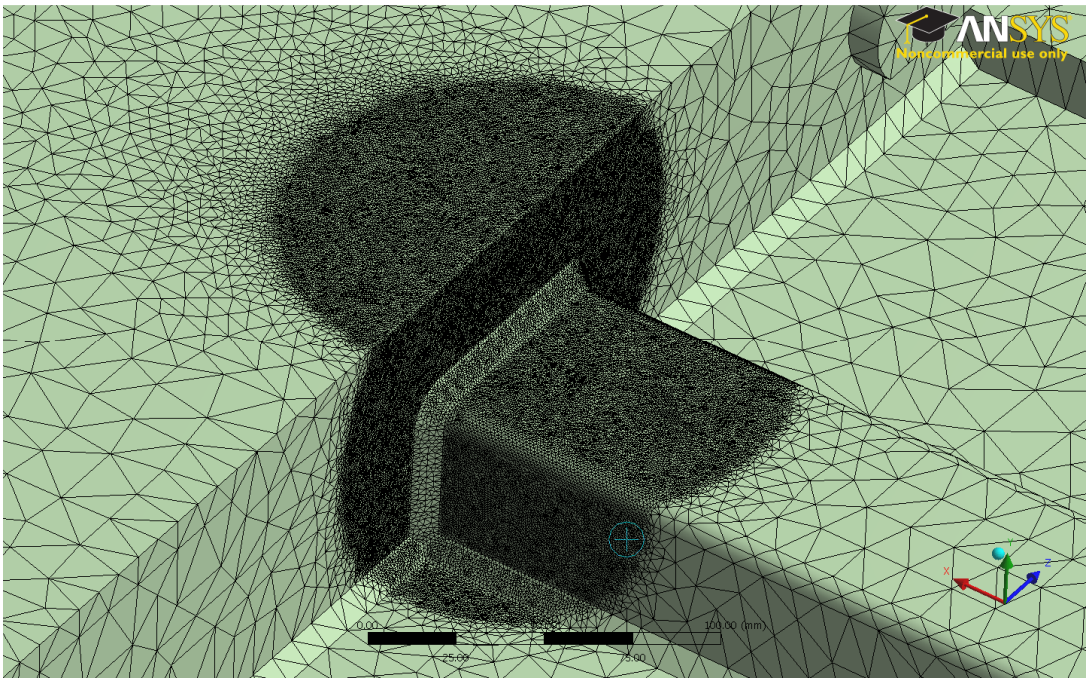

Figure 4-12: showing the submodel mesh detail using the "sphere of influence" mesh control

4.3.3 Simulation results and discussion

The sub-modeling analysis of the critical area has confirmed the presence of the high stresses in that region. This correlated well with the location where cracks have been observed on the actual chassis, as shown in the Figure 1-2. The maximum principal stresses obtained in the

sub-modeling analysis for the normal loading conditions are below the yield stress of the material. However the factor of safety calculated is lower than the company recommended standards for static design. The STEELBRO standard specifies 60% (FOS 1.6) of the yield stress to be the allowable stress for the static design. The maximum stress obtained and the corresponding factor of safety is tabulated in the Table 4-4. The factor of safety calculated for the static design at STEELBRO as

$$FOS = \frac{Yield\ stress\ of\ the\ material}{Maximum\ allowable\ stress}$$

Figure 4-14 and Figure 4-15 show the maximum principal stress at the critical points in the normal loading conditions. The stress convergence carried out to confirm the mathematical accuracy of the model is also shown in the Figure 4-13.

Max principal stress in MPa	334	341	200	323	322
Factor of safety	1.04	1.02	1.75	1.08	1.09

Table 4-4: Factor of safety at the critical points in the normal loading conditions

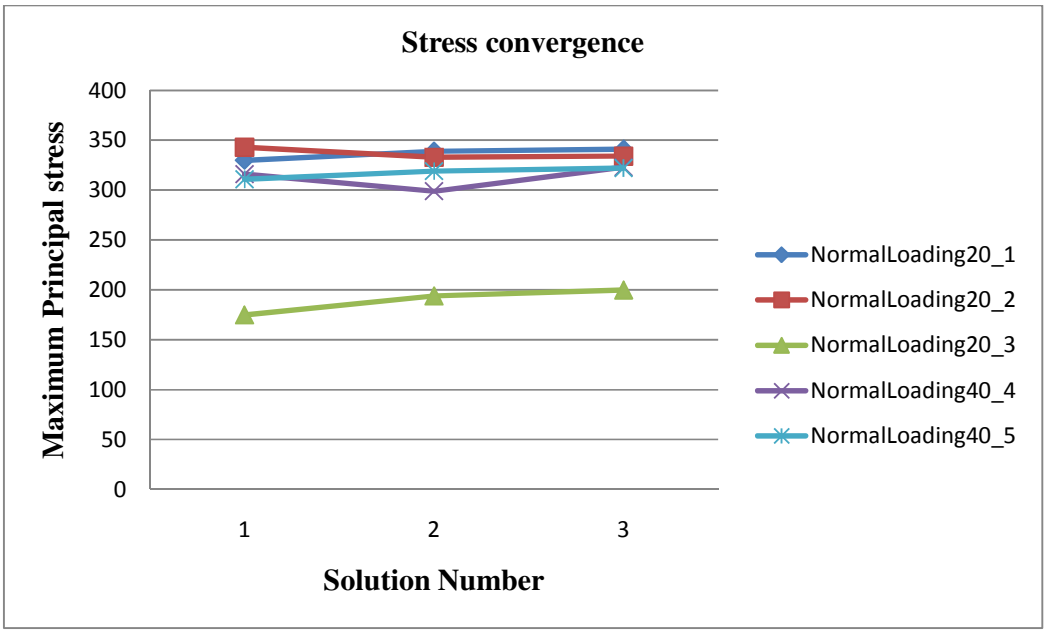

Figure 4-13: Graph showing the stress convergence in normal loading condition.

The sub-modeling analysis of the “worst case” service condition showed that the maximum principal stresses exceeds the yield stress of the material, which means either the structure will fail or plastic deformation will occur. The analysis performed on the trailer uses only “elastic model”, which indicates that any value beyond the elastic region will be a linear estimate at the critical point and may not be an actual value. More accurate results at this situation would require modelling trailer as an “elasto-plastic” model. However, determining the stress in the plastic zone is not the aim of this analysis, as the main objective of this research is to determine the causes of the failure and redesign the component to reduce the maximum stresses below the failure criteria, which is 60% of the yield stress. The Figure 4-16 and Figure 4-17 shows the maximum stresses for the “worst case” service conditions.

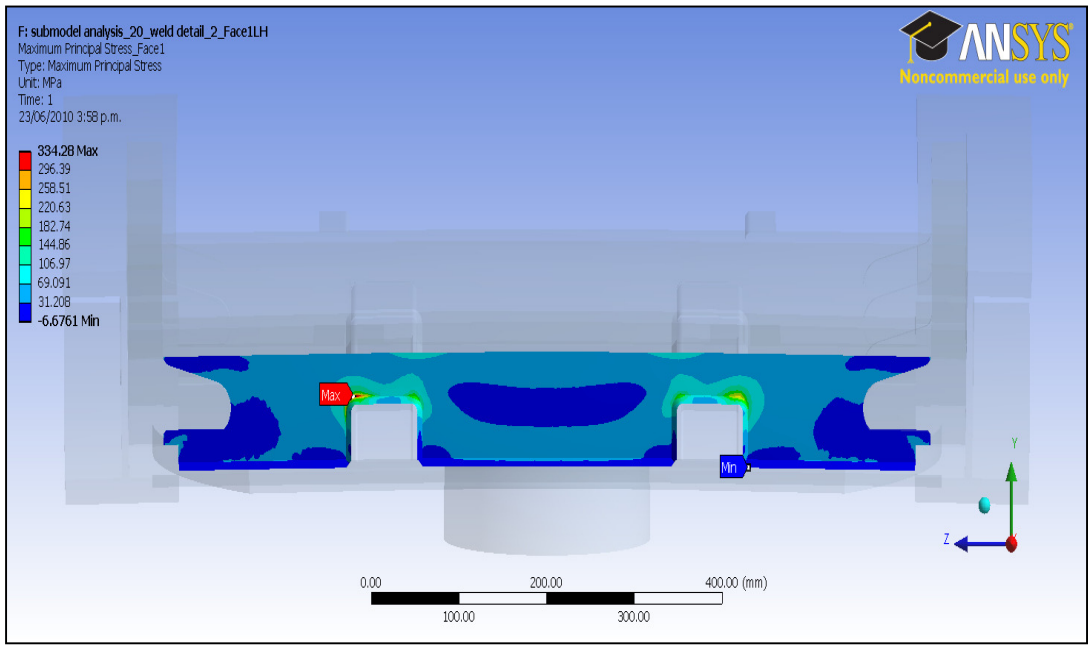

Figure 4-14: showing the critical maximum principal stress at the rub-plate cross- member for 20’ loading condition

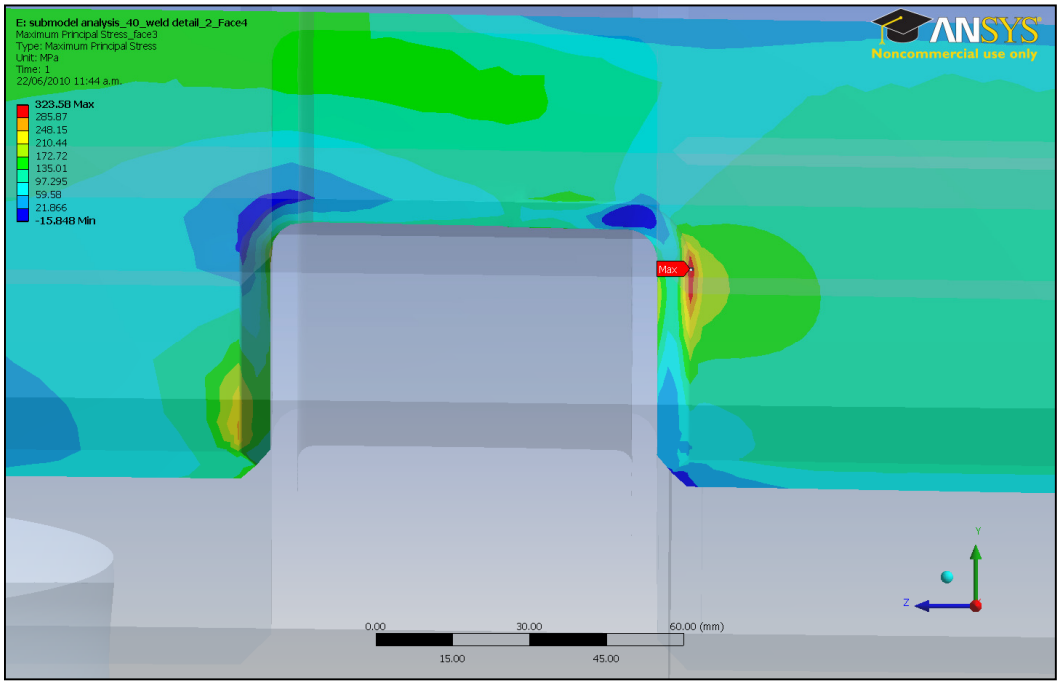

Figure 4-15: showing the critical maximum principal stress at the rub-plate cross- member for 40' loading condition

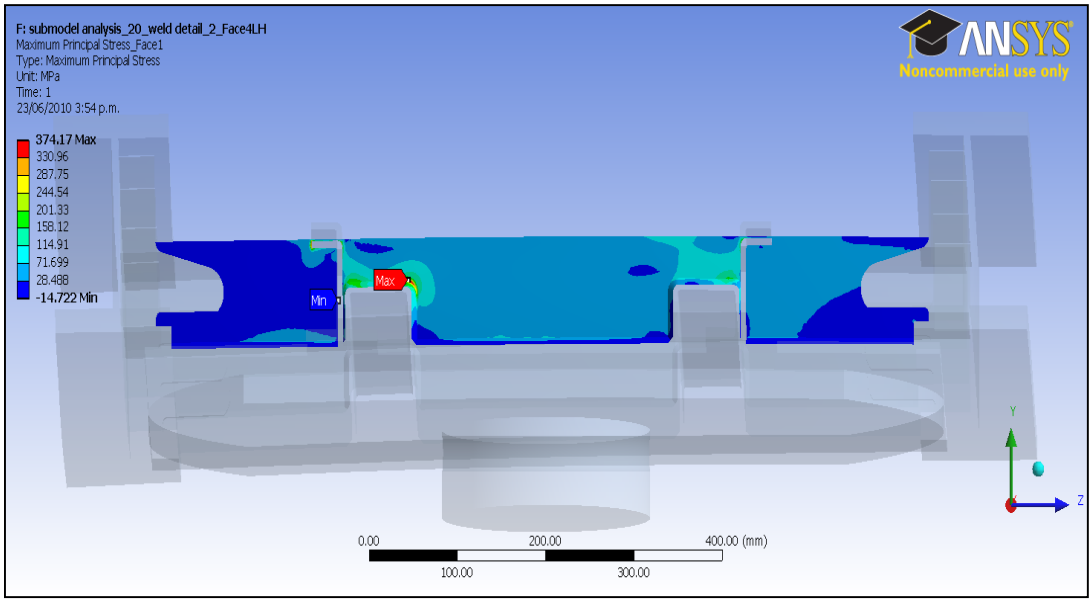

Figure 4-16: showing the critical stress more than the yield stress of the material in the "worst case" 20' container position.

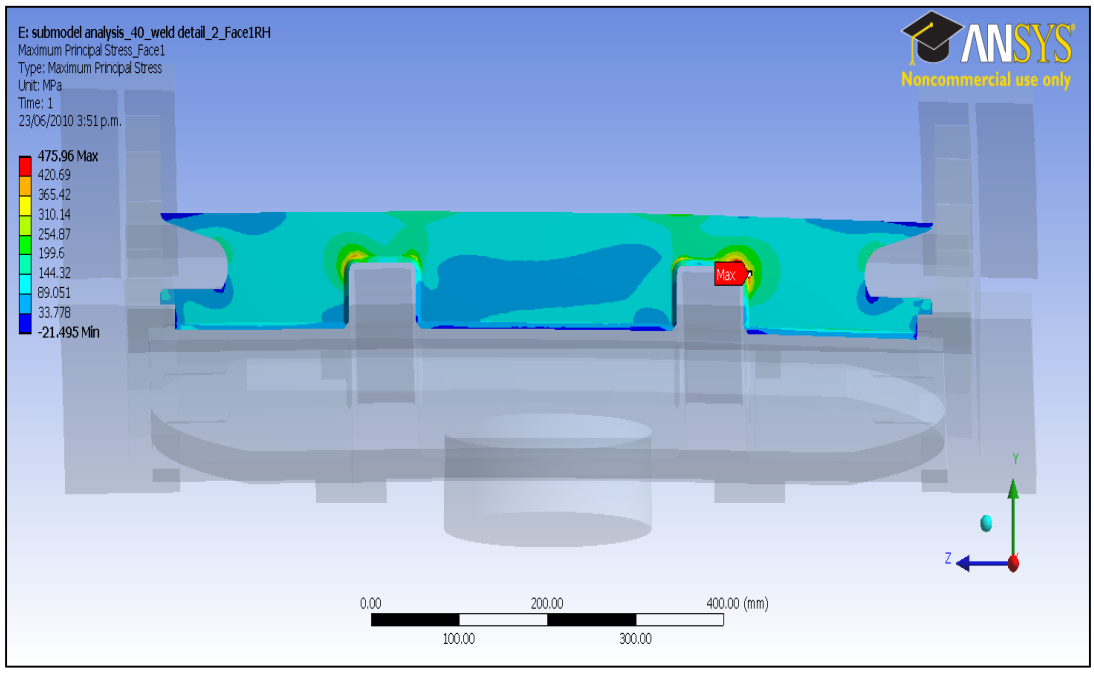

Figure 4-17: showing the critical stress more than the yield stress of the material in the "worst case" 40' container position.

5 VALIDATION OF THE FEA MODEL

5.1 Introduction

An important part of a Finite Element analysis is to validate the model used for the analysis to ensure acceptable quality of results is achieved for available computational resources. This could be done analytically, experimentally and /or using software capability as discussed in the third chapter of the thesis. In this study the FEA model is validated using the shape checking capability of the ANSYS Workbench and experimentally by applying the strain gauges on the actual trailer. The details and the outcome of both methods used for the validation of the FEA model are reported in the following sections.

5.2 Geometric validity of the FEA model

The accuracy of the finite element model is important obtain accurate results, as it represents the physical part of the problem. Therefore, the geometry of the finite element model of the trailer is checked as per the guidelines discussed in Chapter 3. Mainly, geometric aspects of the elements such as Aspect ratio, Jacobian ratio, Warping factor, Maximum corner angle, and Skewness are checked to ensure the mesh quality is within the acceptable limits. Figure 5-1 shows the majority of the mesh volume is within the acceptable limits according to the shape checking criteria established in Chapter 3.

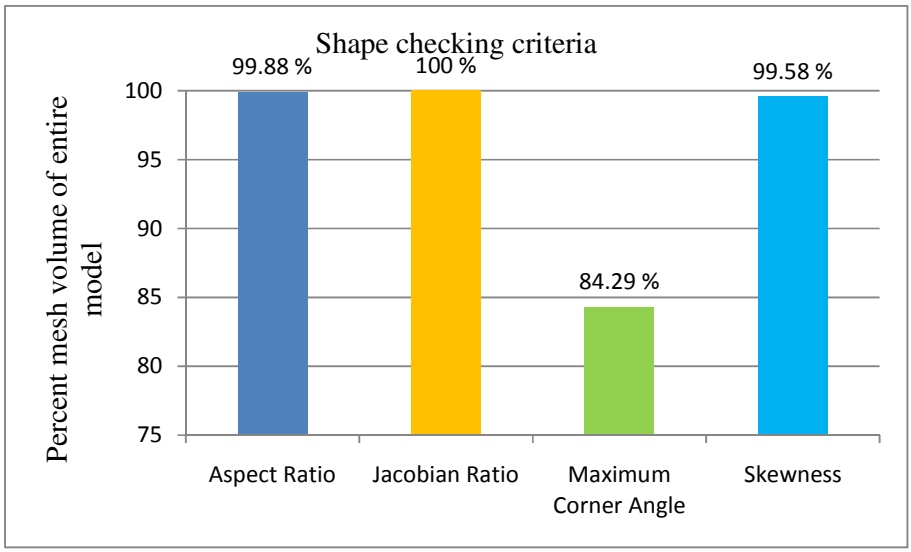

Figure 5-1: Graph showing the total percentage volume of the mesh of the FEA model satisfying the shape checking criteria for 20' normal container loading condition.

5.3 Experimental method to validate the FEA model

The company uses traditional engineering mechanics approach in designing the chassis main-frame, which involves solving a statically determinate system. This design approach is based on full static load acting on the chassis, and to overcome the dynamic affect the main-frames are designed to 40% of the yield stress of the material at the point of concern. There are two main-frames in the chassis, which are the main structural members of the chassis. The current chassis calculation as shown in appendix A, which independently determine the strength of the main-frame. This calculation does not consider load sharing between the two main structural members of the chassis and also does not calculate the stress at the crack region determined in section 5.2. Finite element analysis done in the section 5.2 clearly shows very low stresses at some points within the chassis and indicated high stress concentration at the rub-plate region under investigation. In this situation, to validate the FEA model, actual strain measurement on the trailer is considered. This process involves measuring the actual stresses on the trailer chassis using strain gauges. There are many

mechanical and electrical methods to measure the strain induced in a structural element. However, Strain gauges are used in this project due to their ease of use and superior measuring characteristics. Strain gauges record the mechanical strain induced due to deformation caused by applied force or loads. These stains could be further converted to stresses and loads to determine the factor of safety of a structural element or validate a FEA model, as in this study.

Before proceeding to the application of the strain gauges in this project, it is necessary to have a good understanding about the relevant engineering terminologies and principals in context with the strain gauge technology. The following sections provide an overview of the relevant terminologies discussed in the strain gauging process.

5.3.1 Fundamentals of Strain, stress, and Poisson's Ratio

External force (P) applied on the body causes the deformation in the elastic material of the body. As the body undergoes deformation, it develops resistance against the deformation. Broadly, this resistance to deformation is known as stress (σ), which could either be tensile or compressive in nature as shown in Figure 5-2. If the force is tensile, the initial length of material extends by ΔL. while compressive forces contract the initial length of the body by ΔL known as Strain (ε) and the ratio of the change in length to the initial length is expressed as follows [32]:

$$\text{(Tensile)}\ \varepsilon = \frac{\Delta L}{L} \quad \text{(Compressive)}\ \varepsilon = \frac{-\Delta L}{L}$$

ΔL = Change in length

L = Initial length

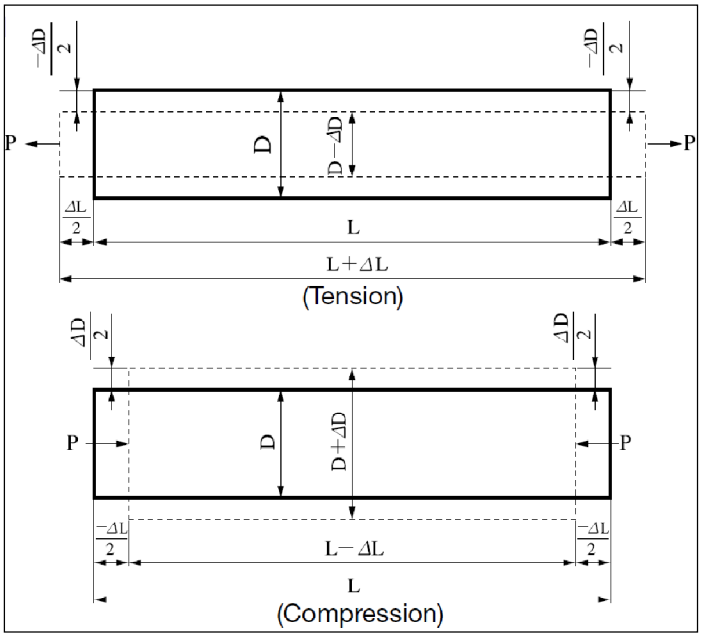

Figure 5-2: Illustrative example showing tensile and compressive force acting on a piece of bar [32].

This strain could be converted to stress using the Hooke's law, which states that the stress is proportional to the strain within the elastic limit of the material. Therefore the stress can be determined by multiplying the corresponding strain with the Elastic Modulus of the material. The Hooke's law is expressed as below:

$\sigma = E\varepsilon$

$\sigma =$ Stress

$E =$ Elastic modulus

$\varepsilon =$ Strain

As shown in the above figure, when a tensile force is applied on the piece of bar, it induces two types of strains in the body; longitudinal strain in the axial direction and transverse strain in the transverse direction of the body. Both strains can be mathematically expressed as follows [32]:

$\varepsilon_1 =$ Longitudinal strain $= \pm \dfrac{\Delta L}{L}$

$$\varepsilon_2 = \text{Transverse strain} = \pm \frac{\Delta D}{D}$$

Poison's ratio is a material property defined as the ratio of the absolute value of the transverse and the longitudinal strains and mathematically expressed as below:

$$\nu = \frac{\varepsilon_2}{\varepsilon_1}$$

where,

$\nu =$ Poisson's Ratio

5.3.2 Strain gauge and Principal of strain measurement

Two types of strain gauges are used in this project. Basically, the strain gauges are made up of fine electrical resistance wire or photographically etched metallic foil. As shown in Figure 5-3, the wire or metallic foil is bonded to an insulated surface and connected to the lead wires. In order to measure strain, the insulated surface is glued onto the test specimen using non-conductive adhesive. When the test specimen undergoes any deformation, a corresponding change in the electrical resistance occurs in the wire or foil. This change in the electrical resistance is recorded as the strain in the test specimen at the point of application of the strain gauge. Linear strain gauges determine the strain in a single direction, while Tri-axial strain gauge rosettes are able to determine the full state of strain at a point via equation 5-1, which includes the Young's modulus and Poisson's ratio of the material. Generally, the tri-axial rosette gauges are used if the direction of the principal axis is uncertain [33]. The strain gauge rosette used in this project is shown in Figure 5-4.

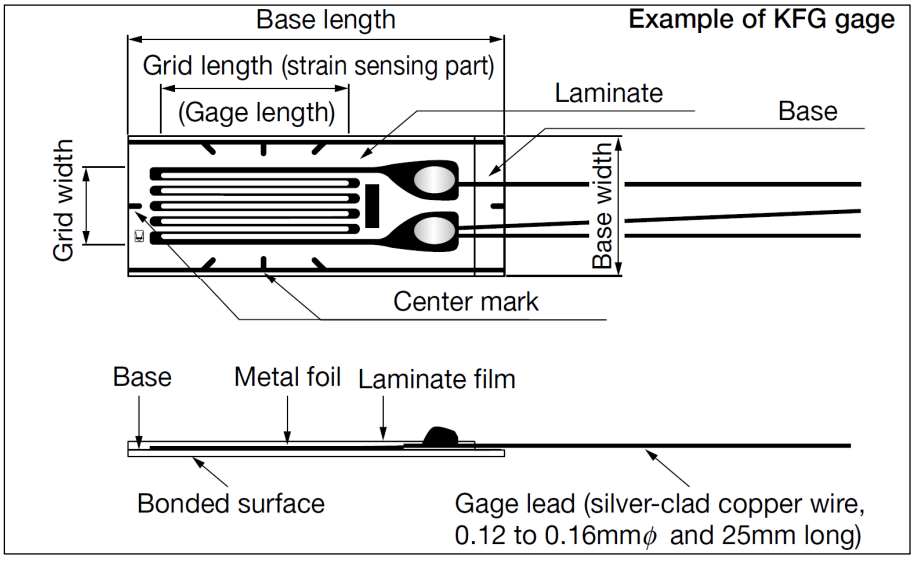

Figure 5-3: Schematic of a general-purpose foil strain gauge (Kyowa, Japan), these were used for the stress measurement on the Mainframe flanges [33].

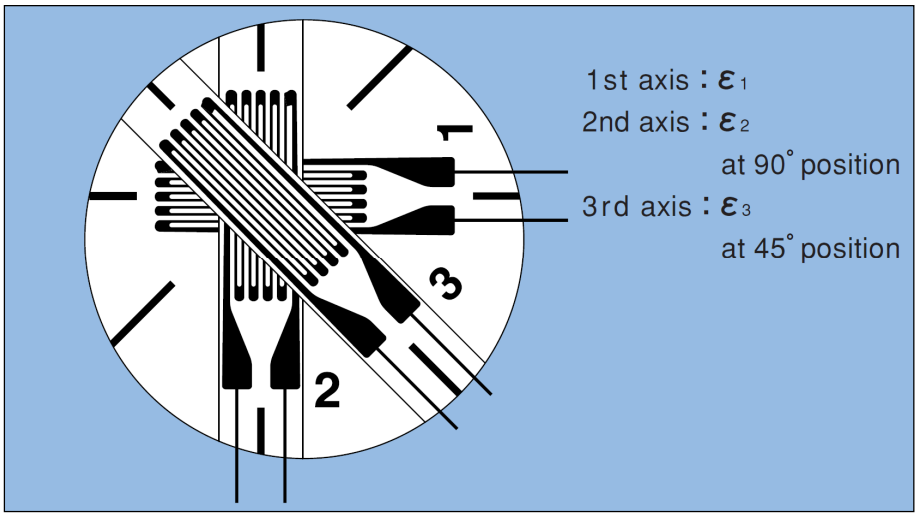

Figure 5-4: Schematic of a 3-element rosette strain gauge (Tokyo Sokki Kenkyujo, Japan), these were used for the stress measurement of the Rub-plate cross-member 'hot spot' areas [33].

Maximum principal stress:

$$= \frac{E}{2}\left[\frac{\varepsilon_1+\varepsilon_2}{1+\nu} + \frac{1}{1+\nu}\sqrt{2\left\{(\varepsilon_1-\varepsilon_3)^2+(\varepsilon_2-\varepsilon_3)^2\right\}}\right] \qquad (5\text{-}1)$$

5.4 Strain gauge system set up

The experiment setup for the strain measurement on the trailer chassis is shown in Figure 5-5. The setup consists of three main components explained as follows:

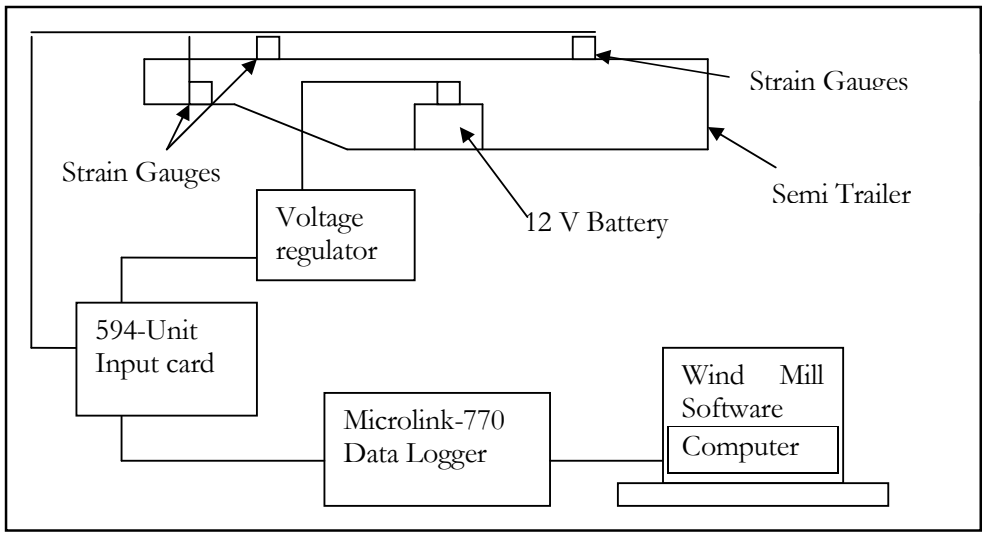

Figure 5-5: Showing the block diagram of the strain-gauge experimental setup.

Microlink-770: The Microlink-770, as shown in Figure 5-6, is a strain gauge data logging system manufactured by Windmill Software Limited, United Kingdom. This device was recording the output form the strain gauges. The unit is equipped with analog and digital connectors. In this project the 37- way analog connector was used to receive 16 differential analog inputs from the strain gauges. This input from the strain gauges was then converted into digital signals and relayed to Windmill data logging software (Computer) through the Universal serial bus (USB) cable [34].

Figure 5-6: Microlink-770 Data acquisition hardware (Biodata Limited, 2000, UK) [34].

594-Unit Screw terminals: This is a 16 bridge input card, which enables the Micrlink-770 unit to receive signals form strain gauge bridges. Two of these units were used in this experiment. The circuit diagram for the stain gauge bridges is shown in Figure 5-7. An active gauge and three fixed resistors are used to make up a quarter bridge circuit for each input channel of the 594-unit [34].

Windmill: Windmill is a data acquisition and control software, which runs on a Windows PC. The windmill software reads the digital strain signals from the Microlink 770 and performs the bridge calculations to produce a reading in micro strain. The recorded micro strain is then transferred to Windows Excel for further analysis [34].

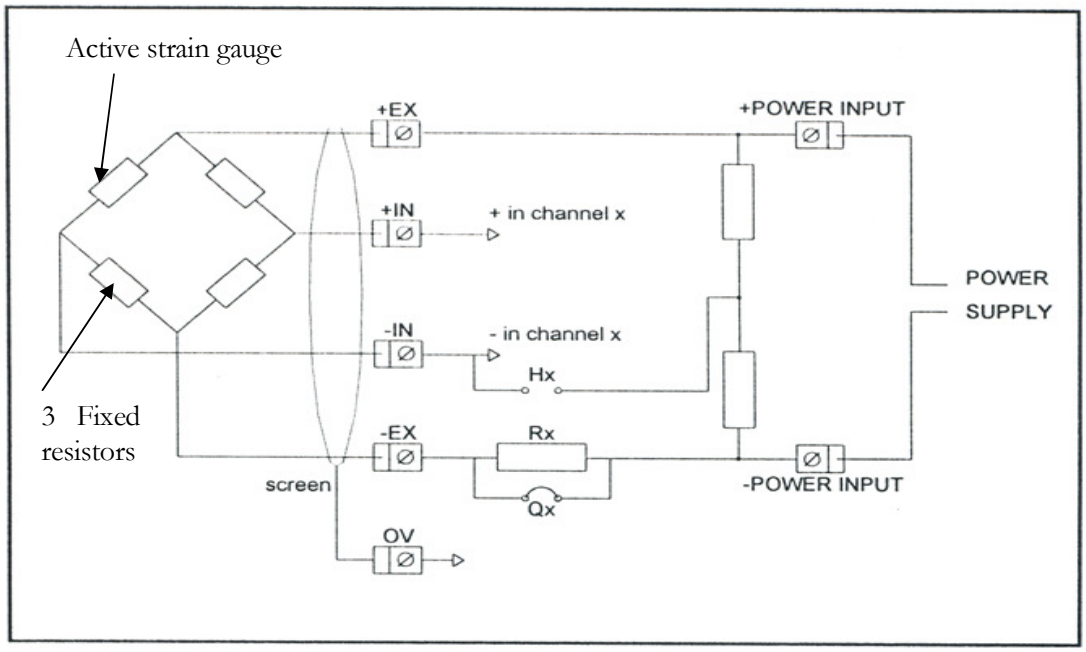

Figure 5-7: Circuit diagram of the quarter bridge connection used in the 594-Unit screw terminal [34].

5.5 Experimental procedure

The strain gauges were applied on the selected points on the trailer and connected to the electronic set up as explained in the section 5.4. In an anticipation of human errors and technical problems, 16 strain gauges were applied on the chassis. Eight of the strain gauges were Rosette gauges attached to the selected points at the rub-plate cross-member region, which is the failure region. As shown in Figure 5-8, each Rosette strain gauge consists of 3 gauges stacked on top of each other and these gauges occupied 24 channels in the 594-Unit screw terminal. The remaining eight linear strain gauges were applied on top and bottom flange of the left hand side mainframe of the chassis. The linear strain gauge application points were selected based on the analytically calculated results, as the points could be compared with strain gauge readings. Figure 5-8 shows the electronic set up of the instruments at the rub-plate region of the trailer.

Figure 5-8: Complete setup of the strain gauge system at the chassis rub-plate, the enlarged view of one of the Rosette strain gauge is shown at the bottom left corner of the picture.

The following two testing scenarios were performed on the trailer to obtain the strain gauge readings.

- Case 1 – Strain gauge data recorded during normal loading/unloading (full load)in static condition for 20’ container position (Figure 5-9)
- Case 2 – Strain gauge data collected during normal loading/ unloading (full load) in static condition for 40’ container position (Figure 5-10)

Figure 5-9: The 20' full load testing position at STEELBRO yard.

Figure 5-10: The 40' full load testing position at STEELBRO yard.

5.6 Results and Discussion

Strain gauge readings obtained for the trailer chassis is utilized in two purposes; first to validate the FEA model and second to determine the difference between the analytically calculated results (STEELBRO design calculation-Appendix A) and the strain gauge measurements. Seven of the applied strain gauges were selected for further comparison with FEA and analytically calculated results. Three of these stain gauges were applied in the sub-model region of the trailer. The remaining four strain gauges were outside of the sub-model region and were compared only with the analytical results. Tables 5-1 and 5-2 report the strain gauge readings in comparison with the FEA and analytically calculated results, respectively. The response curve for one of the strain gauges during the loading of the trailer is shown in Figure 5-11. The strain gauge readings are taken from the stabilized region of the curve.

20' Container loading position			40' Container loading position		
FEA- Stress at gauge positions (MPa)	Strain Gauge readings converted in stress (MPa)	Percentage difference (%)	FEA- Stress at gauge positions (MPa)	Strain Gauge readings converted in stress (MPa)	Percentage difference (%)
151.84	162.56	6.82	171.48	184.23	7.17
132.62	143.32	7.76	186.49	174.28	6.77
119.42	125.91	5.29	206.16	189.89	8.22

Table 5-1: Showing the percentage difference between the FEA and Strain gauge measurements.

20' Container loading position			40' Container loading position		
Analytical - Stress at gauge positions	Strain Gauge readings converted in stress (MPa)	Percentage difference (%)	Analytical - Stress at gauge positions	Strain Gauge readings converted in stress (MPa)	Percentage difference (%)
190	158.84	17.86	196	181.33	7.78
198	155.23	24.22	134	101.73	27.38
120	33.39	112.93	169	49.97	108.72
102	16.94	143.03	158	48.84	105.55

Table 5-2: Showing the percentage difference between the Analytical and Strain gauge measurements.

The percentage difference between calculated FEA results and the strain gauge readings at the cross-member region is between 5 to 9 % within the sub-model cross-member region of the trailer. Considering the level of noise in the system due to diesel engine mounted on the trailer, this is a good level of correlation between the FEA and experimental values. On the other hand, comparison with the analytical values showed that the percentage difference was large, especially at the strain gauges mounted at the rear end of the trailer. This large percentage difference could be due to the simplification done in the analytical calculation for the mainframe.

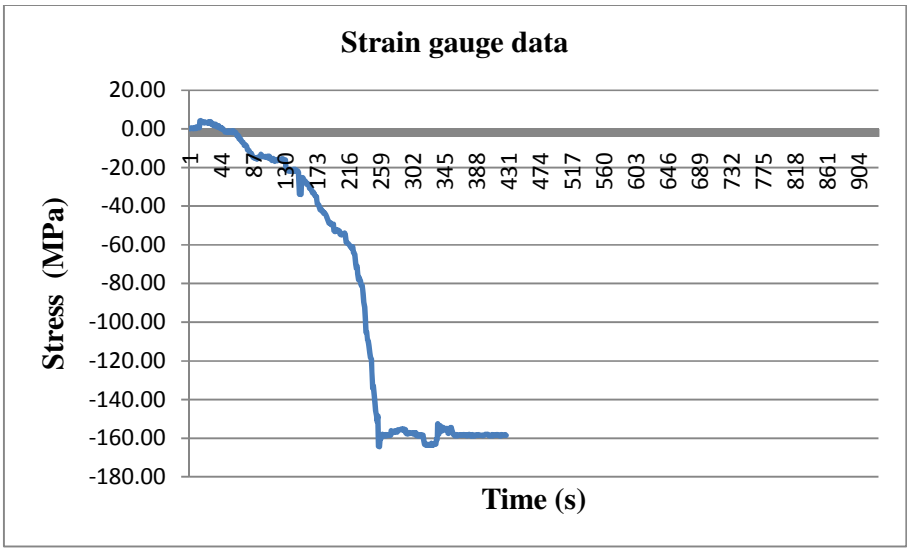

Figure 5-11: Showing the nature of the curve at a strain gauge location in 20' container loading position. The maximum value of 158.84 MPa is recorded in the stable region of the graph.

6 FEA: REVISED DESIGN

6.1 Introduction

The aim of this study is to determine the cause of the observed failure, so that the component can be redesigned to resist cracking. The analysis of Chapter 4 showed that "worst case" service condition could be the cause of the failure, however if it is assumed that the trailer never come across the "worst case" service condition, then the study must focus on normal loading/unloading conditions. Even though the stresses determined in the static analysis are below the yield stress, the phenomenon of metal fatigue could cause the failure under the cyclic loading conditions. Therefore, this chapter further investigates the effect of cyclic loading on the critical region identified in the static analysis for normal loading/unloading conditions.

6.2 Fatigue analysis of the current design

Generally, the objective of fatigue analysis is to estimate the number of repeated cycles of loading a component may experience in it's life time so that the component can be designed to withstand more than the desired number of loading cycles. For the fatigue analysis of the current design, it is important to understand the nomenclature associated with the cyclic loading, as shown in Figure 6-1.

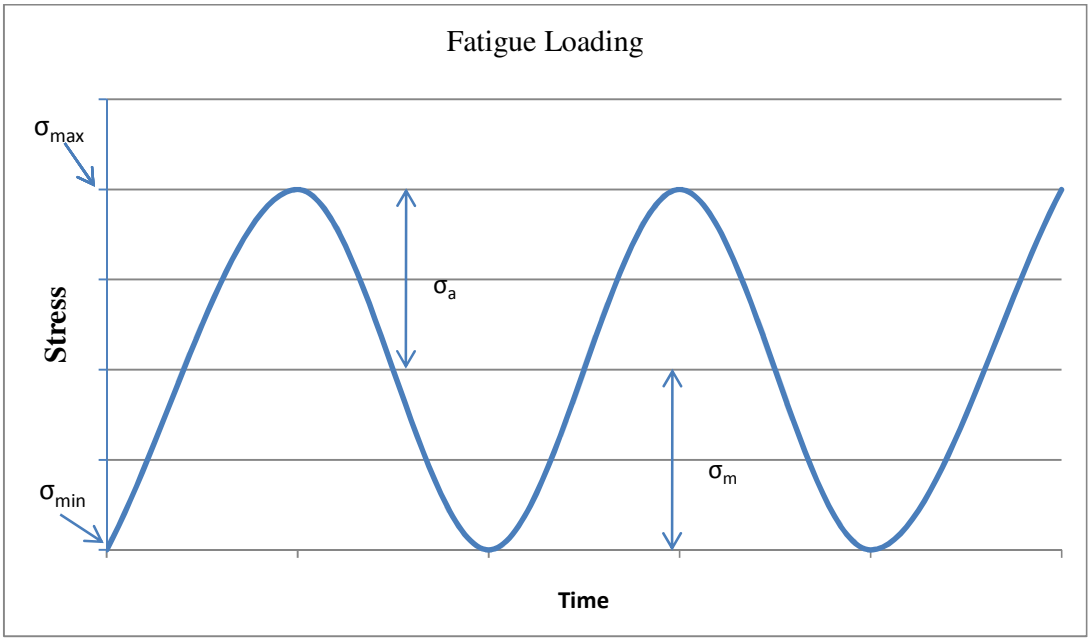

Figure 6-1: showing the nomenclature of fatigue loading.

Stress range : $\Delta\sigma = \sigma_{max} - \sigma_{min}$ (6-1)

Stress amplitude: $\frac{\Delta\sigma}{2}$ (6-2)

Mean stress : $\sigma_m = \frac{\sigma_{max} + \sigma_{min}}{2}$ (6-3)

Stress ratio : $R = \frac{\sigma_{min}}{\sigma_{max}}$ (6-4)

where, σ_{max} and σ_{min} are the maximum and minimum stress respectively.

Currently, there are three major fatigue life prediction methods available for design and analysis. They are as follows:

- LEFM Method
- Stress-Life Method
- Strain-Life Method

6.2.1 LEFM Method

Generally fatigue failures can be characterized into three stages: crack initiation, crack propagation, and fracture. The three stages of fatigue failure are schematically represented in the Figure 6-2 below.

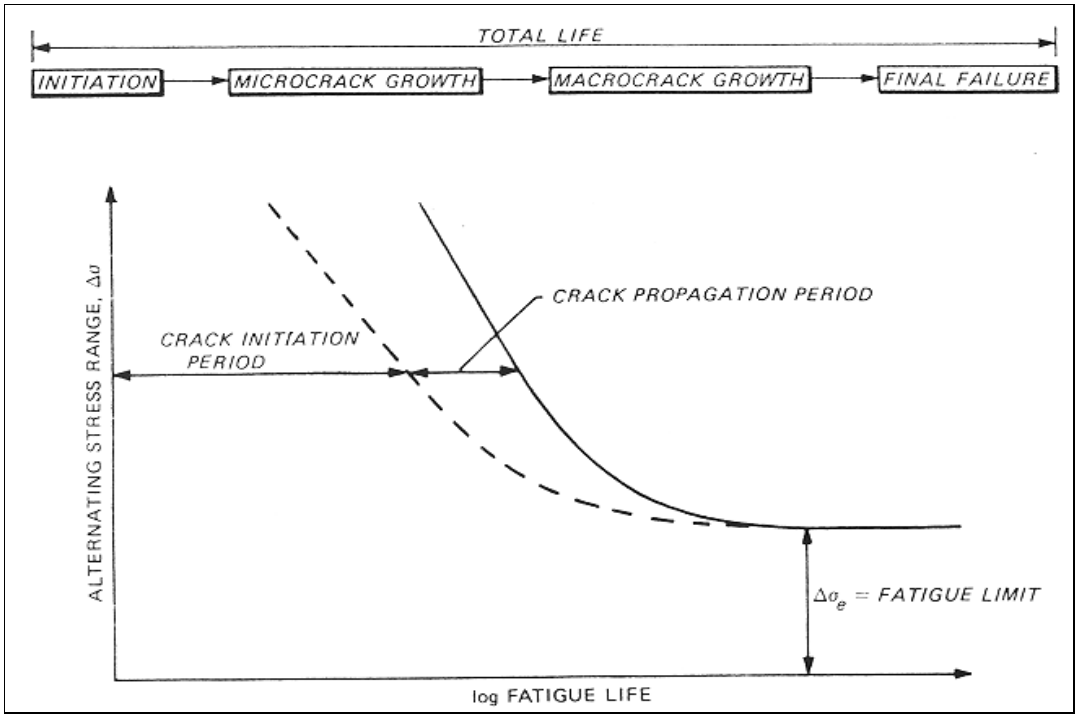

Figure 6-2: showing the total fatigue life and effect of the stress intensity on the fatigue life. [35]

As shown in Figure 6-2, the majority of the time spent in the crack initiation stage and then crack propagation and finally the component fails due to total fracture.

Usually, a fatigue crack initiates at surface cracks, marks, sharp corners, dents, corrosion pits or similar discontinuities. Then the crack grows, forming striations depending on the stress intensity due to cyclic loading. The crack continues to grow until the stress intensity is equal or greater than the fracture toughness of the material. This leads to the final fracture of the component.

The LEFM method assumes an initial flaw size, as shown in Figure 6-3, where initial flaw size is just below the detectable flaw limit and then calculate the number of cycles to failure for the crack to grow to the critical crack size.

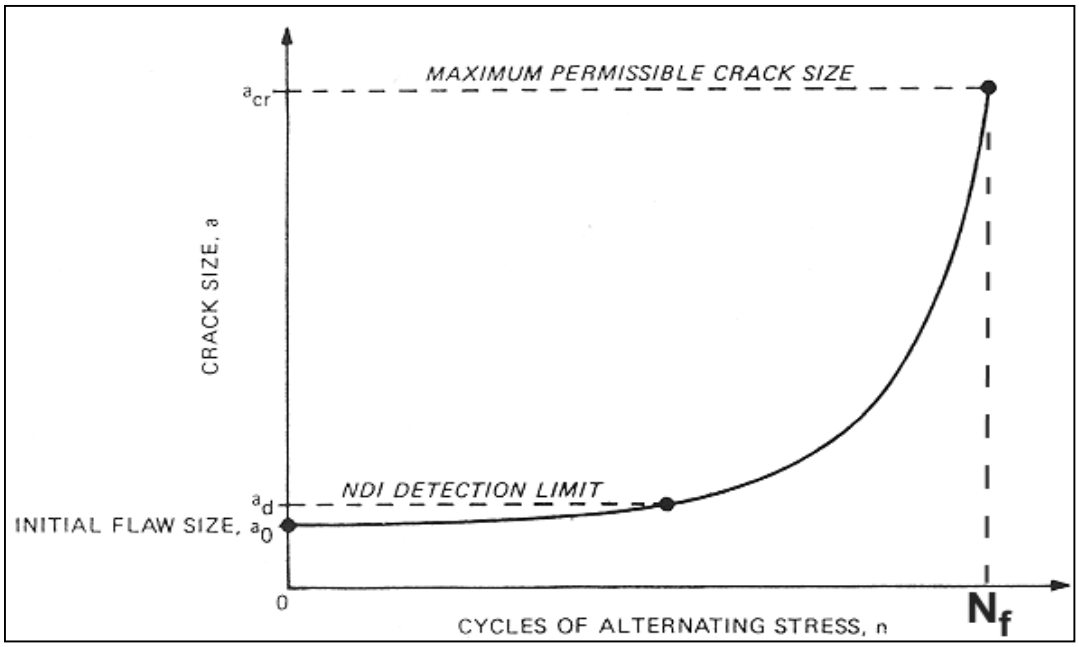

Figure 6-3: Showing the number of cycles to failure from initial crack size to critical crack limit [35].

The mathematical expression by Paris provides a relationship between the crack growth rate and the range of the stress intensity factor, which determines the number of cycles between a_o and a_c, given as [36]:

$$\frac{\partial a}{\partial N} = C(\Delta K)^m \quad (6\text{-}5)$$

where,

$\frac{\partial a}{\partial N}$ = cyclic crack growth rate

ΔK= Stress intensity range

C= material constant

m= material constant

In addition to this equation, Walker and Forman presented the following equations that also consider the stress ratio other than zero, such as loading conditions other than the completely reversed loading condition [36].

$$\text{Walker Equation:} \quad \frac{\partial a}{\partial N} = \frac{C_0}{(1-R)^{m(1-\gamma)}}(\Delta K)^m \quad (6\text{-}6)$$

$$\text{Forman Equation:} \quad \frac{\partial a}{\partial N} = \frac{C_2(\Delta K)^{m_2}}{(1-R)K_c - \Delta K} \quad (6\text{-}7)$$

where,

C_0 ,C_2, m_2, and γ are the constants for the material

R= Stress ratio

K_c = Fracture toughness of the material for the thickness of interest

This fracture mechanics approach to fatigue analysis is more widely used in places like aircraft industries, where the number of cycles to failure will be determined from minimum detectable flow size to critical crack size. This is done to set the inspection intervals so that the crack can be detected before it reaches the critical size. The objective of this study is to estimate the total life at the critical region, so that the structure survives the desired length of

time before any further inspection. This is more easily achieved using either stress-life method or strain-life method, as explained in the following sections.

6.2.2 Stress-Life Method

The Stress-Life method is a traditional approach to analyze metal fatigue based on a stress-life curve called S-N curve. It is derived from experimental data conducted on a test specimen. This method was first introduced by German engineer August Wöller. This is also called the "nominal stress" approach as it uses nominal or average stress acting on the component for the fatigue analysis [36].

Generally, experimental data for a test specimen could be obtained by various fatigue testing machines depending on the loading condition; for example, R. R. Moore rotating beam machine is used for applying pure bending by means of weights [37]. Due to statistical nature of the fatigue, several tests are required to determine the fatigue strength of a material which eventually produces the S-N curve. Figure 6-4 shows the typical S-N curve for steels and non-ferrous alloys.

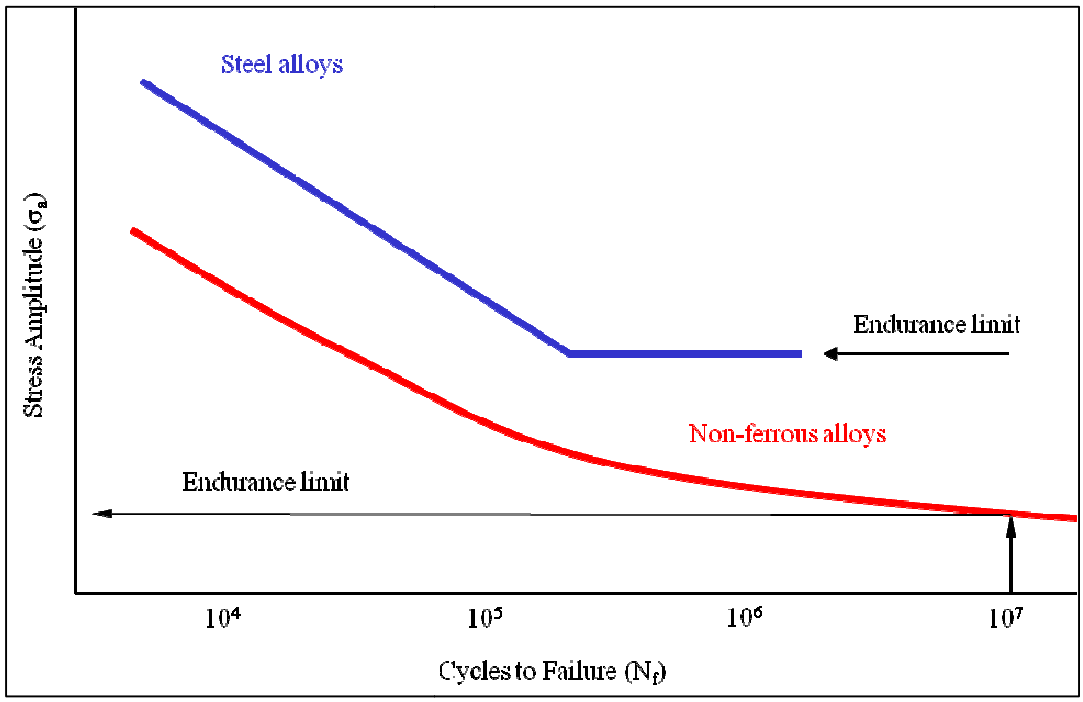

Figure 6-4: showing the typical S-N curve for steel and non-ferrous alloys [35].

The S-N curve is usually obtained by plotting the data points on semi-log or log-log paper. The resulting curve could be fitted by mathematical equation as shown below, which relates the stress amplitude and number of cycles to failure [36].

$$\sigma_a = \sigma_f^{'}(2N_f)^b \qquad (6\text{-}8)$$

where,

$\sigma_f^{'}$ = fatigue strength of material

b = fatigue strength exponent

For steels, fatigue failures less than 10^3 cycles are considered as low cycle fatigue and high cycle fatigue deals with failures at more than 10^3 cycles. As shown in Figure 6-4, for steels, a "knee-bend" can be observed in the graph which indicates the "endurance limit" or "fatigue limit" of the material ($S_e^{'}$). Beyond this limit the material will not fail for any amount of

cycling. The non-ferrous alloys do not exhibit any endurance limit. The endurance limit of such material is set as 10^7 number of cycles to failure arbitrarily [36]. The endurance limit obtained for test specimen (S_e') can be related to endurance limit of the actual machine element (S_e) using endurance limit modifying factors as follows [37]:

$$S_e = K_a K_b K_c K_d K_e K_f S_e' \quad (6\text{-}9)$$

Where,

K_a= surface condition modification factor

K_b= size modification factor

K_c= load modification factor

K_d= temperature modification factor

K_e = reliability factor

K_f = miscellaneous modification factor

This is due to the differences between the conditions of the test specimen and actual machine element. At this stage, it should be noted that Wöller's experimental S-N curve do not consider the mean stress effects, as it considers only completely reversed cyclic loading. In reality this may not be the only case and non-zero mean stress may exist, as in the case of simple tension, where the load is applied and removed. In order to consider the effects of mean stresses Goodman, Gerber, Morrow, and Soderberg proposed the following equations, realizing that for curves R≠0, the woller's work is conservative [35].

Modified Goodman: $$\sigma_a = \sigma_{ar}\left[1 - \frac{\sigma_m}{\sigma_{uts}}\right] \quad (6\text{-}10)$$

Gerber: $$\sigma_a = \sigma_{ar}\left[1 - \left(\frac{\sigma_m}{\sigma_{uts}}\right)^2\right] \quad (6\text{-}11)$$

Soderberg: $$\sigma_a = \sigma_{ar}\left[1 - \frac{\sigma_m}{\sigma_{ys}}\right] \quad (6\text{-}12)$$

Morrow: $$\sigma_a = \sigma_{ar}\left[1 - \frac{\sigma_m}{\sigma_f'}\right] \quad (6\text{-}13)$$

Where,

σ_m = mean stress

σ_{uts} = ultimate tensile strength

σ_{ys} = yield strength

σ_a = fatigue strength when $\sigma_m \neq 0$

σ_{ar} = fatigue strength in fully reversed loading condition, when $\sigma_m = 0$

Out of all the above equations, Soderberg is considered to be most conservative, as it uses the yield stress to be the failure criteria. The Gerber equation more closely fits the experimental data where mean tensile stress is involved and is not suitable for compressive mean stress. Similarly the Goodman equation best fit the data for low-ductile material like high tensile steel or brittle material and the equation modified by Morrow seems to have the best correlation with ductile material experimental data when the true fracture stress is in tension where a material constant (σ_f') is considered as the failure criteria [36]. Therefore, proper selection of the mean stress equation depends on many variables.

As mentioned previously, the Stress-Life approach is mainly based on experimental data. It is reasonable to use this method to estimate fatigue life, for estimating fatigue life, if the S-N curve or experimental fatigue data exist for the material. This method is accurate for high cycle fatigue, where the fatigue life is dominated by elastic strain of the component.

In this project ANSYS Workbench FEA fatigue module has been used to estimate the fatigue life of the component. The FEA fatigue module requires an S-N curve, which is not readily available for the trailer material to be used as a input to calculate the fatigue life in the stress-life method. Although the S-N curve could be produced analytically using the limited experimental data available for the material, the process could be more complex and it would be easier to use strain-life method, which would need only fatigue parameters to estimate fatigue life in ANSYS Workbench fatigue software. The Strain-Life method used to estimate the fatigue life at the critical location of the component is explained in the next section.

6.2.3 Strain-Life Method

Fatigue cracks normally start at local discontinuities. Strain-Life fatigue analysis considers deformation as a cumulative effect of elastic and plastic strains. This method is very successful in defining shorter life span of components, where plasticity causes the majority of the damage. The method can also be used for high cycle fatigue problems as it considers the elastic and plastic strain responsible for fatigue failure. Strain-Life method can thus considered as comprehensive approach to deal with the fatigue problem [36].

This strain based approach estimates local stress and strain at the crack region. Most importantly, it considers the local yielding at the crack region and uses cyclic stress-strain and strain-life curves in the fatigue life estimation process. For this study, the strain-life curve shown in Figure 6-5 was constructed in ANSYS fatigue module using previously published fatigue properties of the trailer material [29].

Figure 6-5 shows elastic, plastic, and total strain components. The total strain is mathematically represented as follows [35]:

$$\in_a = \in_{ea} + \in_{pa} \qquad (6\text{-}14)$$

Where, $\in_{ea}$ = elastic strain amplitude, $\in_{pa}$ = plastic strain amplitude

The elastic and plastic strain lines in the strain-life curve are fitted with following equations respectively [35]:

$$\in_{ea} = \frac{\sigma_a}{E} = \frac{\sigma_f'}{E}\left(2N_f\right)^b \qquad (6\text{-}15)$$

$$\epsilon_{pa} = \varepsilon_f'(2N_f)^c \qquad (6\text{-}16)$$

Where c = fatigue ductility exponent, E = Young's modulus.

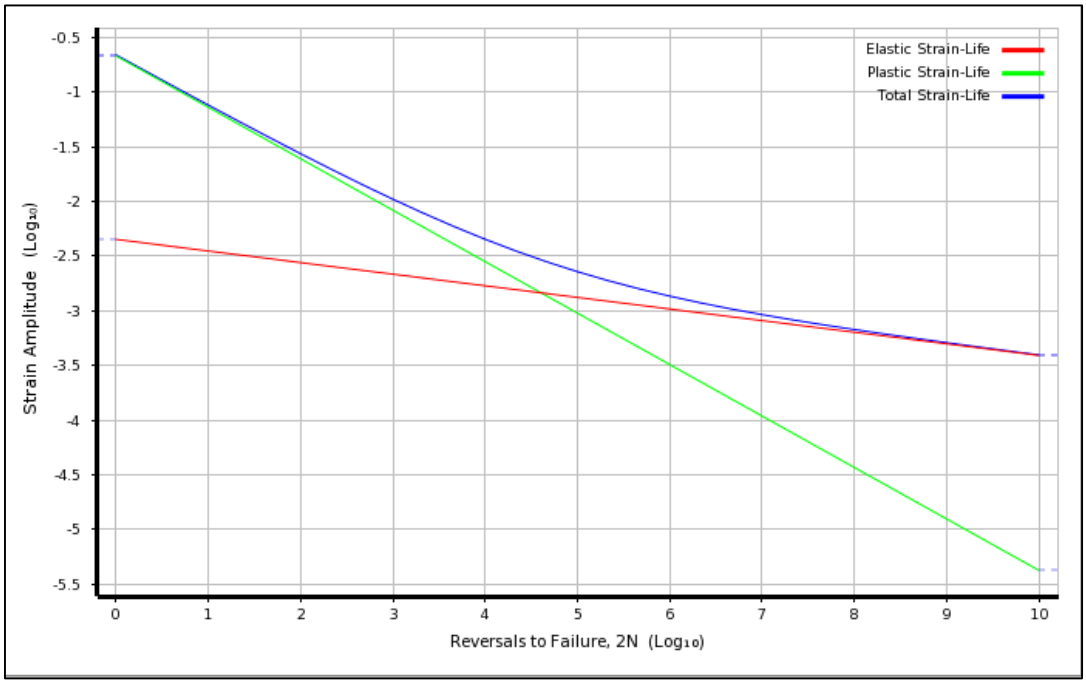

Figure 6-5: The strain life curve constructed in ANSYS using fatigue material properties.

According to the Coffin-Manson relation, when the elastic and plastic equations are combined, the total strain can be related to total life. The Coffin-Manson relation is presented as below [35]:

$$\epsilon_a = \frac{\sigma_f'}{E}(2N_f)^b + \varepsilon_f'(2N_f)^c \qquad (6\text{-}17)$$

Similarly, for cyclic stress-strain curve, the Ramberg-Osgood equation can be presented as follows [35]:

$$\in_a = \frac{\sigma_a}{E} + \left[\frac{\sigma_a}{H'}\right]^{\frac{1}{n'}} \quad (6\text{-}18)$$

Here total strain amplitude is the sum of elastic and plastic strains, H' is strain hardening coefficient, and n' is the strain hardening exponent.

Equations 6.17 and 6.18 can be defined using six parameters; four strain-life material properties and two cyclic stress-strain material properties. Given these fatigue material properties, the ANSYS Workbench fatigue module can construct the strain-life curve and cyclic stress strain curve for estimating the fatigue life.

As mentioned before, the strain-life equations uses elastic and plastic strain inputs to calculate fatigue life. This collective approach can lead to a lengthy finite element simulation to determine the total response. If the total life is dominated by elastic strain, the time spent on plastic deformation analysis will not provide any significant result. Therefore ANSYS fatigue module assumes nominal elastic response and then uses Neuber's equation to relate local stress/strain to nominal stress/strain at the critical area. [38].

Neuber's rule used in ANSYS is presented below:

$$\in \sigma = K_t^2 eS \quad (6\text{-}19)$$

Where,

$\in$ = total local strain

σ = local stress

S = nominal elastic stress

K_t = elastic stress concentration factor

e = nominal elastic strain

The ANSYS fatigue module simultaneously solves the above equation along with Ramberg-Osgood cyclic strain equation to calculate the total response at the local region using only the elastic strain. In the above calculation, ANSYS sets the value of Kt as 1, assuming a perfectly refined mesh of the component [38]. It is therefore necessary to achieve the best possible stress convergence in the static finite element analysis at the region of fatigue interest before the fatigue analysis is carried out.

In order to perform the fatigue analysis using strain-life method, two decisions need to be made to define the fatigue simulation in ANSYS Workbench fatigue module. First the type of cyclic loading applied on the structure must be identified. In this study, only the container loading/unloading scenario is considered. In this case a constant load applied and removed. This could be identified as constant amplitude loading. This is a simple bending load, which does not change the direction of the principal stress axis. Therefore it could further be identified as proportional loading and collectively this scenario could be explained as constant amplitude proportional loading, where the load applied once and then removed (the load fluctuates between maximum constant value and zero). As this loading is analyzed as proportional loading, only a single set of maximum principal stress from the static finite element results are fed to fatigue module to estimate the fatigue life at the critical location of the structure [38]. Figure 6-6 showing the graphical representation of the zero based loading type applied on the trailer.

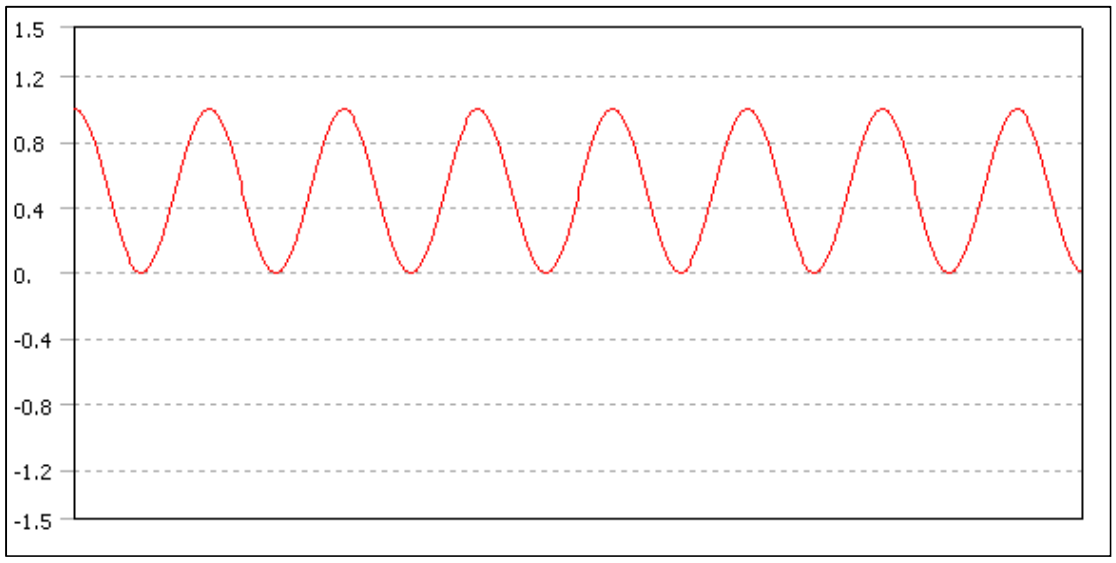

Figure 6-6: constant amplitude zero-based loading; load fluctuates between zero and constant maximum value.

The second important decision in this fatigue analysis is the consideration of the effect of mean stresses, as the loading is Zero-based and not completely reversed cyclic loading. The ANSYS Workbench fatigue module provides two methods to account for mean stress. They are SWT and Morrow mean stress correction methods. Among the two equations, the one yielding the conservative estimate of fatigue life is chosen in this study. The SWT and Morrow mean stress correction equations employed in the fatigue analysis are presented respectively as follows [35]:

SWT equation :

$$(\sigma_m + \sigma_a)\,\epsilon_a = \frac{(\sigma_f')^2}{E}(2N_f)^{2b} + \sigma_f'\varepsilon_f'(2N_f)^{b+c} \qquad (6\text{-}20)$$

Morrow equation:

$$\epsilon_a = \frac{\sigma_f'}{E}\left\{1 - \frac{\sigma_m}{\sigma_f'}\right\}(2N_f)^{b} + \varepsilon_f'(2N_f)^{c} \qquad (6\text{-}21)$$

Thus using the fatigue material properties and strain life relations, the fatigue life of the component at the critical region could be determined using strain-life method.

6.2.3.1 Results and discussion

The fatigue tool from ANSYS fatigue module is inserted into the simulation environment and then the static FE results are fed to fatigue tool to perform the fatigue calculations. The result of the fatigue analysis in terms of factor of safety is tabulated in Table 6-1. Figure 6-7 shows the factor of safety at one of the critical location in the sub-model of the trailer. The factor of safety obtained at the critical locations is more than one. That means the component will serve the desired number of cycles of loading. However, it is less than the recommended Factor of safety for fatigue, which is from 1.5 to 3[39]. The critical region under the study is at the region of the weld beed, which is the area of greatest uncertainties in the design. Therefore the best practice would be to design for a higher factor of safety or completely eliminate the stress concentration at the region if possible.

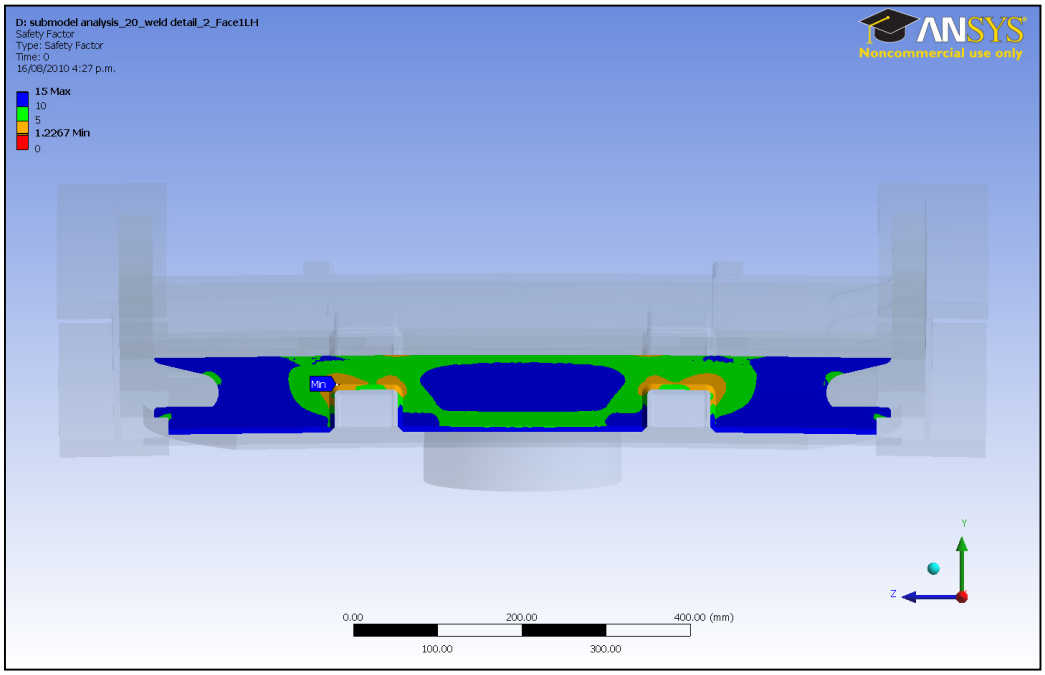

Figure 6-7: showing factor of safety at one of the critical location in 20' normal loading condition.

FOS	1.24	1.22	1.44	1.59	1.247

Table 6-1: showing the factor of safety obtained at the critical locations for the normal loading condition in the fatigue analysis of the current design.

6.3 Evaluation of the proposed new design

The trailer chassis is subjected to two static loading conditions; normal container loading/unloading and a "worst case" service condition. The analysis of the "worst case" service showed that the critical stress in the "worst case" service condition at the "hot spots" exceeds the yield stress of the material while in normal container loading conditions these stresses exceeds the static design safety limit set by STEELBRO. Further analysis of this loading condition for fatigue revealed that the margin on design life at the critical region is very low. This outcome of the static analysis of the trailer chassis warrants the redesign of the critical region.

The SB330 trailer model under the study is one of STEELBRO's highest demanded light weight trailers. Any substantial changes in the chassis design would disrupt the production planning and manufacturing facilities. Therefore, the proposed new design incorporates changes in the critical region in such a way that it would not affect any manufacturing facilities or production planning of the trailer. The sub-model of the proposed new design is shown in Figure 6-8 below.

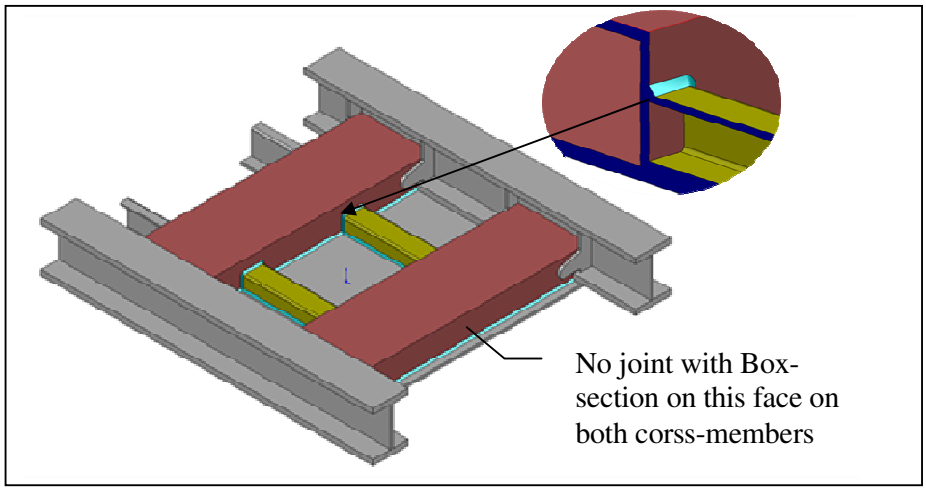

Figure 6-8: Showing the revised design at the cross-member joints and joints at the two opposite faces of the cross-members are eliminated.

Cracks have appeared at the intersection of the rub-plate cross-member and box-section as shown in Figure 1.1. The finite element analysis has also confirmed the critical spots in the rub-plate sub-model. Therefore effort has been made to change the joint design at the cross-member without affecting the structural integrity of the chassis. As shown in the Figure 6-8, this is achieved by removing the notches in the cross-member for the box-section and shortening the box-section at both ends. Originally the box-sections were passed through the cross-members. This is not necessary, as the load transfers from the king-pin through the rub-plate and cross-member. The proposed new design is subjected to both loading conditions and results are presented in the Figure 6-10 to Figure 6-13 respectively.

The proposed new design has simplified the joint design at the cross-member region and eliminated the stress intensity at the stress region, as shown in Figure 6-10 through Figure 6-13. More importantly, this design change is at the drawing level and will not affect any manufacturing facilities or production planning of the current manufacturing system at the company.

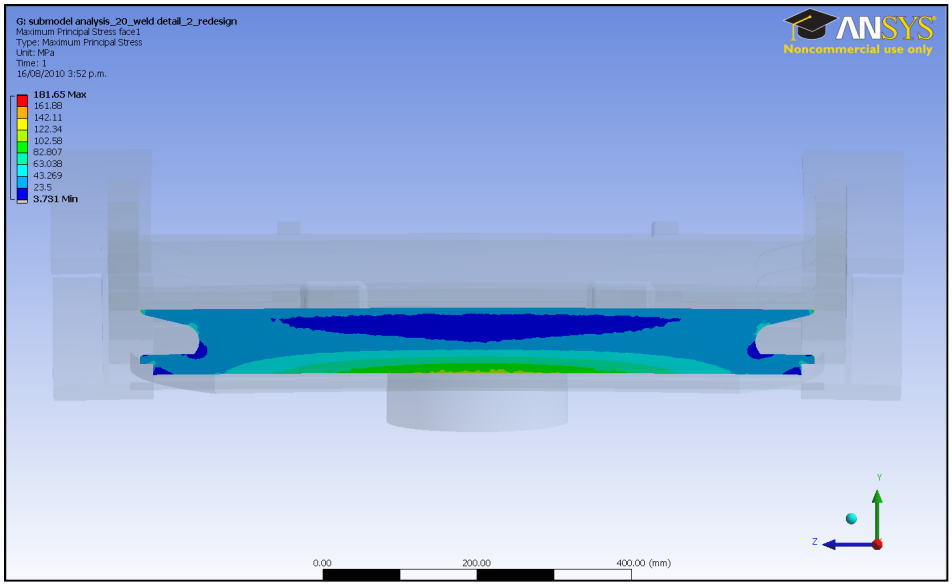

Figure 6-10: showing the stress distribution on one of the critical locations identified in the old design for 20' normal loading condition.

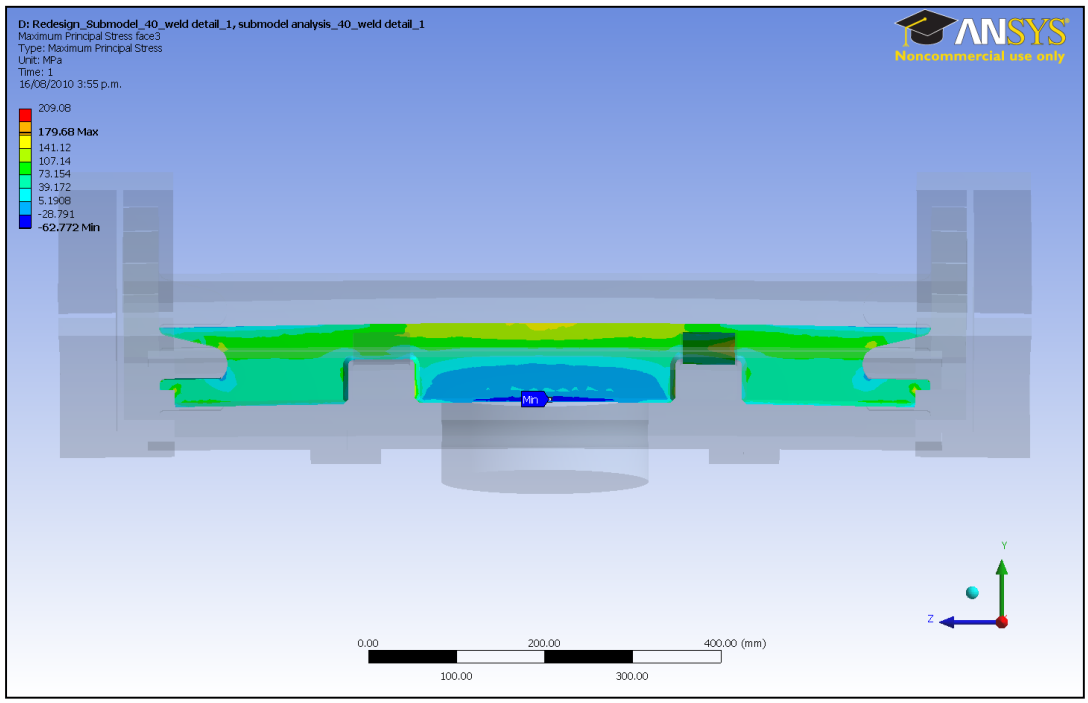

Figure 6-11: showing the stress distribution on one of the critical locations identified in the old design for 40' normal loading condition.

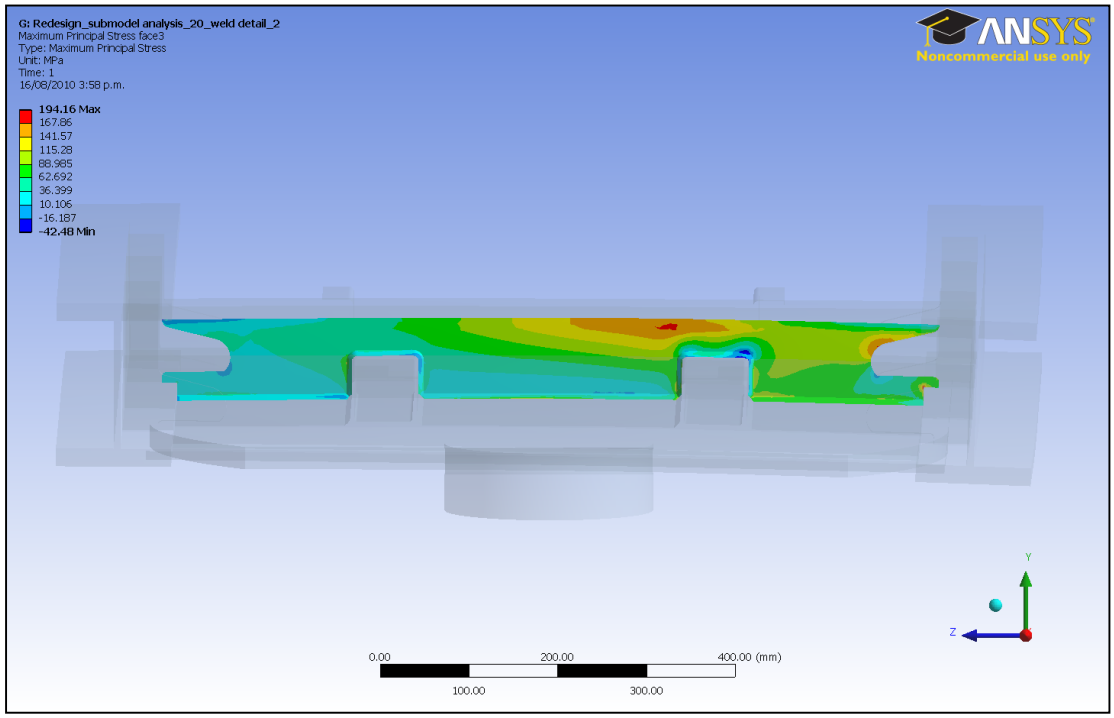

Figure 6-12: showing the stress distribution on one of the critical locations identified in the old design for 20' "worst case" service condition.

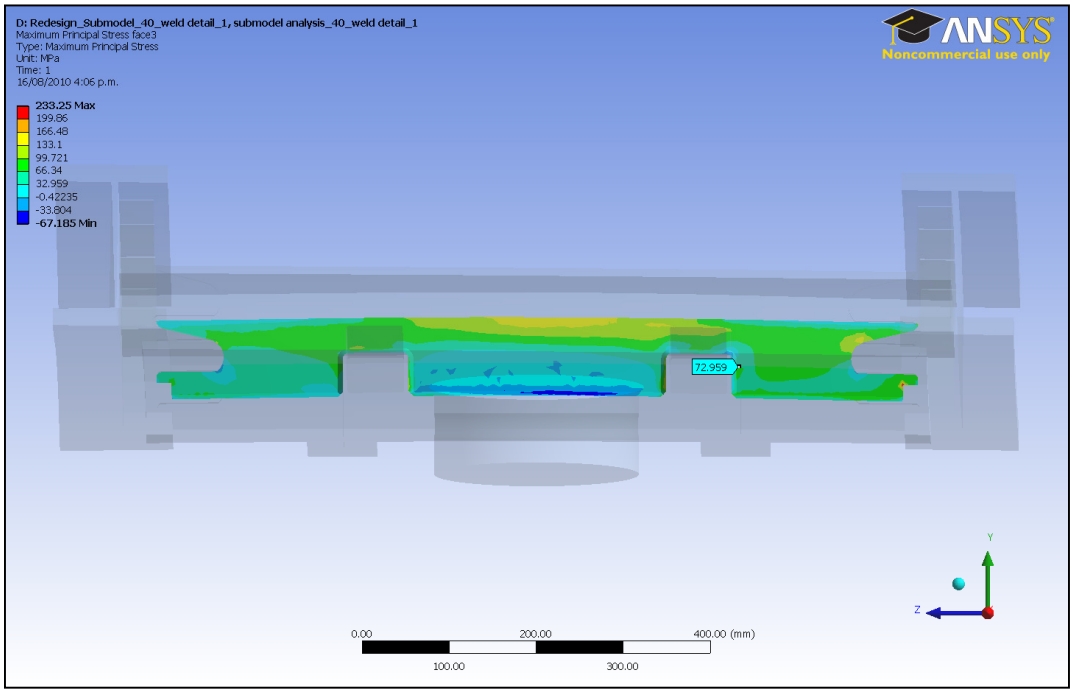

Figure 6-13: showing the stress distribution on one of the critical locations identified in the old design for 40' "worst case" service condition.

7 CONCLUSION AND RECOMMENDATIONS

7.1 Conclusion

The structural analysis of the trailer using Finite element analysis is carried out in this study for two loading conditions; normal loading/unloading condition and a “worst case” loading condition. These two cases were selected to determine their influence on the cross-member cracks at the rub-plate region of the trailer. Based on the outcome of the analysis performed in this study, the following can be concluded.

- If the trailer chassis under goes the “worst case” service condition, it has high potential to cause damage at the critical region and could be the cause of the failure.
- Static analysis of the normal loading/unloading condition showed that the maximum stress is below the yield stress. However, the maximum stresses are more than the recommended static design safety limit.
- Fatigue analysis performed on the normal loading/ unloading condition revealed that the margin of safety at the critical region against the fatigue loading is low and could cause failure considering the statistical nature of fatigue failure.
- Finally, a new design is proposed to overcome the potential failure in the static loading condition for the two loading conditions.

7.2 Recommendations

This research was carried to determine the effect of the two loading conditions on an ongoing problem. In this quest, the above conclusions showed that the trailer chassis subjected to these loading conditions has a significant effect. However, some recommendations to be considered in future development of the trailer chassis:

- Fatigue analysis for the normal loading condition showed that the factor of safety is low at the critical region, even without subjecting the trailer to dynamic loading conditions. This loading condition could occur for example when trailer is transporting a loaded container. Therefore fatigue analysis sould be performed considering the dynamic stress hysteresis to more accurately determine the fatigue life at the critical region.
- Finite element analysis performed in this research provides global picture of stress distribution on the chassis. At some locations it can be seen that the stress is very low, which warrants further investigation for weight to strength ratio optimization of the chassis. This investigation should also extend to detailed dynamic analysis of the trailer.
- This thesis is focused on investigating “area of interest”, rub-plate region. Therefore some assumptions were made at the suspension area and experimental results were found consistent at the area of interest. However, for future analysis such as dynamic or complete structural analysis, true characteristics of the suspension assembly should incorporated in the analysis.
- Fatigue analysis performed using the finite element method should also be validated by experimental methods.

8 REFERENCES

[1] Adams, V., & Askenazi, A. (1999). *Building Better Products With Finite Element Analysis.* Santa Fe, USA: OnWard Press.

[2] Cook, R. D., Malkus, D. S., Plesha, M. E., & Witt, R. J. (2002). *Concepts And Aplications Of Finite Element Analysis* (4th Edition ed.). USA: John Wiley & Sons, Inc.

[3] Transport Canada. (n.d.). *Transport Development Centre:Energy-efficient Light Trailer Engineering Design (TP 12982E).* Retrieved August 28, 2009, from Transport Canada Web site: www.tc.gc.ca/innovation/tdc/summary/12900/12982e.html

[4] Rahman, A. R., Tamin, M. N., & Kurdi, O. (2008). Stress analysis of heavy duty truck chassis as a preliminary data for its fatigue life prediction using FEM. *Journal Mekanikal* , 76-85.

[5] Kassahum, M. (2008). *Static And Dynamic Analysis of a Commercial Vehical With Van Body.* Unpublished Master's Thesis, Addis Ababa University. Ethiopia: Retrieved from http://etd.aau.edu.et/dspace/handle/123456789/1535.

[6] Wang, E., & Rauch, R. (2008). Fatigue Analysis and Design Optimization of a Trailer Hitch System. *Proceedings of International ANSYS Conference.* Germany: Retrived from http://www.ansys.com/events/proceedings/2008.asp.

[7] Bekah, S. (2004). *Fatigue Life Prediction In A Door Hinge System Under Uni-axial and Multi-axial Loading Condition.* Master's Thesis, Ryerson University, Toronto, Canada.

[8] Petracconi, C. L., Ferreira, S. E., & Palma, E. S. (2009). Fatigue Life simulation of A Rear Tow Hook Assembly of A Passenger Car. *Engineering Failure Analysis* , doi:10.1016/j.engfailanal.2009.09.002.

[9] Topac, M. M., Gunal, H., & Kuralay, N. S. (2008). Fatigue Failure Prediction of A Rear Axle Housing Prototype by Using Finite Element Analysis. *Engineering Failure Analysis , 16*, 1474-1482.

[10] Fermer, M., & Svensson, H. (2001). Industrial Experiences of FE-based Fatigue Life Predictions of Weldid Automotive Structures. *Fatigue and Fracture of Engineering Materials and Structures , 24*, 489-500.

[11] Ye, N., & Moan, T. (2007). Static And Fatigue Analysis of Three Types of Aluminium Box-stiffener Frame Connections. *International Journal of Fatigue , 29*, 1426-1433.

[12] Yongming, L., Startman, B., & Mahadevan, S. (2006). Fatigue Crack Initiation Life prediction of Railroad Wheels. *International Journal of Fatigue , 28*, 747-756.

[13] Zhao, J., Li, Q., & Shen, X. (2008). Finite Element Analysis and Structural Optimisatin for Improving the Fatigue Life of Rubber Mounts. *Journal of Macromolecular Sciience,Part A , 45:6*, 479-484.

[14] Karaoglu, C., & Kuralay, N. S. (2002). Stress Analysis of A Truck Chassis with Riveted Joints. *Finite Elements in Analysis and Design , 38*, 1115-1130.

[15] Colquhoun, C., & Draper, J. (2000). Fatigue Analysis of a FEA Model of A Suspension Component and Comparsion with Experimental Data. *Proceedings NAFEMS Conference: Fatigue Analysis from Finite Element Models*. Wiesbaden,Germany.

[16] Cowell, J. M. (2006). Development of A Practical Fatigue Analysis Methodology for Life Preciction of Rotary-Wing Aircraft Components. *Master's Thesis* . Raleigh, North Carolina.

[17] He, B., Wang, S., & Gao, F. (2010). Failure Analysis of an Automobile damper Spring Tower. *Engineering Failure Analysis* , 498-505.

[18] Palma, E. S., & Santos, E. S. (2002). Fatigue Damage Analysis in an Automobile Stabilizer Bar. *Proceedings of the Institution of Mechanical Engneers Part D: J Automobile Engineering, 216*, pp. 865-871.

[19] Madenci, E., & Guven, I. (2007). *The Finite Element Method and Applications in Engineering Using ANSYS*. New York, USA: Springer Science+Busness Media,LLC.

[20] Mac Donald, B. J. (2007). *Practical Stress Analysis with Finite Elements*. Dublin,Ireland: Glasnevin Publishing.

[21] Cook, R. D. (1995). *Finite Element Modeling for Stress Analysis*. New York, USA: Johan Wiley & Sons , Inc.

[22] Fagan, M. J. (1992). *Finite Element Analysis*. Singapore: Longman Singapore Publishers (Pte) Ltd.

[23] Dadkhah, F., & Jack Zecher, P. E. (2007). *Ansys Workbench: Software Tutorial with Multimedia CD Release 11*. Mission,KS,USA: SDC Publications.

[24] Edwards, K. S., & McKee, R. B. (1991). *Fundamentals of Mechanical Components Design*. New York,USA: McGraw-Hill,Inc.

[25] Juvinall, R. C., & Marshek, K. M. (1991). *Fundamentals of Machine Componet Design* (2nd Edition ed.). New York,USA: John Wiley & Sons.

[26] ANSYS Inc. (2009). Manual :Theory Reference for the Mechanical APDL and Mechanical Applications. (ANSYS Release 12.1). Canonsburg, USA.

[27] ANSYS Inc. (2007, January). Manual: Advanced Analysis Techniques Guide. (ANSYS Release 11). canonsburg, USA.

[28] ANSYS Inc. (2009). Manual: ANSYS Workbench Meshing Guide. *ANSYS Release 12.1*. Canonsburg, USA.

[29] Dusicka, P., Itani, A. M., & Buckle, I. G. (2007). Cyclic Response of Plate Steels Under Large Inelastic Strains. *Journal of Constructional Steel Research* , 156-164.

[30] ANSYS Inc. (2007). Structural Analysis.

[31] Looman, D. (2007). Submodeling In Ansys Workbench. *Ansys Advantage , I* (2), pp. 34-36.

[32] KYOWA Electronic Instrument Co., Ltd. (n.d.). *howsgw.pdf*. Retrieved July 10, 2009, from KYOWA Electronic Instrument Co., Ltd's website: www.kyowa-ei.co.jp/english/products/gages/pdf/howsgw.pdf

[33] Tokyo Sokki Kenkyujo Co., Ltd. (n.d.). *TML Pam E-101R STRAIN GAUGES*. Retrieved 02 03, 2009, from Tokyo Sokki Kenkyujo Co., Ltd's website: www.tml.jp/e/product/strain_gauge/catalog_PDF/straingauge1.pdf

[34] Biodata Limited,2000. (2000). *Microlink Hardware and Software User Manual*. Manchester, UK: Biodata Limited.

[35] Karl, M. (n.d.). *Fracture Mechanics and Failure Analysis*. (Powerpoint slides) Retrieved from http://blackboard.canterbury.ac.nz

[36] Dowling, N. E. (2007). *Mechanical Behavior Of Materials* (3rd Edition ed.). New Jersey, USA: Pearson Prentice Hall.

[37] G, R., Budynas, J, K., & Nisbett. (2008). *Shigley's Mechanical Engineering Design* (8th Edition ed.). USA: McGraw−Hill Primis.

[38] Hancq, A., & Browell, R. (2006, March 29). *Calculating And Displaying Fatigue Results*. Retrieved August 05, 2009, from ANSYS,Inc: www.ansys.com/assets/white-papers/wp-fatigue.pdf

[39] Autodesk.inc. (n.d.). *Safety Factors : Safety factor of fatigue loaded weld joint* . Retrieved April 2010, from Autodesk.inc website: http://wikihelp.autodesk.com

[40] Heckathorn, D. (n.d.). *Codfficient of Friction-Slide 1 (Powerpoint Slides)*. Retrieved 10 2009, from www.web.cvcaroyals.org

9 APPENDIX

Bending stress calculations from STEELBRO is presented below. For points form the bending stress results were selected to compare with the strain gauge results.

Mainframe Analysis C969-e MF NZ SB33 8500 FD 40opt.mcd

Constants: $g := 9.81$ $kN := 1000$ $kNm := kN \cdot 1000$ $kg := g$

Functions: $s(x, a) := (x - a) \cdot \Phi(x - a)$ $fb(BM, yf, I) := BM \cdot \frac{yf}{I}$

Static Load Case.

Geometry:

$L := 13600$	Length O/A
$FL2 := 9250$	Forward length
$FOH := 1600$	Forward overhang
$AX1 := 1500$	Axle 1-2 spacing
$AX3 := 1500$	Axle 2-3 spacing
$c := 485$	Hanger pivot-Axle centres (HT230TA15)
$d := 650$	Hanger pivot-Airbag centres (HT230TA15)
$FL = 9250$	Effective forward length

Payloads

$PL := 8250 \cdot g$ Nominal Payload per load point (N) $PL = 81 \cdot kN$

$Mm := 1100 \cdot g$ Module Mass (MK6 2500. SB33 2200) $Mm = 11 \cdot kN$

Discrete Loads	Distance from KP	Distr. loads	Distance from KP to start of Pd	Distance from KP to start of Pd
$P := \begin{pmatrix} Mm \\ PL \\ PL \\ Mm \\ 0 \\ 0 \end{pmatrix}$	$I := \begin{pmatrix} 1819 \\ 2274 \\ 8187 \\ 8581 \\ 0 \\ 0 \end{pmatrix}$	$Pd := \begin{pmatrix} 0 \\ 0 \\ 0 \\ 0 \\ 0 \\ 0 \end{pmatrix}$	$Id1 := \begin{pmatrix} 0 \\ 0 \\ 0 \\ 0 \\ 0 \\ 0 \end{pmatrix}$	$Id2 := \begin{pmatrix} 0 \\ 0 \\ 0 \\ 0 \\ 0 \\ 0 \end{pmatrix}$

KP reaction

$Rkp = 80 \cdot kN$

$Rkp = 8133 \cdot kg$

Total Suspension reaction

$Rsusp = 104 \cdot kN$

$Rsusp = 10566.8 \cdot kg$

Bending Moment

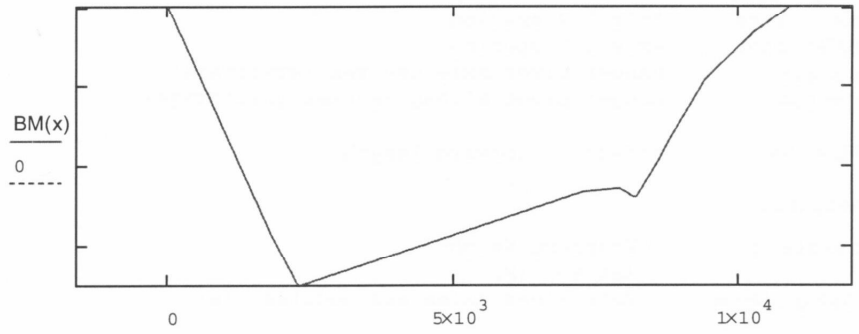

Distance K/Pin to Section

I-Section Size: Depth;Width;Thickness;Web

Fibre distance:

$$xs := \begin{pmatrix} -1600 \\ -1246 \\ -794 \\ -606 \\ -431 \\ -159 \\ 149 \\ 421 \\ 1096 \\ 1819 \\ 2274 \\ 2463 \\ 3789 \\ 5200 \\ 7146 \\ 7901 \\ 8127 \\ 8581 \\ 8646 \\ 9400 \\ 10146 \\ 10907 \\ 11193 \\ 11647 \end{pmatrix} \quad SP := \begin{pmatrix} 145 & 130 & 20 & 8 \\ 170 & 130 & 20 & 8 \\ 187 & 130 & 20 & 8 \\ 195 & 130 & 20 & 8 \\ 195 & 130 & 20 & 8 \\ 195 & 130 & 20 & 8 \\ 195 & 130 & 20 & 8 \\ 195 & 130 & 20 & 8 \\ 195 & 130 & 20 & 16 \\ 273 & 130 & 20 & 16 \\ 330 & 130 & 20 & 16 \\ 352 & 130 & 20 & 16 \\ 515 & 130 & 12 & 5 \\ 515 & 130 & 12 & 5 \\ 515 & 130 & 12 & 5 \\ 515 & 130 & 12 & 5 \\ 515 & 130 & 12 & 5 \\ 515 & 130 & 12 & 4 \\ 515 & 130 & 12 & 4 \\ 515 & 130 & 12 & 4 \\ 515 & 130 & 12 & 4 \\ 515 & 130 & 12 & 4 \\ 515 & 130 & 12 & 4 \end{pmatrix}$$

$$yf := \begin{bmatrix} SP_{(1,1)} \cdot 0.5 \\ SP_{(2,1)} \cdot 0.5 \\ SP_{(3,1)} \cdot 0.5 \\ SP_{(4,1)} \cdot 0.5 \\ SP_{(5,1)} \cdot 0.5 \\ SP_{(6,1)} \cdot 0.5 \\ SP_{(7,1)} \cdot 0.5 \\ SP_{(8,1)} \cdot 0.5 \\ SP_{(9,1)} \cdot 0.5 \\ SP_{(10,1)} \cdot 0.5 \\ SP_{(11,1)} \cdot 0.5 \\ SP_{(12,1)} \cdot 0.5 \\ SP_{(13,1)} \cdot 0.5 \\ SP_{(14,1)} \cdot 0.5 \\ SP_{(15,1)} \cdot 0.5 \\ SP_{(16,1)} \cdot 0.5 \\ SP_{(17,1)} \cdot 0.5 \\ SP_{(18,1)} \cdot 0.5 \\ SP_{(19,1)} \cdot 0.5 \\ SP_{(20,1)} \cdot 0.5 \\ SP_{(21,1)} \cdot 0.5 \\ SP_{(\ldots,1)} \cdot 0.5 \end{bmatrix} \quad yf = \begin{pmatrix} 73 \\ 85 \\ 94 \\ 98 \\ 98 \\ 98 \\ 98 \\ 98 \\ 98 \\ 137 \\ 165 \\ 176 \\ 258 \\ 258 \\ 258 \\ 258 \\ 258 \\ 258 \\ 258 \\ 258 \\ 258 \\ 258 \end{pmatrix}$$

Calculated bending stress along the length of the mainframe is tabulated in the third column below.

$$BMs = \begin{pmatrix} 0 \\ 0 \\ 0 \\ 0 \\ 0 \\ 0 \\ -12 \\ -34 \\ -87 \\ -145 \\ -177 \\ -174 \\ -158 \\ -142 \\ -118 \\ -115 \\ -120 \\ -98 \\ -94 \\ -47 \\ -21 \\ -0 \\ 0 \\ -0 \\ -0 \end{pmatrix} \cdot kNm \qquad Ixx = \begin{pmatrix} 21 \\ 31 \\ 39 \\ 42 \\ 42 \\ 42 \\ 42 \\ 42 \\ 45 \\ 100 \\ 158 \\ 184 \\ 247 \\ 247 \\ 247 \\ 247 \\ 247 \\ 237 \\ 237 \\ 237 \\ 237 \\ 237 \\ 237 \\ 237 \end{pmatrix} \cdot 10^{6}$$

$$\text{Stress} \quad fb = \begin{pmatrix} 0 \\ 0 \\ 0 \\ 0 \\ 0 \\ 0 \\ -27 \\ -77 \\ -190 \\ -198 \\ -185 \\ -167 \\ -165 \\ -148 \\ -124 \\ -120 \\ -125 \\ -107 \\ -102 \\ -51 \\ -23 \\ -0 \\ 0 \\ -0 \\ -0 \end{pmatrix}$$